Single-molecule studies of nucleosome reorganization by FACT during eukaryotic replication

Barbara Safaric

Vollständiger Abdruck der von der Fakultät für Physik der Technischen Universität München zur Erlangung des akademischen Grades einer

Doktorin der Naturwissenschaften (Dr. rer. nat.)

genehmigten Dissertation.

Vorsitzender:	Prof. Dr. Martin Zacharias
Prüfer der Dissertation:	1. Prof. Dr. Karl Duderstadt
	2. Prof. Andreas Ladurner, Ph.D.

Die Dissertation wurde am 09.12.2021 bei der Technischen Universität München eingereicht und durch die Fakultät für Physik am 07.02.2022 angenommen.

Excerpts of this thesis have appeared in the following publication:

Scherr, M.J.*, Safaric, B.*, and Duderstadt, K.E. (2018). Noise in the Machine: Alternative Pathway Sampling is the Rule During DNA Replication. Bioessays 40.
*equal contribution

Table of content

List of figures

List of tables

List of abbreviations

Å – Angstrom

aa – amino acid

ALEX – Alternating-Laser Excitation

ARS – autonomously replicating sequence

bp – base pair

CMG – Cdc45-MCM-GINS complex

cryo-EM – Cryogenic electron microscopy

dsDNA – double-stranded DNA

*E** – apparent FRET

EMSA – electrophoretic mobility shift assay

FACT – Facilitates Chromatin Transactions

fl – full-length

FRET –Förster resonance energy transfer

kbp – kilobase pair

kDa – kilodaltons

PDB – Protein Data Bank

PIFE – Protein Induced Fluorescence Enhancement

Pol – polymerase

PTM – post-translational modification

RC – replication complex

s. d. – standard deviation

Zusammenfassung

Die Chromosomenreplikation hängt von einer effizienten Entfernung der Nukleosomen durch akzessorische Faktoren ab, um einen schnellen Zugang zur genomischen Information zu gewährleisten. Gleichzeitig muss die epigenetische Information durch Sicherung der entfernten Histone und ihrer anschließenden Wiederanlagerung an neu synthetisierte DNA-Stränge erhalten bleiben. In dieser Arbeit werden die dynamischen Vorgänge untersucht, die der Nukleosomenverarbeitung vor der Replikationsgabel zugrunde liegen, wobei der Schwerpunkt auf dem Histonchaperon FACT liegt. Eine systematische Untersuchung von FACT-Kürzungen mittels Einzelmolekül-FRET ergab, dass die C-terminalen H2A/H2B-Bindungselemente beider FACT-Untereinheiten, Spt16 und Pob3, für die Bindung von FACT an das Nukleosom Essentiell sind. Im Gegensatz dazu wurde festgestellt, dass der N-Terminus von Spt16 keine Rolle bei der Reorganisation des Nukleosoms spielt. Um diese Interaktionen im Zusammenhang mit der Chromatinreplikation besser zu verstehen, wurden potenzielle FACT-Bindungsstellen innerhalb der Replikationsmaschinerie mit strukturgeleiteten Pulldowns untersucht. Diese Studien ergaben eine neue Interaktion zwischen FACT und Tof1, einer Proteinuntereinheit des Komplexes zum Schutz der Replikationsgabel, vor der Gabel platziert. Die Interaktionsschnittstelle zwischen dem N-Terminus von Spt16 und dem C-Terminus von Tof1 stimmt mit jüngsten Strukturstudien überein. Die Interaktion positioniert FACT vor der Replikationsgabel, so dass die mittleren und C-terminalen Domänen von Spt16 und Pob3 für den Kontakt mit den elterlichen Nukleosomen zur Verfügung stehen. Schließlich wurde die Bedeutung der entdeckten Interaktionen für eine effiziente Replikations-gabelprogression durch Chromatin durch vollständig *in vitro* rekonstituierte *S. cerevisiae* Chromatin-Replikationsassays bestätigt.

Die in dieser Arbeit präsentierten Ergebnisse bieten Einblicke in die Art und Weise, wie FACT Nukleosomen reorganisiert, und unterstützen einen Mechanismus, bei dem Nukleosomen durch die koordinierte Einbindung mehrerer FACT-Domänen entfernt werden. Darüber hinaus wird das Netzwerk von Interaktionen aufgedeckt, das den ersten kritischen Schritten im Histonprozessierungsweg während der Replikation zugrunde liegt und FACT durch eine Interaktion mit der Untereinheit des Gabelschutzkomplexes, Tof1, an die Spitze der Replikationsgabel stellt.

Abstract

Chromosome replication depends on efficient removal of nucleosomes by accessory factors to ensure rapid access to genomic information. At the same time, the epigenetic information needs to be preserved by securing removed histones and their subsequent redeposition onto newly synthesized DNA strands. In this thesis, the dynamic events that underlie nucleosome processing ahead of the replication fork are investigated with a central focus on the histone chaperone FACT. A systematic study of FACT truncations by single-molecule FRET revealed that the C-terminal H2A/H2B binding elements of both FACT subunits, Spt16 and Pob3, are essential for FACT engagement with the nucleosome. In contrast, the N-terminus of Spt16 was found to have no role in nucleosome reorganization. To better understand these interactions in the context of chromatin replication, potential FACT binding sites within the replication machinery were investigated using structure-guided pulldowns. These studies revealed a new interaction between FACT and Tof1, a subunit of the fork protection complex. The interaction interface between the N-terminus of Spt16 and the C-terminus of Tof1 is consistent with recent structural studies. The interaction positions FACT in front of the replication fork, such that the middle and C-terminal domains of Spt16 and Pob3 are available for engagement with parental nucleosomes. Finally, the importance of the discovered interactions for efficient replication fork progression through chromatin was confirmed by fully *in vitro* reconstituted *S. cerevisiae* chromatin replication assays.

The findings presented in this thesis offer insights into how FACT reorganizes nucleosomes, supporting a mechanism in which nucleosomes are removed through the coordinated engagement of multiple FACT domains. Further, the network of interactions underlying the first critical steps in the histone processing pathway during replication are revealed and place FACT at the front of the replication fork through an interaction with the fork protection complex subunit, Tof1.

Chapter 1: Introduction and background

Balancing the competing demands of storage versus transmission of genetic information is a fundamental challenge faced by all cellular organisms. Chromosomes must be folded and compacted in an orderly fashion to fit inside cells but retain dynamic flexibility to allow for rapid information access. To meet these challenges, eukaryotes organize their chromosomes using fundamental units, known as nucleosomes, consisting of 147-base pair (bp) segments of DNA tightly wrapped around histone octamer core (Kornberg, 1977; McGhee and Felsenfeld, 1980). These intricate structures enforce region specific regulatory programs and compact DNA. They also allow for rapid disassembly and reassembly during vital cellular processes (Widom, 1989). To facilitate diverse transformations of chromosomes, cells employ an array of histone chaperones and remodelers. No clear consensus has emerged for how these factors are regulated during DNA replication and to what extent they become integral members of replication complexes or remain passing collaborators. Further, how histone chaperones facilitate the transfer of histones to newly synthesized DNA strands during DNA replication is not well understood.

Histone chaperones are involved in multiple processes, from storage and histone transport to the nucleosome assembly. As a highly diverse group of proteins, they share no (or very low) sequence similarity, which is also reflected in their structure and function. This thesis investigates how the histone chaperone FACT engages with the nucleosome in the context of DNA replication. The histone chaperone FACT (FAcilitates Chromatin Transactions) is a multi-subunit protein indispensable for chromatin replication *in vitro*. FACT was shown not only to interact with the nucleosome, but also it harbors binding sites for all nucleosome components. Taken together, these features point towards a crucial role of FACT in histone inheritance and preservation of epigenetic information during DNA replication. To secure parental histones in a timely manner, FACT would need to be present in a close proximity to, or at the front of, the replisome approaching the parental nucleosome. How this process is coordinated, and which factors are involved, is not clear.

The primary goal of this thesis is to resolve the details of FACT interactions with the nucleosome to reveal contributions of the individual FACT domains to the nucleosome engagement. For this purpose, a single-molecule FRET assay reporting on the nucleosome conformation was developed. The second aim of this study was

to investigate how FACT is implicated in the chromatin replication. First, numerous replisome factors were screened for their potential physical interaction with FACT. Building upon the findings from the first part of the project, the contributions of particular FACT domains to chromatin replication were evaluated by an *in vitro* chromatin replication assay.

The single-molecule FRET assays reveal the details of how FACT engages with the nucleosome, uncovering intricate dynamic events and resolving seemingly overlapping roles of the individual FACT domains. Further, investigating replisome architecture and probing for potential interacting factors will uncover a so-far unknow interaction between FACT and the fork protection complex. Based on the most recent structural data, this interaction would place FACT right at the front of the replication fork, positioning it in a prime location to secure parental histones.

In the introductory chapters of this thesis, a short overview of chromatin science and the major discoveries, basics of chromatin, together with chromatin replication are presented. The following chapter further contextualizes the research by providing the background information on the heart of this thesis - histone chaperone FACT. Chapter 4 of this thesis summarizes the findings from single-molecule FRET assays revealing the contributions of the individual FACT domains to its interaction with the nucleosomes. Following a short overview of the fluorescence and its fundamental properties, the concept of FRET is introduced, together with the experimental approach for the observation of single molecules used in this work. In the chapters that follow the results of the single-molecule FRET assays are presented and discussed. In the Chapter 5, the role of FACT is investigated in the context of chromatin replication. First, a short description of the *in vitro* replication assay is provided, detailing how the evaluation of the FACT contribution to replisome progression through chromatin is conducted. Next, by summarizing the key structural findings, the overall architecture of the replisome is introduced. The results presented in the chapters following describe a search for replisome factor(s) that potentially interact with FACT and detail the implications of distinct FACT domains in chromatin replication. In closing, Chapter 6 draws together the various strands of the thesis with a brief summary of the main findings of the work presented.

1.1. A brief history of chromatin science

The nineteenth century was a time of great changes. Coinciding with the Industrial Revolution, that fundamentally changed the way people lived and worked, this century was also a time of outstanding scientific discoveries which shaped modern science as we know it today.

The onset of the 19th century is marked by John Dalton who published his atomic theory in 1808. According to the atomic theory, each chemical element is composed of atoms, with the same mass, differing from atoms of another element only in their weight. Pollen found itself in the middle of a major discovery in 1822 when Robert Brown, a botanist who was investigating pollen grains under the microscope, noticed they move randomly in the water. To honor the discovery, this phenomenon is today known as Brownian motion. In 1905, Albert Einstein provided an explanation of Brownian motion by mathematical laws behind the movements of particles based on kinetic–molecular theory, showing that the phenomena is caused by moving water molecules which randomly collide with suspended particles resulting in their random movement (Einstein, 1905). Jean Baptiste Perrin provided experimental evidence supporting Einstein's theory of Brownian motion, and was awarded the Nobel Prize in Physics in 1926. This was the pivotal piece of evidence that confirmed the existence of atoms and molecules, and Dalton’s atomic theory was finally universally accepted by scientists.

Brown’s discoveries did not stop there. Few years later, in 1831, when studying the fertilization of plants, Brown noticed pollen grains were moving into oval structure within cells and named this structure ‘nucleus’. He further learned that the nucleus is crucial for fertilization and development of an embryo. Brown’s work, together with the first description of cells by Robert Hook (Hooke, 1667), laid foundations for a new paradigm in biology − the ‘cell theory’. The theory was formulated by botanist Schleiden and zoologist Schwann in 1838, when they both independently came to the same conclusion that the cell is a basic structural unit of all organisms. Another major breakthrough was centered around plants, even though it was overlooked till the early 20th century. In 1866, Georg Mendel published his findings on hybridization experiments in pea plants, formulating the laws of inheritance, which consequently led to establishment of genetics (Mendel, 1866).

It was the beginning of 1870s when Friedrich Miescher and Albrecht Kossel, researchers in Felix Hoppe-Seyler's laboratory, made two seminal discoveries. First,

Miescher isolated a substance from white blood cell nuclei which he characterized as a phosphorus-rich acid and named it ‘nuclein’, what we today know as nucleic acids. Shortly after, Kossel expanded the findings by the discovery of a ‘histon’ in acidic extracts from erythrocyte nuclei. At the same time, Walther Flemming, a pioneer of cytogenetics, was making strides in studying the cell division. Flemming used aniline dyes which stained cell nucleus and uncovered fibrous structures within. Inspired by Greek word for color ‘khroma’, Flemming named these structures ‘chromatin’ (Flemming, 1882). Further experiments revealed that fibrous structures change their shape and position in the nucleus, which led to incredibly detailed and correct description of mitosis. Few years later, Heinrich Wilhelm Waldeyer named the nuclear threads observed by Flemming a 'chromosome', meaning stainable bodies (Waldeyer, 1888).

The decades that followed lacked major breakthroughs in biological research. It wasn’t until 1911 when Thomas Morgan, a researcher working on fruit flies, devised a theory of genetic linkage, describing that genes situated on the same chromosomes are inherited together and not randomly distributed to daughter cells as was believed. In 1928, Frederick Griffith discovered one bacteria can obtain the characteristics of another by means of what he named a 'transforming principle'. In fact, this was the first documented bacterial transformation, a commonly used technique today. Only a year later, heterochromatin was described for the first time by Emil Heitz, botanist and geneticist, who noticed certain parts of chromosomes are more densely stained than others (Heitz, 1929). This led to a distinction between heterochromatin and euchromatin, with the idea that more densely stained regions, heterochromatin, present ‘passive’ regions which don’t carry genes. Familiar with Morgan’s work, Heitz continued the studies together with Bauer and identified polytene chromosomes in flies, observing the characteristic pattern of heterochromatin (Heitz and Bauer, 1933). A group of scientists continued the course of investigations and in 1944 identified that DNA, in fact, accounts for the ‘transforming principle’. Contrary to the belief at the time, Avery, MacLeod and McCarty proposed that DNA, rather than histone protein, is the hereditary material of bacteria. In their paper they concluded “The evidence presented supports the belief that a nucleic acid of the deoxyribose type is the fundamental unit of the transforming principle” (Avery et al., 1944).

Shortly after the discovery of the protein α-helix (Pauling et al., 1951), the X-ray photograph obtained by Rosalind Elsie Franklin revealed the helical structure of the DNA with two chains (Franklin and Gosling, 1953a). With the knowledge of Franklin’s

research, Watson and Crick formulated a model of DNA structure (Watson and Crick, 1953), and together with Maurice Wilkins, received the Nobel prize for the discovery of the structure of DNA in 1962.

The discovery of the DNA structure shifted the focus away from the histones, which were thought at the time to only hold the DNA together. However, in the early 1960s, biochemist Vincent Allfrey, who curiously studied the amino acid composition of histones, found that some histone proteins had significant levels of acetyllysine residues. His team concluded that histones are post-translationally modified by acetylation and methylation, and that such modifications alter DNA-histone interactions. This knowledge allowed Allfrey to lay the foundation for epigenetics research, correctly formulating the connection between histone modifications and control of gene expression (Allfrey et al., 1964). Driven by the development of electron microscopy and methods to isolate chromatin, during the 1970's when examining the micrographs of nuclei the widespread little particles were discovered, named ν (nu) bodies by the researchers (Olins and Olins, 1974). Together with measurements of the size of ν bodies (70 Å), the team proposed a model for chromatin in which each ν body contains two of each of the histone in a complex with a DNA. Similarly, Christopher Woodcock also visualized the chromatin particles (Woodcock, 1973). Initially, his work was rejected from a journal with a reviewer noting that to accept it would require "rewriting our textbooks on cytology and genetics" – speaking to the monumental impact of his discovery. At the same time, two laboratories working on histones discovered the existence of histone–histone interactions and their assembly in the histone core of the chromatin subunit (D'Anna and Isenberg, 1974; Roark et al., 1974). Based on nuclease digestion and histone crosslinking data, a model of chromatin structure was proposed, in which four histone pairs form a complex with around 200 base pairs of DNA (Kornberg, 1974; Kornberg and Thomas, 1974). Finally, in 1975, the chromatin subunit was named 'nucleosome', incorporating previously described ν bodies and their spherical nature (Oudet et al., 1975).

The discovery of the nucleosome was a turning point in chromatin research, profoundly changing the way the field looked at fundamental cellular processes like DNA replication and transcription. The small nucleosome became the focal point of the research, and scientists focused their efforts on better understanding the composition and structure of the individual nucleosomes, as well as their distribution and organization in the genome. In 1984, the first high resolution crystal structure of

a nucleosome was published (Richmond et al., 1984). This pivotal study confirmed many of the previous findings, including the fact that DNA is wound around the histone core in 1.8 turns, the composition of the octameric histone core and the arrangement of histones within a histone core in form of two H2A/H2B dimers and an H3/H4 tetramer. The structure also provided several new insights showing that DNA in not uniformly wrapped around the histone core, but there are a few regions of tighter bending at the H3/H4-DNA interfaces. Further, it became apparent that histone-DNA interactions are confined to the inner DNA interface and that histones do not grasp around the DNA.

With the knowledge that the globular domains of a histones are located in the histone core, the question of the function of histone tails arose. These were later found to be involved in formation of higher-ordered chromatin states as well as a place of numerous post-translational modifications (PTMs) (Wu et al., 1986). In 1993, recognizing the potential behind PTMs, Bryan Turner proposed a hypothesis that PTMs of histones could be a way of information storage and transfer, with each single PTM potentially resulting is a specific effect — either by modifying the nucleosome structure or by acting as a marker for a specific histone binding protein (Turner, 1993). After decades of investigation on the PTMs of histone tails, in 2000 Brian Strahl and David Allis presented a hypothesis known as the ‘histone code’ proposing that specific histone modifications, sequentially or in combination, can be read by other proteins, prompting distinct downstream events (Strahl and Allis, 2000). Today, it is generally accepted that the ‘histone code’, together with other epigenetic mechanisms, such as DNA methylation and histone variants, determines heritable changes in gene expression.

The breakthrough findings of the 19th century mark the beginning of a new era of scientific discoveries and modern science as we know it today. From unsuspecting pollen to the nucleosome structure, this brief historic overview of the key findings in the chromatin research paints a clear picture that science has been inherently interdisciplinary right from the early days. Also, it sets the stage for the work presented in this thesis, where some of the basic nucleosome interactions implicated in chromatin replication are investigated by a combination of biochemical and biophysical approaches. None of which would have been possible without the numerous breakthrough findings by the awe-inspiring scientists mentioned here, and many more.

1.2. Chromatin – more than meets the eye

Since the discovery of DNA and chromatin, the continued development of methods enabled their extensive study, revealing an intricate system inside the cell nucleus and details of the fundamental biological processes, such as DNA replication and transcription. In eukaryotic cells, genomic DNA is in a form of a chromatin, organized in complexes with histone proteins in an arrangement which allows for extensive and ordered DNA compaction. The structural and functional unit of chromatin is a nucleosome, comprising of 147 bp of DNA that wraps around histone octamer core approximately 1.7 times in a left-handed manner (Luger et al., 1997) (Figure 1.2). The histone core consists of a highly conserved set of four histone proteins — two copies of the H2A/H2B heterodimer, and an H3/H4 heterotetramer. The seemingly simple formation of a small nucleosome complex, only around 11 nm in diameter (Richmond et al., 1984), shortens the DNA seven-fold (Iashina et al., 2017). Individual interconnected nucleosomes are described by the 'beads on a string' model, defining the primary structure of chromatin. Linker DNA, a short DNA stretch of varying length, connects neighboring nucleosomes thereby establishing a foundation for chromatin fiber formation. Further interactions between chromatin fibers form secondary and tertiary chromatin structures (Woodcock and Dimitrov, 2001), which lead to large-scale compaction and chromosome condensation (Figure 1.1).

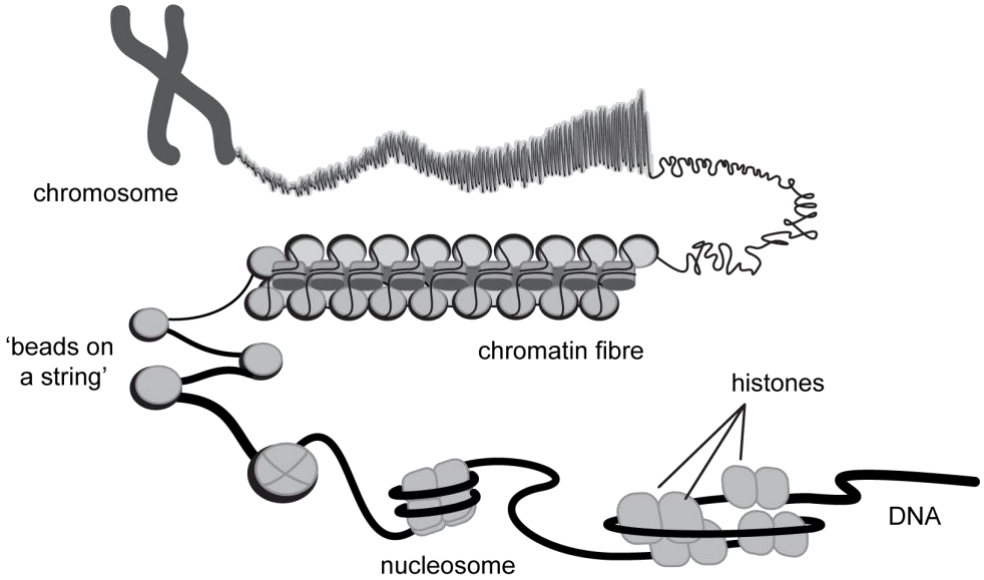

Figure 1.1. Chromatin organization.
The first step of DNA compaction is formation of complexes with histone proteins, forming nucleosomes. Nucleosome arrays are described by a 'beads on a string' model, depicting the basic uniform organization of chromatin. These arrays further form higher-order chromatin structures, chromatin fibers, which are subsequently folded into chromosomes.

The structure and the compaction state of chromatin are used for further classification of chromatin regions into heterochromatin and euchromatin. The majority of chromatin exists in a highly condensed structure, the heterochromatin, which is transcriptionally less active, while euchromatin is more open and highly transcriptionally active (Morrison and Thakur, 2021). This classification is a reflection of nucleosome packaging, histone post-translational modifications (PTMs) and histone variants (Ahmad and Henikoff, 2002; Martire and Banaszynski, 2020; Zhang et al., 2015).

Histones are small globular proteins, usually between 10 and 15 kDa in size. Their characteristic feature is their histone fold domain, composed of three α-helices, which forms a stable histone fold that dimerizes with another histone (Luger et al., 1997; Marino-Ramirez et al., 2006) (Figure 1.2). These protein-protein interactions stabilize the octameric histone core, while the basic nature of histones is crucial for their interactions with the negatively charged DNA by electrostatic and hydrogen bonding (Davey et al., 2002; Luger et al., 1997; Rohs et al., 2009). A single DNA base pair, positioned at the H3:H3 – DNA interface, forms the strongest interaction between histones and DNA, and defines the nucleosome symmetry axis known as nucleosome dyad (Luger et al., 1997) In addition to a globular core, histone tails are unstructured and protrude away from the DNA. Not only do these flexible regions engage with the neighboring nucleosomes, significantly contributing to the stabilization of higher ordered chromatin structures, but they also interact with transcription factors and chromatin remodelers (Du and Patel, 2014). Particularly, the H4 tail was shown to be central for chromatin condensation (Dorigo et al., 2003; Gordon et al., 2005; McBryant et al., 2009), interacting with a surface region of neighboring nucleosomes termed the ‘acidic patch’. The acidic patch is formed by several acidic surface residues of H2A and H2B, clustered together to create a negatively charged interface (Kalashnikova et al., 2013). This binding interface was shown to mediate interactions with multiple proteins, leading to a hypothesis that nucleosome-binding proteins interact with the acidic patch to trigger remodelling of higher order chromatin structure (Kalashnikova et al., 2013).

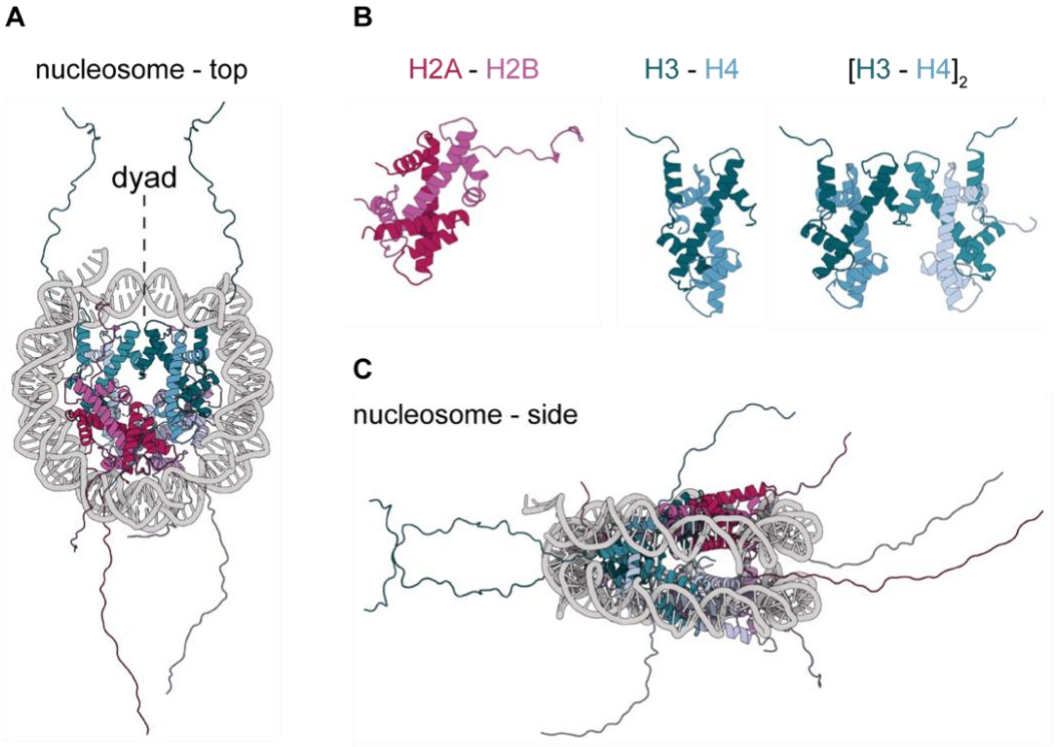

Figure 1.2. Canonical nucleosome.
(**A**) Structure of the canonical *S. cerevisiae* nucleosome (PDB 1ID3) with unstructured histone tails added separately in Coot. Nucleosome dyad, defining the nucleosome symmetry axis, is indicated. (**B**) Structures of *S. cerevisiae* H2A/H2B, H3/H4 dimers and $[H3–H4]_2$ tetramer (PDB 1ID3), showing the characteristic α-helix histone fold. (**C**) Side view of (A) showing the extent of unstructured histone tails. Histone H2A is red, H2B is pink, H3 is teal, H4 is light blue, and DNA is grey.

The structure of chromatin is also modulated by histone variants. Even though histone sequences are highly conserved throughout the tree of life, there is some divergence which results in histone variants. In addition to the four canonical histones (H2A, H2B, H3 and H4), eight variants of H2A (H2A.X, H2A.Z.1, H2A.Z.2.1, H2A.Z.2.2, H2A Barr body deficient (H2A.B), macroH2A1.1, macroH2A1.2 and macroH2A2) and six variants of H3 (H3.3, CENP-A, H3.1T, H3.5, H3.X and H3.Y) have been found so far in human somatic cells. Further, two testis-specific variants of H2B (H2BFWT) and testis-specific histone H2B (TSH2B) were identified (Buschbeck and Hake, 2017). Histone variants were found to have specific roles (Buschbeck and Hake, 2017), distinct cell cycle stage dependent expression profiles, and are incorporated in specific regions of chromatin (Tachiwana et al., 2021). In contrast to canonical histones, which are expressed in S phase, histone variants H2A.Z and H3.3 are expressed throughout the cell cycle and are incorporated in both open chromatin and pericentric heterochromatin (Ahmad and Henikoff, 2002; Boyarchuk et al., 2014). MacroH2A is found at transcriptionally suppressed

chromatin, and is the feature of the inactive X chromosomes (Costanzi et al., 2000). CENP-A (centromere protein A) is an H3 variant, essential for centromere definition and maintenance (Carroll et al., 2010; Tachiwana et al., 2011).

However, it is not only the sequence of histones that shapes the chromatin. Histone tails are carriers of the majority of post-translational modifications (PTMs) which not only are crucial for regulation of transcription, replication and DNA repair, but are also key for epigenetic inheritance and preservation of cell identity. These chemical modifications change the local microenvironment due to their size and/or charge, which in turn, has an influence on the protein-protein as well as protein-DNA contact network. So far, a plethora of histone modifications has been discovered, whereby the most common ones include methylation, acetylation and ubiquitination of lysine, methylation of arginine, and phosphorylation of serine, threonine and tyrosine residues (Bannister and Kouzarides, 2011). Methylation alters the hydrophobic character and size of the modified residue, without changing the overall charge. Methylation is associated with the gene silencing and is considered to have a major role in transcriptional regulation. Acetylation is associated with a transcriptionally active chromatin as it neutralizes the charge of lysine residues, thereby weakening the interaction with the negatively charged DNA resulting in a more open chromatin structure. Similarly, phosphorylation alters the electrostatic properties of histones by adding a bulky, negatively charged group and is essential in DNA damage response pathways, mitosis and transcriptional regulation (Musselman et al., 2012). Additional levels of complexity arise from (potentially) cooperative action of PTMs and cross-talk.

The intricate process of chromatin packing allows for more than two meters of DNA to fit inside of a nucleus in humans cells, achieving a 10 000-fold (Li et al., 1998) condensation of DNA. Such tremendous DNA compaction in chromatin significantly restricts the access of protein machinery to DNA for fundamental DNA-templated processes, including replication, transcription, and DNA repair. The highly dynamic nature of chromatin accommodates this great demand for DNA access, realized through the aforementioned histone variants and covalent modifications, and chromatin associated proteins such as chromatin remodelers and histone chaperons. Histone variants and histone PTMs are pivotal for recruitment of a number of proteins to chromatin in a site-specific manner, including ATP-dependent remodelling machineries that can move or eject nucleosomes, and chromatin-binding proteins that recognize specific chromatin architectures. And even though scientists in the 19th century first wrongly believed that the histone

proteins are carriers of the genetic information, new insights into chromatin and the continuously growing field of epigenetics show they were not completely mistaken. With the great methodological developments in the last few decades, is has become clear that chromatin is not merely a stiff scaffold for DNA compaction, but rather a complex and dynamic structure forming a unique and active environment — implications of which we are only beginning to understand.

1.3. Chromatin replication and the replisome architecture

Genome duplication is performed by large protein complexes, known as replisomes, that couple the disassembly and unwinding of parental chromosomes with the synthesis and repackaging of daughter chromosomes. In eukaryotes, the CMG (Cdc45, Mcm2-7, GINS) helicase lies at the center of this process serving as the hub for replisome assembly. CMG unwinds parental double-stranded (ds)DNA and guides the separated strands to distinct polymerases on the leading and lagging strands (Burgers and Kunkel, 2017), where they serve as templates for synthesis of new daughter stands (Figure 1.4). The DNA replication machinery is an example of a multicomponent system for which our mechanistic understanding is rapidly evolving due to single-molecule observations. The foundation of our understanding of replication mechanism derives from several seminal experiments conducted in the second half of the 20th century which suggested DNA replication is performed by a single static complex with highly defined operating principles. In contrast to this view, single-molecule observations have revealed that dynamic exchange of core components, pausing events, and several types of DNA loops may underlie coordination of daughter-strand synthesis (Beattie et al., 2017; Duderstadt et al., 2016; Geertsema et al., 2014; Georgescu et al., 2014; Graham et al., 2017; Lewis et al., 2017a). Individually, these events support different mechanistic models which cannot always be reconciled in a single reaction mechanism. However, when viewed as alternative, sometimes parallel, pathways, a more complete and coherent picture emerges. Nonetheless, this multi-pathway view of replication is often at odds with experimental observations that still dominate our textbook view of the process. Given the numerous compelling studies supporting this dynamic view (Beattie et al., 2017; Duderstadt et al., 2016; Geertsema et al., 2014; Georgescu et al., 2014; Graham et al., 2017; Lewis et al., 2017a) we must re-examine the early experiments that underlie our core theories.

The view that DNA replication is a highly coordinated process first emerged from autoradiography and pulse-chase experiments conducted by Cairns and others (Friedberg et al., 2006; Kornberg and Baker, 1992), which revealed that DNA unwinding is coupled to the synthesis of the daughter strands. The pioneering work of Arthur Kornberg, Okazaki and many others that followed, led to the discovery of the first DNA polymerases and the asymmetric mechanism of daughter-strand synthesis (Nelson and Cox, 2005). This revealed that while the polymerase on the leading strand can synthesize co-directionally with unwinding, the polymerase on the

lagging stand performs synthesis discontinuously, in the opposite direction, by repeatedly restarting on RNA primers generated by primase. Discontinuous synthesis on the lagging strand leads to the formation of a series of Okazaki fragments (OF), which are later converted into a continuous strand.

The fundamental asymmetry in the synthesis of the daughter strands presents a coordination challenge: How can a single protein complex accommodate the opposite directionalities of synthesis? Based on rapid dilution experiments suggesting replication is performed by a single protein complex, Alberts came up with the elegant proposal that each cycle of lagging-strand synthesis involves the formation of a 'trombone loop' that allows both polymerases to reside in the same complex while moving in opposite directions (Alberts et al., 1983). These early observations created a paradigm in the field that efficient DNA replication is a consequence of highly refined operating principles. In the decades that followed, intensive research focused on clarifying the role of the key players and the precise sequence of events that underlies each replication cycle.

As our understanding of the replication machinery has advanced, many central questions have nonetheless persisted. In particular, several divergent models have been put forward to explain how daughter-strand synthesis remains synchronized given that lagging-strand synthesis involves a series of slow enzymatic steps (priming and polymerase cycling) while leading-strand synthesis is continuous (Corn et al., 2005; Dixon, 2009; Frick and Richardson, 1999; Hamdan et al., 2009; Lee et al., 2006; Lee and Richardson, 2002; Li and Marians, 2000; Mangiameli et al., 2017; Manosas et al., 2009; Pandey et al., 2009; Tanner et al., 2008; Yuzhakov et al., 1999). Several recent observations of replication with single-molecule approaches have revealed more intrinsic stochasticity in replisome function suggesting many of these models are not mutually exclusive. Instead, they may represent different pathways whose sampling depends on environmental conditions and the current configuration of the replication machinery (Figure 1.3).

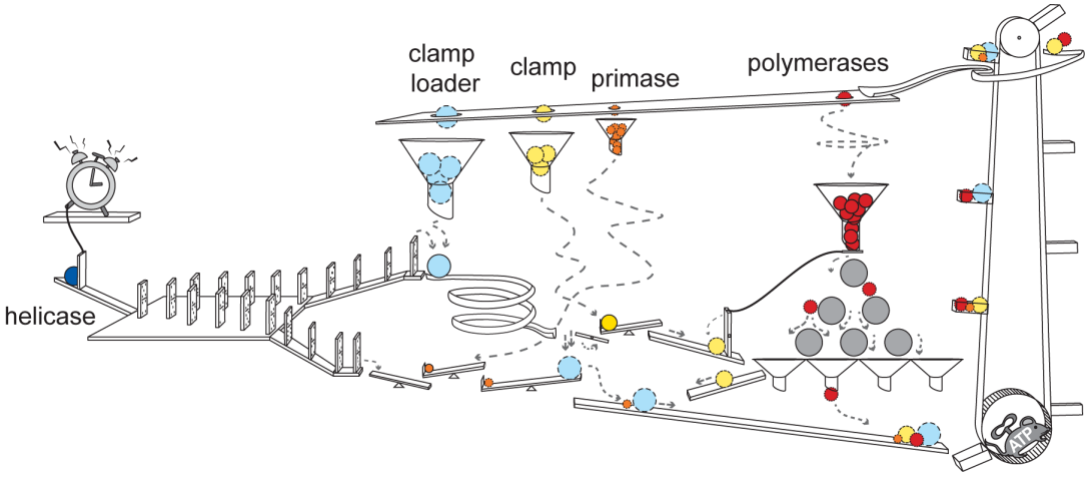

Figure 1.3. Stochastic sampling of molecular pathways during DNA replication.

The first step towards genome duplication consists of replisome assembly and activation during the initiation process. The initiation process in eukaryotes is divided in two major steps: origin licensing and origin firing which separately happen in G1- and S-phase of the cell cycle, respectively (Blow and Laskey, 1988; Diffley et al., 1994). During origin licensing, the replicative helicase is loaded on origins. In contrast to bacteria, eukaryotes have multiple origins whose sequence seems to be more defined by chromatin organization rather than on a primary DNA level. Origins in *S. cerevisiae* are, in this sense, unique - they show well-defined sequences, called autonomously replicating sequences (ARS) (Stinchcomb et al., 1979). ARS are recognized by the heterohexameric origin recognition complex (ORC) which subsequently recruits the helicase loader Cdc6 to close a hexameric ring around dsDNA. Contrary to bacterial DnaA, the ORC-Cdc6 complex has no DNA unwinding activity, instead its primary role is helicase loading. The eukaryotic helicase is a heterohexameric complex with a defined order of minichromosome maintenance (Mcm) 2–7 subunits (Li et al., 2015). Helicase activation involves separation of the double hexamer, dsDNA melting and exclusion of one strand to allow ssDNA translocation in 3′-5′ direction (along the leading strands). Two S-phase kinases play critical roles during this process: Dbf4-dependent kinase (DDK) and S-Phase cyclin-dependent kinase (S-CDK). First, DDK phosphorylates Mcm4/6 subunits, which exposes a binding site for Sld3 (in complex with Sld7). Cdc45 is then recruited to Mcm2-7, presumably by Sld3. Second, S-CDK phosphorylates Sld2 and Sld3 which enables binding to Dpb11. Subsequently, the tetrameric complex GINS and Pol ε are recruited, forming the full 11-subunit replicative helicase CMG (Cdc45-Mcm2-7-GINS).

Following helicase activation and CMG formation, three different polymerases are recruited to the replication fork: Pol ε and Pol δ, which are generally assumed to perform leading and lagging-strand synthesis, respectively, and Pol α which performs priming. While in bacteria, the clamp loader acts as central hub in the replisome by tethering Pol III on both strands to the helicase, CMG plays a crucial role in organizing the eukaryotic replisome (Gambus et al., 2006b; Gambus et al., 2009). Direct association of Pol ε to CMG ensures robust leading-strand synthesis (Georgescu et al., 2017; Georgescu et al., 2014; Langston et al., 2014; Sengupta et al., 2013; Sun et al., 2015; Zhou et al., 2017) and three central complexes have been implicated in coordinating daughter-strand synthesis. First, Ctf4 (chromosome transmission fidelity 4), a homotrimeric complex, has been shown to couple CMG and Pol α (Gambus et al., 2009; Kang et al., 2013; Simon et al., 2014; Sun et al., 2015). Second, Mcm10 has a versatile role in origin melting, CMG assembly and stimulation, and Pol α recruitment to CMG (Perez-Arnaiz et al., 2017). Finally, Mrc1 (mediator of replication checkpoint), Tof1 (topoisomerase I interacting factor), and Csm3 (chromosome segregation in meiosis), together forming the fork protection complex (FPC) may link helicase to polymerase activity (Cho et al., 2013; Gambus et al., 2006b; Katou et al., 2003) and has recently been shown to simulate replication to *in vivo* rates both in bulk and single molecule assays (Lewis et al., 2017b; Yeeles et al., 2017). Taken together, these observations highlight the numerous interactions between CMG and other replisome components that can serve to modulate replication fork progression. Recent single-molecule studies of bacterial replication strongly hint that dynamic exchange and a constantly evolving contact network underlie this modulation, but further studies are needed to elucidate the unique importance of each core subassembly and the global architecture of the eukaryotic replisome.

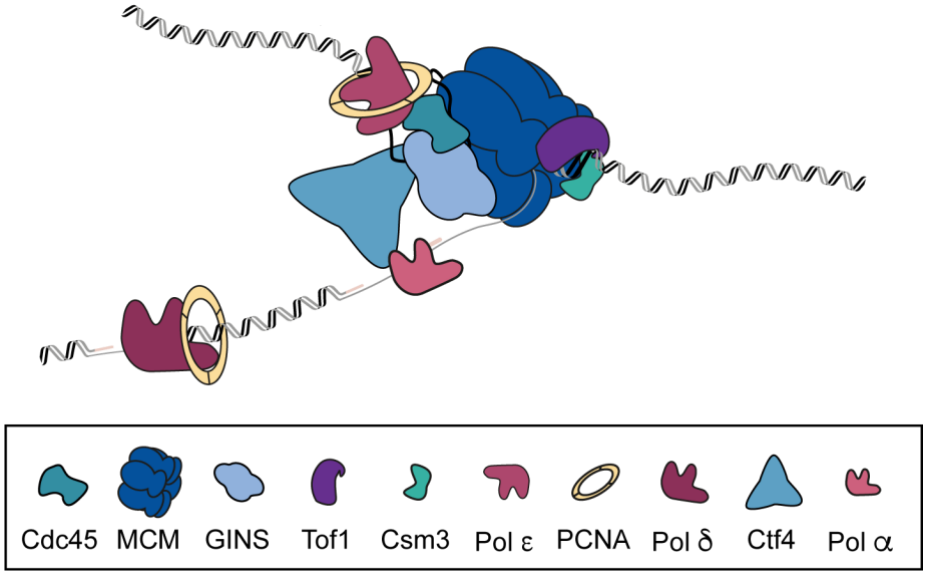

Figure 1.4. Composition of the replisome.
The *S. cerevisiae* replisome is a large and dynamic assembly comprised of ~50 proteins. On the schematics, arrangement of some of the core of the replisome factors is depicted, including the CMG (Cdc45-MCM-GINS) helicase, PCNA clamp, the leading strand DNA polymerase (Pol) ε, lagging strand Pol δ, Pol α, Ctf4 and Tof1- Csm3.

While biochemical and genetic studies have revealed numerous functions of replisome factors and their interactions, questions about the underlying mechanisms remain open. Understanding the architecture of the replisome will provide a complete picture of the process, however, obtaining structures of the multi-protein replisome machinery proved to be very challenging due to its complexity and subunit dynamics.

The first glimpse of replisome organization showed the CMG that lies in the center of the eukaryotic replisome, composed of Mcm2-7 hexamer, Cdc45 and GINS. The Mcm2-7 hexamer has distinct N- and C-terminal domains forming two tiers, N- tier and C-tier. The C-tier contains the ATP sites driving translocation and DNA unwinding. Cdc45 and GINS are placed on a side of the Mcm2-7 hexamer where they close MCM2-7 ring (Costa et al., 2011). Next, the pre-RC intermediate was visualized, containing the ORC-Cdc6-Cdt1–MCM2-7 (OCCM) complex bound to DNA (Sun et al., 2013). Helicase loading was shown to progress through a transient ORC–Cdc6–Mcm2–7-Mcm2–7 (OCMM) complex - a loading intermediate with an OCM and a second Mcm2–7 single hexamer in which the N- tiers of each Mcm2–7 in the double hexamer are facing each other (Sun et al., 2014). Although the head-to-head loading orientation of the Mcm2-7 double-hexamer is widely accepted (Evrin et al., 2009; Remus et al., 2009), the orientation of double-hexamer separation has long been a topic of discussion. The debate heated up with conflicting reports of

single MCM hexamer arrangement, which resulted in a conundrum about double-hexamer resolution and subsequent orientation of the opposing replication forks. In the classical model of Mcm2-7 separation, the C- tier faces the replication fork with the N-tier is behind. This model is supported by structural and FRET studies (Costa et al., 2014; Itsathitphaisarn et al., 2012; McGeoch et al., 2005; Rothenberg et al., 2007). In contrast, high-resolution structural analysis suggested the N-tier faces the replication fork. Thus, upon double-hexamer separation, the Mcm2-7 helicases would need to pass each other by translocating on opposing ssDNA strands (Georgescu et al., 2017). This occurs by strand ejection by one CMG helicase, which then becomes the translocation strand of the second CMG, by a so far unresolved mechanism. The model where CMG translocates with the N-tier facing the replication fork, and the leading-strand template enters the CMG in a 3′–5′ orientation, is today widely accepted (Douglas et al., 2018; Georgescu et al., 2017).

Even though the structure of the eukaryotic CMG helicase at a replication fork provided many insights into the replisome organization, from the *in vitro* replication studies, detailed in Chapter 5.1, it was clear that a few factors vital for proper replication fork progression are missing from thus far obtained structures. These include components of the replisome progression complex (RPC), primarily the proteins found to be responsible for the increased replication rates — Mrc1 and Csm3-Tof1, shown to form the fork protection complex (FPC). A recent cryo-EM structure of the FPC bound to CMG at a replication fork, together with Ctf4, provides one of the most complete pictures of the replisome today (Baretic et al., 2020). The structure shows that the Ctf4 trimer is placed at the GINS-Cdc45 interface, protruding away from the CMG (Figure 1.5). With one Ctf4 monomer interacting with CMG, the other two monomers are left free for dynamic interaction with multiple factors, in addition to its stable interaction with Pol α (Yuan et al., 2019). Further, this is the first structure of Tof1 and Csm3 complex, extending on the previously resolved N-terminus of Timeless, a human orthologue of Tof1, and biochemical characterization of its interaction with Tipin, a human orthologue of Csm3 (Holzer et al., 2017). Interestingly, in the cryo-EM structure by Baretic et al. (2020), Csm3-Tof1 is located on the N-tier of the MCM helicase, binding dsDNA before it enters into the CMG, thus redefining the architecture of the replisome by placing the Csm3-Tof1 in front of CMG. Additionally, cross-linking mass spectrometry showed multiple Mrc1-CMG contacts, extending from the Mrc1 N-terminal interaction with Tof1, to Mrc1 C-terminus positioned at the rear of the CMG, close to Cdc45. Together with data from *in vitro* replication assays (Yeeles et al., 2017), this work suggests that

dsDNA binding by Csm3-Tof1 is important for the stabilization of Mrc1 on the replisome, and consequently, for DNA replication enhancement (Baretic et al., 2020).

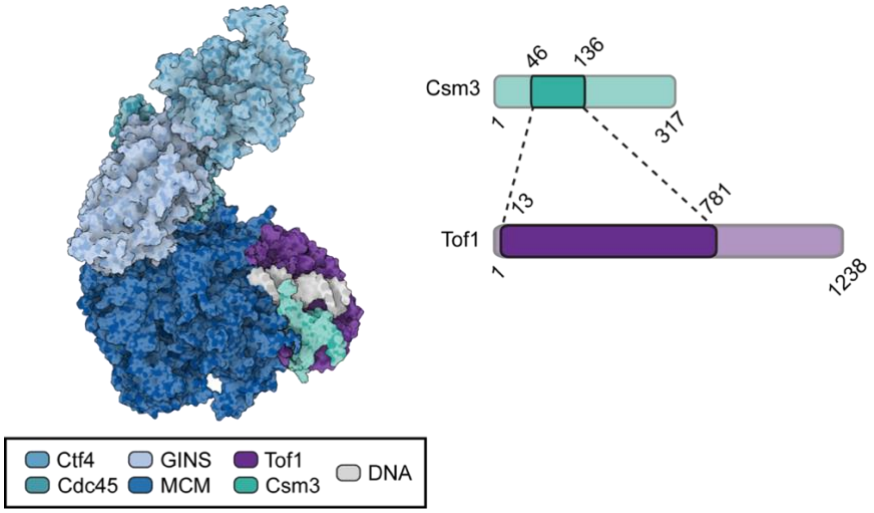

Figure 1.5. Structure of FPC bound to CMG.
Left: Structural model of CMG-Ctf4-Tof1Csm3 (PDB 6SKL). The figure was prepared with Protein Imager (Tomasello et al., 2020). Right: Schematic showing resolved parts of Tof1-Csm3 complex in 6SKL.

There are several further factors whose structural arrangement will be the key in understanding replisome organization — replicative polymerase ε, δ and α. Data suggests all three polymerases are retained in the replisome for multiple rounds of Okazaki fragment synthesis (Kapadia et al., 2020; Lewis et al., 2020). Pol α was shown to only transiently interact with Ctf4, thereby forming a Mcm2–Ctf4–Pol α cluster (Yuan et al., 2019), which positions Pol α conveniently for nucleosome transfer from parental DNA to the lagging daughter DNA (Gan et al., 2018b). How exactly Pol α and Pol δ are retained at the replication fork is not clear. Pol ε was shown to form a stable complex with CMG, with the Pol ε subunits Pol2 and Dpb2 contacting Mcm2, 3, 5 and GINS (Goswami et al., 2018).

Recently, a cryo-EM structure of a human replisome was resolved, comprising the CMG replicative helicase, TIMELESS-TIPIN (*S. cerevisiae* Tof1-Csm3 and Mrc1), CLASPIN (*S. cerevisiae* Mrc1), AND-1 (*S. cerevisiae* Ctf4), Pol ε and fork DNA (Jones et al., 2021). Comparison of the *S. cerevisiae* and human replisome structures shows that both follow the same blueprint, with the replisome factors placed in equivalent positions. Reflected in the high conservation of replisome architecture, such an arrangement highlights the fundamentally conserved mechanism of DNA replication. To develop a full picture of chromatin replication and to better understand the replisome coordination additional studies will be needed. The underlying mechanisms of the priming process, substrate handoff between Pol α, δ, ε, and parental histone transfer are still poorly understood.

1.4. Histone shuffle

With the approaching replication fork, nucleosomes are believed to undergo structural changes that include unwinding of the DNA from the histone core and disruption of the histone octamer. Here, the capture of parental histones, together with their handover and subsequent re-incorporation onto new DNA strands, is crucial for preservation of the epigenetic information. This critical process is orchestrated by the action of several histone chaperones and chromatin remodelers that ensure preservation of the epigenome.

As the engine of unwinding, the CMG is positioned to make first contact with parental nucleosomes that must be disassembled. Several other important protein complexes assemble with the CMG and could be involved directly or indirectly in processing of parental nucleosomes (Figure 1.6). Among them is the fork protection complex (Csm3-Tof1-Mrc1), which modulates replisome speed (Lewis et al., 2017b; Yeeles et al., 2017). Pol ε was shown to have an intrinsic H3/H4 chaperone activity and facilitate replication-coupled nucleosome assembly (Bellelli et al., 2018; Yu et al., 2018). Further, an H3/H4 interacting motif in the terminus of MCM2 has been reported and structurally characterized in complex with H3/H4 and the histone chaperone Asf1, but a direct role in chromatin replication has not been established (Groth et al., 2007; Huang et al., 2015; Richet et al., 2015). Further, together with Ctf4 and Pol α, MCM2 was shown to participate in parental $(H3\text{-}H4)_2$ tetramer handover to the lagging-strand DNA (Gan et al., 2018a). Also, it has been shown that CAF1 (chromatin assembly factor 1) is the main chaperone involved in H3/H4 tetramer deposition, directly interacting with the replication machinery through PCNA (proliferating cell nuclear antigen) (Moggs et al. 2000). There is an open question whether or not the H3/H4 tetramer separates into dimers (Tagami et al., 2004) during fork passage, or is it inherited as a tetramer (Xu et al., 2010). Mattiroli et al. (2017) provided further insights into the intermediate steps of H3/H4 deposition by CAF1. However, speculations about preferential tetramer separation based on the chromatin context or the possibility that parental dimers are reunited into a tetramer on a daughter strands (Groth et al., 2007) remain unresolved. The model for deposition of newly synthesized H3/H4 dimers involves binding of Asf1 to H3/H4 dimers in the cytoplasm followed by transport to the nucleus. Asf1 binds dimers at their tetramerization interface, thus preventing premature tetramer formation. In the nucleus, H3/H4 dimers are handed over to CAF1. However, the mechanism of inheritance of parental H3/H4 dimers remains elusive. Huang et al. (2015) showed

the first structure of a co-chaperone complex and proposed a model in which MCM2 binds the evicted parental H3/H4 tetramer, followed by binding of Asf1, which disrupts the tetramer by evicting one of the H3/H4 dimers and ultimately forming a co-chaperone complex MCM2-H3-H4-Asf1. As Asf1 on its own is not able to disrupt H3/H4 tetramer-DNA contact (Donham et al., 2011), there is space for speculations about potential contributions of other chaperones in tetrasome destabilization, beyond MCM2.

In contrast to H3/H4, the inheritance of H2A/H2B dimers is less clear. It is known that Nap1 delivers H2A/H2B dimers into the nucleus and is involved in their deposition (Ito et al., 1996). Polymerase α (Pol α), which is vital for initiation of DNA replication by synthetizing short RNA primers on the leading and lagging strand, has a specific H2A/H2B histone-binding motif (Evrin et al., 2018). Pol α was also shown to interact with FACT (Wittmeyer and Formosa, 1997) which is believed to be involved in H2A/H2B deposition as well (Mao et al., 2016; Orphanides et al., 1999; Ransom et al., 2010; Wittmeyer and Formosa, 1997). In addition, FACT was recently shown to bind to the H3/H4 complex, indicating that FACT can function in H3/H4 depositions as well (Liu et al., 2020; Tsunaka et al., 2016; Wang et al., 2018). However, the importance of these interactions and whether histones are handed downstream of the replication fork by FACT remain unknown.

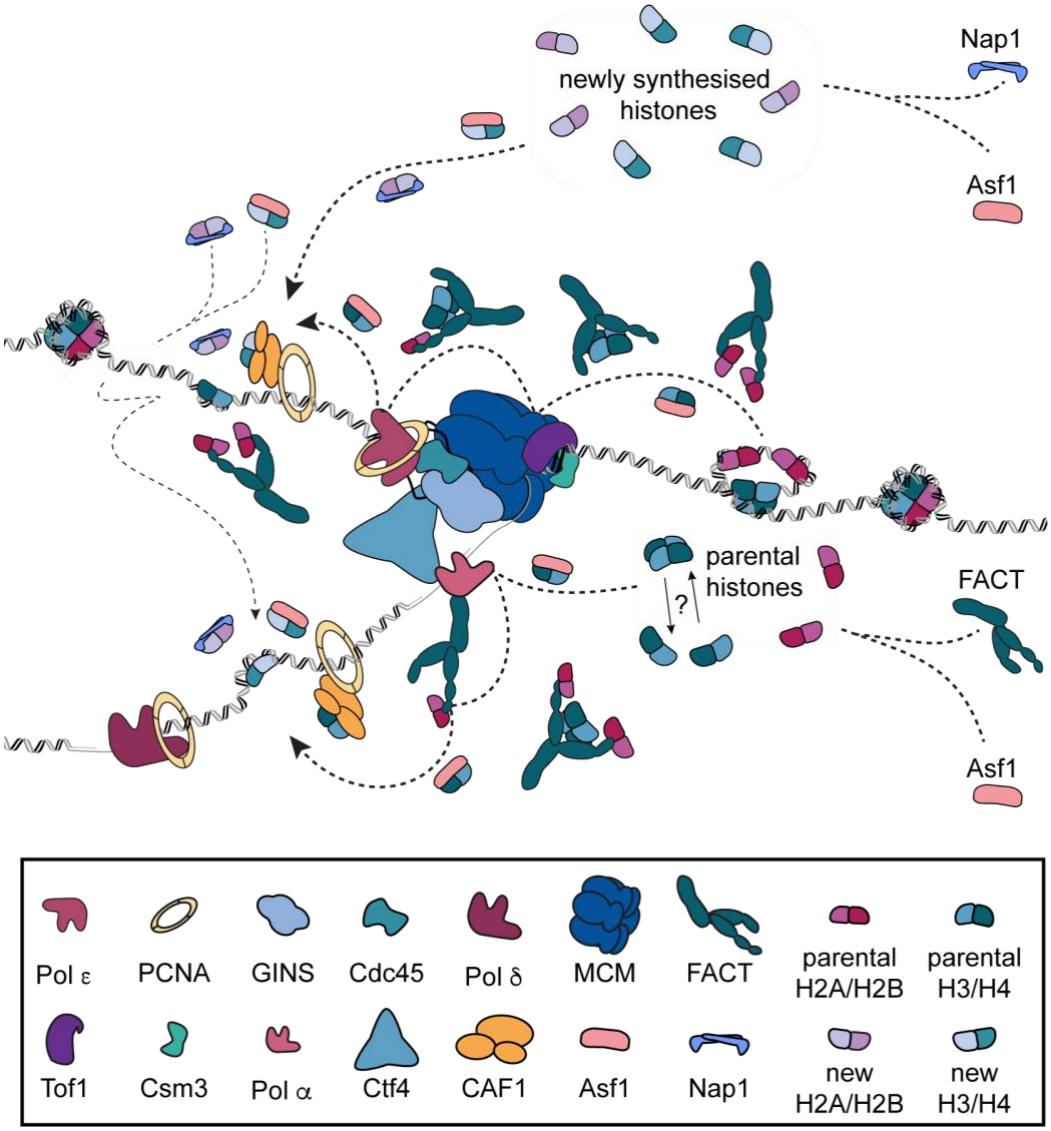

Figure 1.6. Histone shuffle at the replication fork.
Illustration of the complex network of events leading to re-establishment of *de novo* chromatin behind the replication fork. Parental histones, upon disruption of parental nucleosomes into two H2A/H2B dimers and an $[H3\text{-}H4]_2$ tetramer, or two H3/H4 dimers, are transferred to the new DNA strands by the action of histone chaperones, presumably FACT and Asf1, among others. FACT might hand off histones directly to the lagging strand through its interaction with Pol α. A similar scenario might take place on the leading strand through FACT interactions with other replisome factor(s). The newly synthetized histones are imported into the cell nucleus as dimers in a complex with their chaperones: Nap1-H2A/H2B and Asf1-H3/H4, and are directed towards the site of incorporation, where Asf1 hands over the H3/H4 dimer to CAF1. The arrows depict the histone route with potential 'touch-downs' – known interacting sites between replisome factors and histones.

1.5. The facilitates chromatin transactions (FACT)

The facilitates chromatin transactions (FACT) complex is an essential and highly conserved histone chaperone, first discovered as a vital factor for promotion of elongation by RNA Pol II (Orphanides et al., 1999). In addition to transcription, FACT was also shown to play important roles in DNA replication and repair (Formosa, 2012; Ho et al., 2002; Mason and Struhl, 2003; Tan et al., 2006). Some of the characterized roles of FACT include repression of transcriptional initiation and preservation of histone modifications (Duina, 2011; Holla et al., 2020; Jamai et al., 2009; Jeronimo et al., 2019), together with facilitating the incorporation of CENP-A for establishment of centromeric chromatin (Chen et al., 2015; Deyter and Biggins, 2014; Okada et al., 2009; Prendergast et al., 2016). Further, FACT has also been implicated in nucleosome destabilization during DNA and RNA polymerase advancement as well as nucleosome eviction (Belotserkovskaya et al., 2003; Chen et al., 2018a; Hsieh et al., 2013; Schwabish and Struhl, 2004; Shakya et al., 2015; Takahata et al., 2009). In addition, there are hints about a possible role of FACT in histone deposition after replication fork passage (Kurat et al., 2017; Mao et al., 2016; Schwabish and Struhl, 2004).

Reason behind such contrasting roles of FACT lies in its ability to bind to nucleosomes and disrupt the intra- and inter-nucleosome contacts in an ATP-independent manner while preserving all of its elements. This ability of FACT activity was termed ‘nucleosome reorganization’ (Formosa, 2012; Winkler et al., 2011). Nucleosome reorganization indeed contributes to accessibility of the DNA, supporting the role of FACT in nucleosome destabilization. However, it has been shown that reorganization by FACT is a reversible process (Chen et al., 2018a; Wang et al., 2018), which supports the FACT involvement in histone deposition. Therefore, FACT can facilitate both nucleosome assembly and disassembly depending on the context. During DNA replication FACT might be involved in destabilization of parental nucleosomes ahead of the replication fork, histone eviction and/or handover, as well as nucleosome assembly behind the fork, establishing *de novo* chromatin.

FACT found in *S. cerevisiae* (yFACT) consists of a heterodimer of Spt16 and Pob3, supported by an HMGB-like, DNA-binding protein Nhp6 (Brewster et al., 2001; Formosa et al., 2001). This arrangement is distinct among eukaryotes, as most lack Nhp6 and instead have an HMGB-fused to Pob3 to form SSRP1 (further referenced

as hFACT) (Brewster et al., 2001; Orphanides et al., 1999; Wittmeyer and Formosa, 1997). Both subunits of FACT have a unique modular organization revealed by the individual domain structures connected by unstructured, flexible linkers (O'Donnell et al., 2004) (Figure 1.7). A shared characteristic among domains is the pleckstrin-homology motif, which forms binding modules for protein ligands (Blomberg et al., 1999). An exception is the N-domain of the Spt16 subunit, which shares a homology with bacterial aminopeptidases, though without any peptidase activity as active site residues are not preserved (Stuwe et al., 2008; VanDemark et al., 2008). Therefore, this domain might be involved in an interaction with unstructured protein regions resembling peptides, such as histone tails, which are the substrate of the aminopeptidases (Gonzales and Robert Baudouy, 1996). The diversity in the basic fold of FACT domains might indicate the ability to bind multiple diverse substrates, maybe even simultaneously.

Extensive efforts have been made both *in vivo* and *in vitro* to map interactions of FACT with the nucleosome. The crystal structures revealed Spt16 and Pob3 dimerize through their middle domains (Keller and Lu, 2002; O'Donnell et al., 2004), which recognize H3/H4 (Kemble et al., 2013) and anchor FACT to nucleosomes (Kemble et al., 2013; Liu et al., 2020). Biochemical assays showed that both subunits of FACT have multiple domains involved in histone binding (Cucinotta et al., 2019; McCullough et al., 2018; Tsunaka et al., 2016; Winkler et al., 2011). Together with the crystal structures of the individual domains bound to histone dimers (Hondele and Ladurner, 2013; Kemble et al., 2015; Tsunaka et al., 2016), these findings show that FACT is able to bind to H2A/H2B dimers as well as the H3/H4 tetramer, potentially at the same time. The extended C-terminal tails of Spt16 and Pob3 both contain histone recognition motifs, a short stretch of around 25 amino acids named the minimal binding domain (MBD), that allow for two H2A/H2B dimers to be bound simultaneously (Kemble et al., 2015). Initially, it was proposed that hFACT destabilizes the nucleosome by eviction of H2A/H2B dimers (Belotserkovskaya et al., 2003). However, this model has been challenged by studies with yFACT (Rhoades et al., 2004; Xin et al., 2009) showing that the displacement of H2A/H2B dimers is a rare event, which may be an indirect consequence of an overall destabilization of the nucleosome by FACT. Moreover, single-molecule FRET studies of FACT mechanism suggest nucleosome destabilization is initiated by DNA uncoiling, with FACT causing unwrapping of around 70% of DNA within a nucleosome, without histone eviction (Valieva et al., 2016). Recently, for the first time the details of FACT engagement with the nucleosome were resolved by

cryo-EM, providing the unprecedent insights into hFACT interaction with the nucleosome as well as coordination of FACT domains (Liu et al., 2020). This structure consolidates many of the previously resolved structures of the individual domains and proposed models of FACT engagement with the nucleosome (Figure 1.7). Confirming the previous findings, the C-terminal tail of Spt16 interacts with H2A/H2B dimer, stretching through the entirety of the dimer-DNA interface thus preventing reassociation of DNA and histones. Surprisingly, a large DNA-binding surface was identified, responsible for extensive interactions between FACT and nucleosomal DNA.

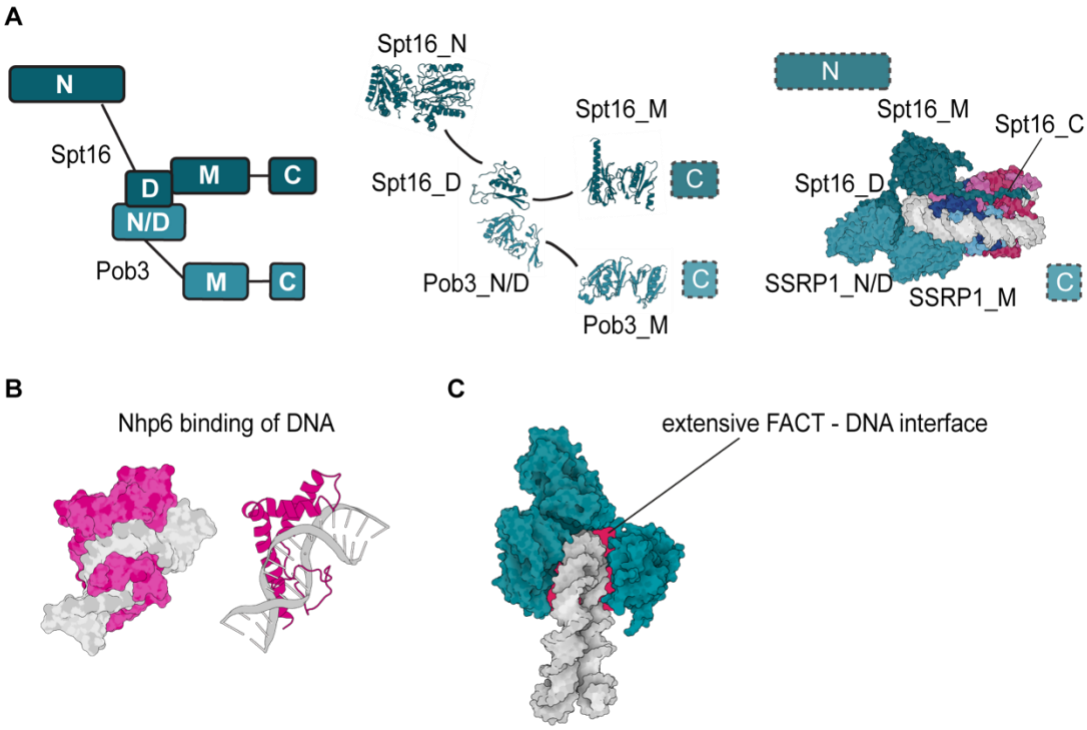

Figure 1.7. Organization of FACT.
(A) Left: Schematics of modular domain organization of FACT. Middle: Crystal structures of the individual FACT domains as follows: Spt16_N (PDB 3BIQ), Spt16_M (PDB 4IOY), Spt16_D-Pob3_N/D (PDB 4KHB), Pob3_M (PDB 2GCL). Right: Cryo-EM structure of the hFACT in complex with a nucleosome (PDB 6UPK). (B) Crystal structure of Nhp6 bound to DNA (PDB 1J5N). (C) Cryo-EM structure of the hFACT (PDB 6UPK) showing the extensive DNA binding interface in red.

However, few questions still remain unanswered. Namely, the mode of action of the HMGB1 domain in higher eukaryotes, and Nhp6 in yeast, is not clear. Nhp6, as well as other HMGB1 proteins, is a DNA binding protein that recognizes the DNA minor groove in a sequence-independent manner. Upon binding, the DNA gets extensively bent (Allain et al., 1999; Sarangi et al., 2019), and Nhp6 was shown to have around 20-fold greater affinity for the nucleosomal compared to the linker DNA (McCauley

et al., 2019). yFACT, which does not bind DNA or nucleosomes on its own, in the presence of Nhp6 can form a nucleosome-Nhp6-FACT complex. Interestingly, it has been shown that Nhp6 does not stably interact with yFACT (Formosa et al., 2001). Taken together, Nhp6 might support formation of FACT-nucleosome complex by DNA kinking, thus exposing histone surfaces which can then be recognized and captured by FACT. Further, from the cryo-EM structure, the middle and terminal domains of the SSRP1 subunit, together with the N-domain of Spt16, are not visible. It will be interesting to see whether and how are these domains are involved in interactions with the nucleosome. Finally, the dynamic conformational rearrangements that ensure coordination of flexibly tethered elements by FACT to either facilitate assembly or promote disassembly of nucleosomes have not been established.

1.6. Research goals and scope of this thesis

Elucidating the dynamics of nucleosomes in front of the replication fork, together with the inheritance of parental histones, is not only essential for understanding the maintenance of chromatin structure and preservation of epigenetic information, it will also reveal how efficient replication of chromatin is achieved. To provide a more complete picture of this complex process, in this study the dynamic events that underlie nucleosome processing ahead of the replication fork, with the main focus on the histone chaperone FACT are investigated. Extensive biochemical and biophysical characterization has demonstrated that FACT restructures nucleosomes (Chen et al., 2018b; Valieva et al., 2016), but the importance of this activity in the context of chromatin replication has not been established. Similarly, whether a minimal region exists within FACT that is sufficient to facilitate chromatin replication has not been explored. A complex network of static and dynamic interactions coordinate histone removal and deposition during replication (Miller and Costa, 2017). The limited spatial and temporal resolution of traditional approaches has posed challenges for studying these dynamic events. As a consequence, the location or locations where FACT participates and how FACT dynamically reorganizes nucleosomes in the context of other replication factors is not well understood.

To study how FACT reorganizes nucleosomes and its role in chromatin replication, I used single-molecule FRET to visualize dynamic changes in nucleosomal DNA during engagement by FACT. Consistent with past reports (Valieva et al., 2016) working with *Xenopus* nucleosomes, large scale structural changes and reorganization of *S. cerevisiae* nucleosomes upon addition of yFACT are observed. A systematic study of FACT truncations revealed that the C-terminal H2A/H2B binding elements of Spt16 and Pob3 are essential for reorganization. However, these binding elements alone retain no activity, demonstrating that nucleosome reorganization depends on the coordinated engagement of multiple, connected interacting regions. Surprisingly, the N-domain of Spt16 was shown not to be involved in the interaction of FACT with the nucleosome. To clarify the importance of these interactions during replication, I identified potential FACT binding sites guided by structures of replisome subcomplexes and investigated the influence of these factors on FACT activity. Combined with systematic pulldowns, these studies revealed a new interaction between FACT and the fork protection complex, more specifically, the N-terminus of Spt16 was found to bind the C-terminus of Tof1,

positioning FACT for engagement of parental nucleosomes. Further investigation revealed that the interaction motif of FACT and Tof1 is adjacent to the main interaction site between Tof1 and Top1. Finally, fully *in vitro* reconstituted chromatin replication assays confirmed the importance of these interactions for efficient fork progression through chromatin. Taken together, the results presented in this thesis provide mechanistic insight into how FACT reorganizes nucleosomes and reveal the network of interactions underlying the first critical steps in the histone processing pathway during replication.

Chapter 2: Principles of fluorescence

In the middle of 16th century, a Spanish physician, Nicolas Monardes, was working with an infusion of a Mexican medicinal wood when he noticed its peculiar blue hue. This is the first known reported observation of fluorescence (Monardes, 1565), a type of photoluminescence - phenomenon describing physical effects emerging upon interaction of light with matter. The basic process of fluorescence can be separated into two main steps, excitation and emission of an absorbing molecule (fluorophore), which affect its electronic state. The energy of a molecule that is not being excited by light presents its ground electronic state, S_0 (Figure 2.1). Excitation involves the absorption of light energy by a fluorophore, where all the energy of individual photons is transferred to the fluorophore, resulting in fluorophore excitation and a shift from its electronic ground state S_0 to a higher energetic singlet state S_2. When the absorbed energy is bigger than a minimum energy required for fluorescence, i.e. the transition of an electron from fluorophore's ground state into lowest excited singlet state (from S_0 to S_1), the fluorophore moves into an even higher electronic orbital (S_2), accompanied by a change in vibration and rotation. The transition between these different electronic states makes it possible to excite a molecule by a range of wavelengths. Electronically excited states are unstable and electrons have to drop back to the ground state. Excited electrons transition between electronic states (e.g., from S_2 to S_1) by internal conversion. At the same time, some of the energy is also released by vibrational relaxation, resulting in the lowest energy in the level S_1. Following, fluorescence occurs as the electron returns from S_1 to the ground state S_0 in one step by releasing the excitation energy in the form of a photon. Another scenario includes intersystem crossing in which electrons in the excited singlet state undergo a spin conversion to the triplet state in a 'forbidden transition'. The triplet state energy levels overlap with the lowest energy level in S_1, permissive of the intersystem crossing followed by internal conversion to the lowest energy of T_1. The transition from a triplet state back to the singlet ground state is comparably a long process, as this transition requires the triplet electron to again undergo an unlikely forbidden transition. Finally, energy is relaxed from T_1 state by emission of a photon in a process called phosphorescence.

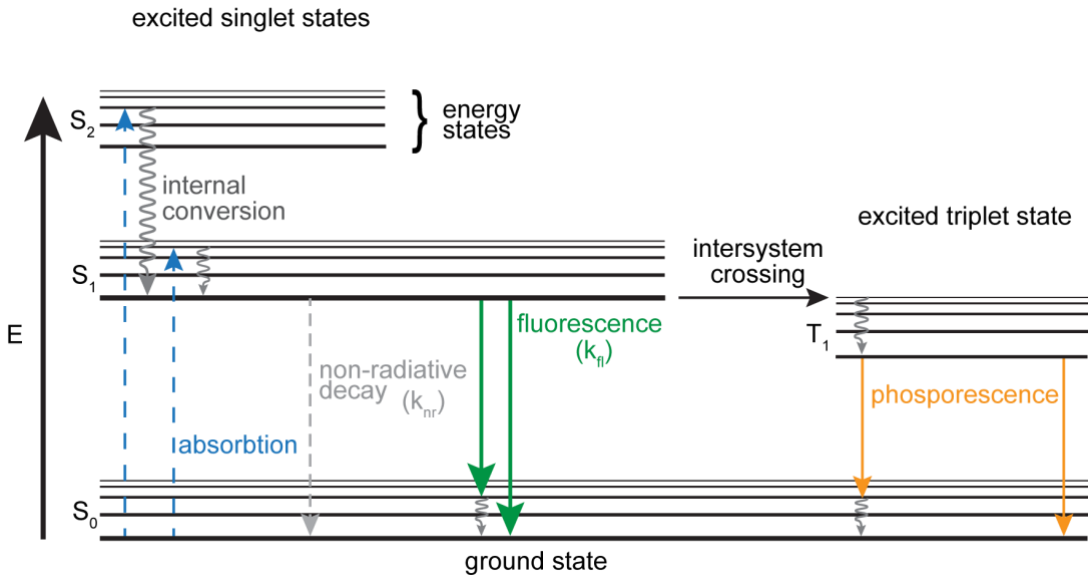

Figure 2.1. Jablonski diagram of photoluminescence.
The y axis is energy E, which increases from the bottom (ground state, S_0) to the top (singlet and triplet excited states or S_1, S_2 and T_1). Horizontal lines represent the energy levels of each electronic state. Absorption of a photon promotes a molecule from its ground state to a higher state (blue arrows). Some of the energy is released by internal conversion (grey arrows), followed by fluorescence (green arrows). Alternatively, a forbidden change in the spin state occurs from the S_1 to the T_1 state resulting in intersystem crossing and phosphorescence (orange arrows). Excitation rate, k_{ex}, non-radiative decay rate k_{nr}, intrinsic fluorescence emission rate k_{fl}.

Due to the loss of energy while reaching the lowest energy level S_1, the emitted photon has less energy than the absorbed photon. As it is known that the light of a short wavelength (toward the blue) has higher energy than one with a long wavelength (toward the red), the light with an increased wavelength and lower energy is emitted by the fluorophore compared to the absorbed (excitation) light. This shift was first described by George Stokes (Stokes, 1852) and later became known as the Stokes' shift. As the transitions between the electronic states are the same during absorbance and emission, the emitted spectrum, albeit shifted to longer wavelengths, mirrors the curve of the absorption spectrum (Figure 2.2).

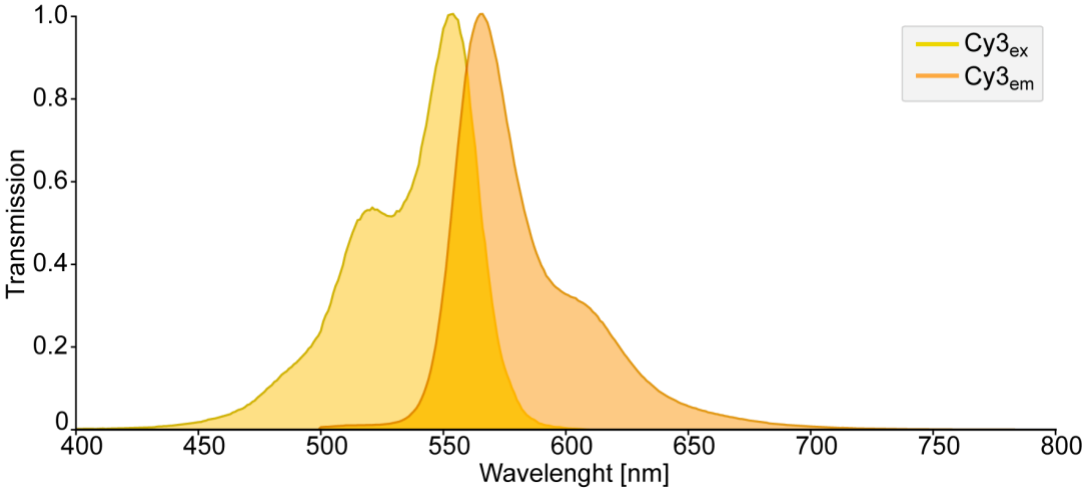

Figure 2.2. The excitation and emission spectra of Cy3.
Cy3 has an excitation peak at 555 nm (yellow) and an emission peak at 569 nm (orange). Data from FPbase (Lambert, 2019).

In addition to absorbance and emission spectra of a fluorophore, other important parameters that characterize a fluorophore are molar extinction coefficient ε, fluorescence lifetime τ and quantum yield ϕ. The molar extinction coefficient ε, corresponds to the probability of a fluorophore absorbing a photon as light passes through a solution with the fluorophore, and is specified for the wavelength at which the absorption maximum occurs. The fluorescence lifetime τ is a measure of how long a fluorophore spends in the excited state before returning to the ground state either by photon emission, described by the fluorescence emission rate k_{fl}, or by non-radiative processes such as internal conversion, intersystem crossing, and Förster resonance energy transfer, described by the non-radiative decay rate k_{nr} :

$$\tau = \frac{1}{(k_{fl} + k_{nr})} \tag{2.1}$$

the quantum yield ϕ is the efficiency of a fluorophore, expressed as the ratio of photons emitted after the excitation to photons absorbed:

$$\phi = \frac{k_{fl}}{(k_{fl} + k_{nr})} \tag{2.2}$$

2.1. Förster resonance energy transfer (FRET)

As the story goes, in the middle of the 20th century, the curiosity of Theodor Förster, a physical chemist, was sparked by the process of photosynthesis due to the extremely efficient capture of the light energy, which should not be possible if this energy would reflect only photons captured by the small reaction centers in the chlorophyl molecules. Förster thought that the energy captured by the leaf surface must somehow travel through the leaf into the reaction centers, resulting in the high efficiency of the photosynthesis. Being familiar with the works of Jean Baptiste Perrin on energy transfer, Förster postulated that the energy travels by rapid bouncing between the molecules. He presented his quantitative theory of non-radiative energy transfer in 1948 (Förster, 1948). By this seminal contribution, Förster laid foundations to new field of science today known as Förster Resonance Energy Transfer (FRET).

Resonance energy transfer is a process that occurs when an excited fluorophore, the donor, is in a close proximity (up to 10 nm) of another molecule, the acceptor, under the condition when the emission spectrum of the donor overlaps with the absorption spectrum of the acceptor. This energy transfer does not include emission of a photon by the donor, but rather the donor and acceptor are coupled by a dipole-dipole interaction. The acceptor that absorbed the energy of the donor is now in the excited state itself, and if the acceptor is another fluorophore, upon energy relaxation it will emit a photon (Figure 2.3), similar to a single excited fluorophore as described above.

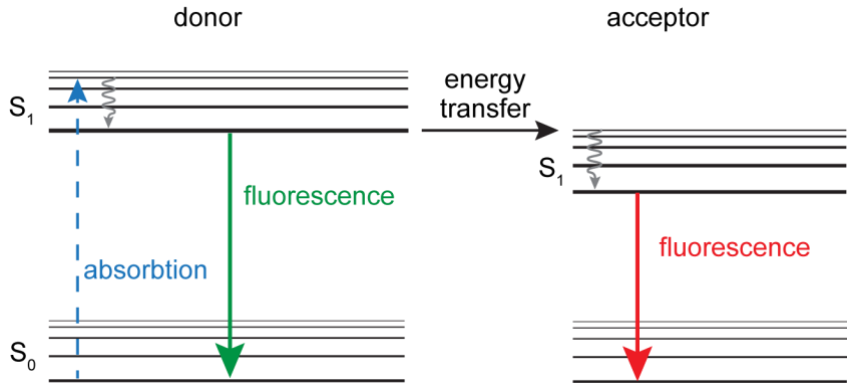

Figure 2.3. Jablonski diagram of FRET.
Absorption of a photon promotes a donor from its ground state to a higher state (blue arrow). Some of the energy is released by internal conversion (grey arrow), followed by fluorescence (green arrow). When acceptor molecule is in the vicinity, energy tranters occurs from the donor to the acceptor, which releases the absorbed energy by fluorescence (red arrow).

As the resonance energy transfer is strongly dependent on the distance between the donor and acceptor, FRET can be used as a molecular ruler (Clegg, 2009). In addition to the distance, the energy transfer is dependent also on the extent of the spectral overlap between donor and acceptor, described by Förster radius. These factors determine the rate of energy transfer k_T:

$$kT = \frac{1}{\tau_{\boldsymbol{D}(\mathbf{0})}}\left(\frac{R_0}{R}\right)^6 \tag{2.3}$$

where $\tau_{D(0)}$ is the fluorescence lifetime of the donor in absence of the acceptor. R_0 is a Förster radius for a given donor-acceptor pair, defined as:

$$\mathrm{R_0} = \frac{9000(\ln 10)\kappa^2\phi_\mathrm{D}}{128\pi^5 \mathrm{N_A}\,\eta^4} J\,(\lambda) \tag{2.4}$$

Förster radius corresponds to the inter-dye distance that results in an energy transfer efficiency of 50 % (Figure 2.4). κ^2 is a geometric factor that depends on the relative orientation of the acceptor and donor transition dipoles, ϕ_D is the quantum yield of the donor, N_A is Avogadro's Number, η is the refractive index of the medium, and $J(\lambda)$ is the overlap integral of the absorption spectrum of acceptor and the emission spectrum of donor. The value of κ^2 depends on the orientation between the acceptor dipole and the donor dipole, which are constantly fluctuating, thus the actual value of κ^2 is an ensemble average, generally approximated to κ^2 =2/3 (van der Meer, 2002). In turn, the efficiency of the energy transfer E is calculated as the ratio of the transfer rate to the total decay rate of the donor in presence of the acceptor:

$$E = \frac{k_T}{k_T + \frac{1}{\tau_D}} \tag{2.5}$$

Substituting in the rate of energy transfer, k_T, simplifies the equation:

$$E = \frac{R_0^6}{R_0^6 + R^6} = \frac{1}{1 + \left(\frac{R}{R_0}\right)^6} \tag{2.6}$$

Finally, from FRET efficiency the intermolecular distance between donor and acceptor *R* can be calculated using the Förster Radius (R_0):

$$R = R_0 \left(\frac{1}{E} - 1\right)^{\frac{1}{6}} \tag{2.7}$$

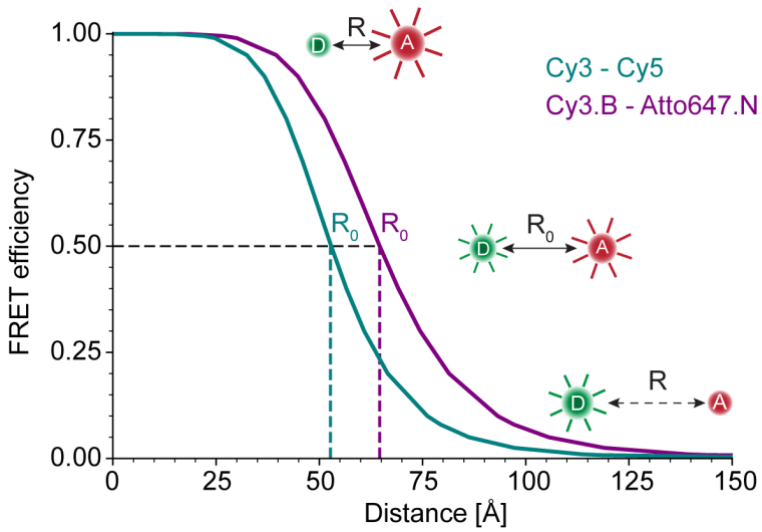

Figure 2.4. FRET efficiency as a function of distance.
When the dyes are in close proximity the FRET efficiency is high, and with increasing distance the FRET efficiency drops. The Förster Radius (R_0) is defined as the donor-acceptor distance at 50% of energy transfer. Distance-dependent FRET efficiencies are shown for two dye pairs with different Förster radii, R0 for Cy3 - Cy5 is 52.65 Å (teal), and for Cy3.B - Atto647N is 64.63 Å (purple). Data from FPbase (Lambert, 2019).

2.2. Alternating-laser excitation (ALEX) single-molecule FRET

Alternating-laser excitation (ALEX) is an imaging technique based on rapid switching between lasers directly exciting donor and acceptor fluorophores. The imaging approach described in this thesis is ALEX single-molecule FRET developed on a confocal microscope with a freely diffusing sample.

In ALEX, the alternating frequency of excitation needs to be high enough to capture the same labelled molecule multiple times during its milliseconds long diffusion period across the confocal volume. The first laser is used to excite the donor directly, and the acceptor indirectly, given it is in the FRET range. In turn, the second laser excites the acceptor directly, specifying its maximum fluorescent intensity (Figure 2.5, top panel). In order to achieve single-molecule resolution, the excitation is constricted to only a few femtolitres of a sample by focusing the laser light, as it passes through an objective, on a micrometer-sized pinhole. The pinhole acts as an aperture and cuts out background (extrafocal) signal, allowing only the sample emission coming from the focal plane to pass towards a detector. Following, emission is split between donor and an acceptor detection channels based on the spectral properties. Another important factor for single-molecule resolution is the concentration of the fluorophores in the sample, which is kept in the picomolar range. The low concentration and diffraction-limited focal volume allow for the detection of fluorescent bursts as each fluorophore passes through the observation volume. A single burst is identified based on a given threshold value, which refers to a number of detected photons within a certain time window, spanning over a continuous set of alternating laser pulses. If all the criteria are satisfied, each individual fluorophore will be detected as a single burst. Donor and acceptor bursts shown in green and red, respectively. If a sample is labelled with both a donor and acceptor fluorophore, a FRET signal is detected in the acceptor channel upon donor excitation, shown in yellow (Figure 2.5, bottom panel).

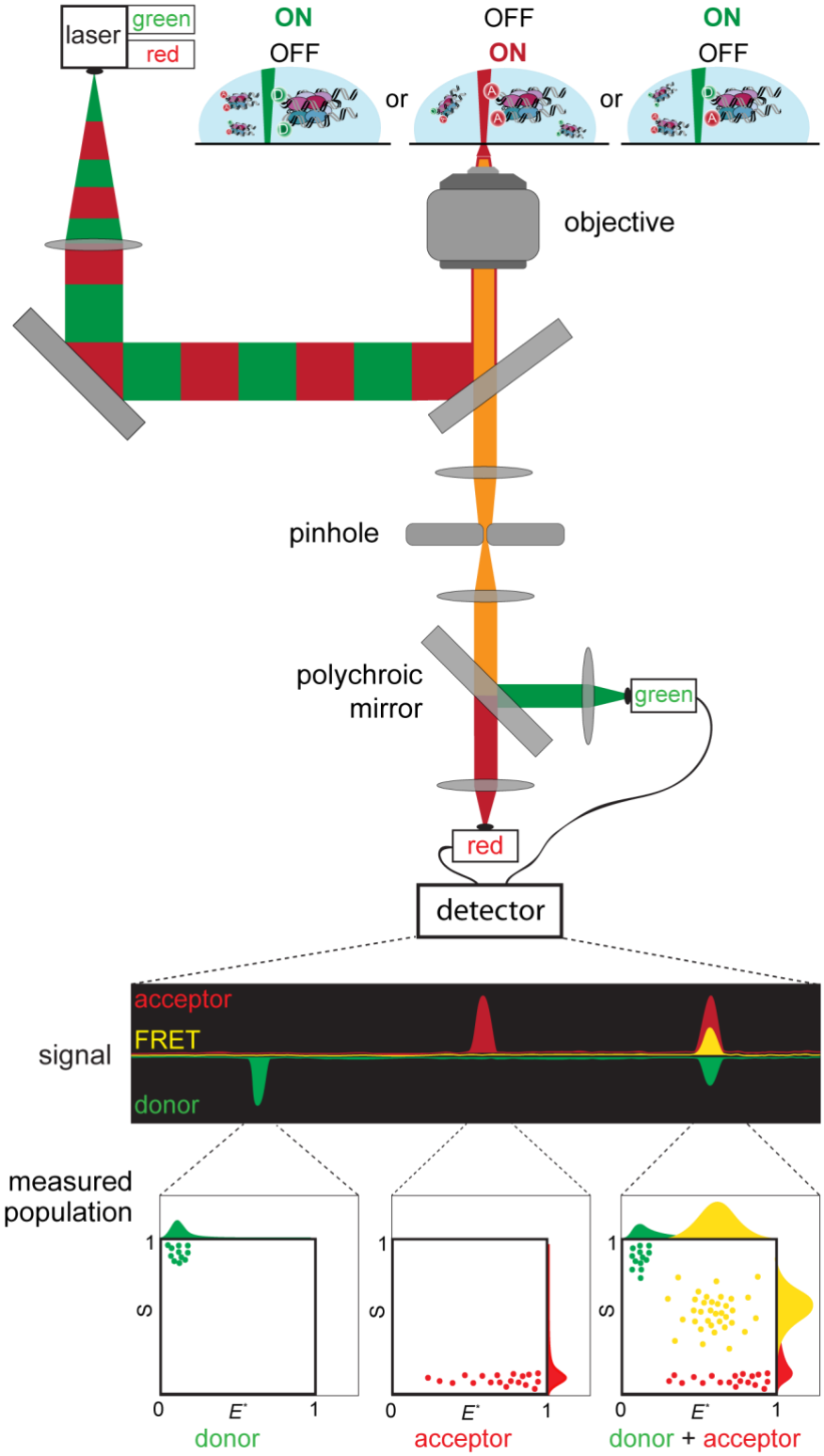

Figure 2.5. ALEX microscopy set-up.
A schematic representation of confocal setup used in this work, with three different scenarios at the confocal spot (top) and the subsequent fluorescent burst detection (bottom). The excitation is generated by quick pulses of green and red laser, which are collimated as they pass through the lens to a polychroic mirror, reflecting the light onto an objective of high numerical aperture, creating a diffraction limited excitation spot. Fluorescence from the sample travels back through the objective, and after passing through a pinhole which cuts out background signal, it is split into a green and a red detection channel.

The detected bursts are further used to determine FRET efficiency, reporting on the energy transfer from donor to acceptor, based on the measured fluorescence intensities of donor ($f_{D_{ex}}^{D_{em}}$) and acceptor ($f_{D_{ex}}^{A_{em}}$) upon donor excitation. These fluorescent intensities are used to calculate apparent FRET (E^*), a setup-dependent value reporting on interdye separation and distance changes:

$$E^* = \frac{f_{D_{ex}}^{A_{em}}}{f_{D_{ex}}^{D_{em}} + f_{D_{ex}}^{A_{em}}} \tag{2.8}$$

It is important to note that apparent FRET reports on the relative distant changes between the fluorophores, and not the absolute distance. This is due to the fact that the photon counts used in the calculations are raw data, not yet corrected for background, detection efficiencies of the dyes and spectral cross-talk. Spectral properties between fluorophores can vary greatly as each fluorophore is defined by particular spectral characteristics, with distinct excitation and emission spectra (Figure 2.6). These spectra between the fluorophores overlap to different extents, resulting in capturing some of the fluorescence in the wrong channel, known as spectral cross-talk. As a consequence of detecting donor emission in the acceptor emission channel, it might not possible to differentiate between e.g. donor only and low-FRET species.

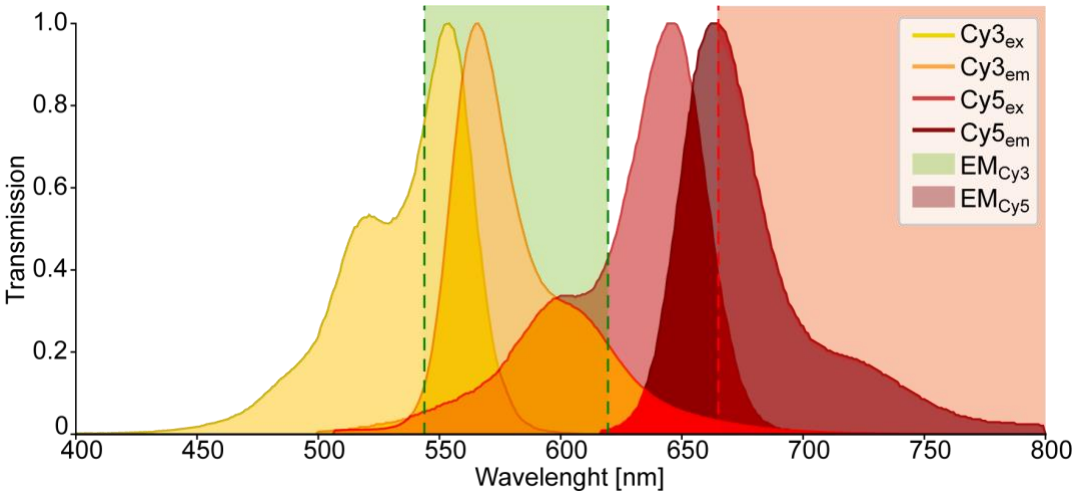

Figure 2.6. Spectral properties of FRET pair Cy3 and Cy5.
Upon the excitation of Cy3 (yellow), energy transfer takes place exciting Cy5 (light red), resulting in Cy5 emission (dark red). Spectral cross-talk happens as some of Cy3 excitation (yellow) results in Cy3 emission (orange), which in turn overlaps with Cy5 emission spectra. To minimize the crosstalk, emission filters are used, shown in green (filtering Cy3 emission), and red (filtering Cy5 emission). Data from FPbase (Lambert, 2019).

ALEX offers an elegant solution address spectral-crosstalk by using direct excitation of the acceptor. By quick excitation pulses of both, donor and acceptor, in addition to fluorescence intensities of donor ($f_{D_{ex}}^{D_{em}}$) and acceptor ($f_{D_{ex}}^{A_{em}}$) upon donor excitation, fluorescence intensities of acceptor upon acceptor excitation ($f_{A_{ex}}^{A_{em}}$) are recorded. These three parameters capture the total fluorescence of a sample and are used to calculate the stoichiometry ratio (S^{raw}), which enables separating populations based on their chromaticity.

$$S^{raw} = \frac{(f_{D_{ex}}^{D_{em}} + f_{D_{ex}}^{A_{em}})}{(f_{D_{ex}}^{D_{em}} + f_{D_{ex}}^{A_{em}} + f_{A_{ex}}^{A_{em}})} \tag{2.9}$$

Each burst in ALEX is therefore described not only by a FRET value, but also with a stoichiometry. Plotting FRET and stoichiometry values in a 2D histogram enables resolving specific populations, which might overlap in 1D histogram. For example, molecules labelled with only a donor fluorophore will center around coordinates $E^* \approx 0$ and $S^{raw} \approx 1$ (Figure 2.5, bottom left panel, green). In contrast, acceptor-only molecules will cluster around low $S^{raw} \approx 0$ (Figure 2.5, bottom middle panel, red). Molecules labelled with donor and acceptor fluorophores will settle in the intermediate stoichiometry range $S^{raw} \approx 0.5$ based on their E^* (Figure 2.5, bottom right panel, yellow).

Chapter 3: Material and methods

3.1. Protein purification

3.1.1. Histone octamer purification

S. cerevisiae histones were codon optimized for the bacterial expression and cloned into pETDuet™ and pCDFDuet™ vectors (#71146, #71340, Novagen). *E. coli* BL21(DE3) codon plus RIL (Agilent) were co-transformed with pETDuet_H2A-H2B and pCDF_H3 -H4 and grown in ZYP-5052 auto-induction medium at 37 °C up to OD_{600} = 0.8. The temperature was lowered to 18 °C and expression continued overnight. All subsequent purification steps were performed at 4 °C. Cells were harvested by centrifugation (4000 x g, 15 min), resuspended in buffer A (20 mM HEPES-NaOH, pH 7.6, 10 % (v/v) glycerol, 1 mM DTT) + 800 mM NaCl, 1 mM EDTA, supplemented with 1× protease inhibitor cocktail and lysed by sonication. The cell lysate was cleared by centrifugation (23666 x g, 45 min) and applied to two HiTrap Heparin HP 5 ml columns equilibrated in buffer A + 800 mM NaCl. The columns were washed with 10 CV buffer A + 800 mM NaCl, 1 mM EDTA, and histone octamers were eluted on an 800 mM – 2 M NaCl gradient. Peak fractions were pooled, spin concentrated with a MWCO 10000 Amicon Ultra Centrifugal Filter unit and applied to a Superdex 200 increase 10/300 gel filtration column equilibrated in buffer A + 2 M NaCl and 1 mM EDTA. Fluorescently labeled histones were generated using quick-change mutagenesis, expressed and purified in a similar manner with the following differences: Peak fractions from HiTrap Heparin HP were applied on a HiPrep 26/10 Desalting column to remove DTT. Immediately afterward, DyLight™ 650 Maleimide (Thermofisher) dye was added in a great excess. After the incubation, the labelling reaction was quenched with addition of excess DTT. Next, labelled histone octamers were run on Superdex 200 increase 10/300 gel filtration column to remove excess dyes and other contaminates. Peak fractions containing histone octamers were pooled, spin concentrated, frozen in aliquots in liquid N_2 and stored at -80 °C. This procedure was performed independently for histone positions H2A_46, H2B_125, H3_135 and H4_83. Nucleosome reconstitution was performed in an identical manner to wild type histones as described below.

3.1.2. FACT purification

S. cerevisiae FACT subunits, Spt16 and Pob3 (ScCD00751519 and ScCD00751520, DNASU), and truncations, were cloned into 12-Ade-B and 12-Trp-U vectors (a kind gift from S. Gradia, UC Berkeley, Addgene plasmids #48298 and #48303) with standard genetic procedures. GST-tagged Pob3 was cloned into 12-Trp-U vector. Plasmids were co-transformed into yeast strain yBS2, and precultures were grown in synthetic defined medium supplemented with 2 % (v/v) raffinose, w/o adenine and tryptophan, at 30 °C. The following day, 12 l YP supplemented with 2 % (v/v) raffinose was inoculated with the precultures, grown at 30 °C up to an OD_{600} ≈ 1, induced by addition of 2 % (v/v) galactose and incubated overnight at 18 °C. Cells were harvested by centrifugation (4000 x g, 15 min), washed once with cold 1 M sorbitol, 25mM HEPES-NaOH, pH 7.6, and resuspended in 1 cell volume of buffer A supplemented with 1× protease inhibitor cocktail and frozen dropwise in liquid N_2. Frozen cells were lysed in a SamplePrep Freezer/Mill and subsequently mixed with 1 cell volume buffer A + 150 mM NaCl, 5 mM imidazole, supplemented with 1 x protease inhibitor cocktail. All subsequent steps were performed at 4 °C. Cell lysate was cleared by ultracentrifugation (290121 x g, 60 min) and applied to two HisTrap HP 5 ml columns equilibrated in buffer A + 150 mM NaCl, 5 mM imidazole. The columns were washed with 15 CV buffer A + 150 mM NaCl, 5 mM imidazole, followed by a 5 CV wash with buffer A + 500 mM NaCl. FACT subunits were eluted using a 5 - 500 mM imidazole step gradient (5, 40 and 100% of buffer A + 500 mM imidazole). Peak fractions were pooled, buffer exchanged to buffer A + 150 mM NaCl, and the His-tag was cleaved by TEV protease overnight at 4 °C. Cleaved protein was purified over HiTrap NiNTA HP 5 ml, and the flowthrough was applied to ENrich™ Q 10 x 100 Column (Bio-Rad) column, equilibrated with buffer A + 150 mM NaCl, 1 mM EDTA. Proteins were eluted using a 150 mM – 1 M NaCl gradient, peak fractions containing Spt16 and Pob3 were pooled, spin concentrated with a MWCO 50000 Amicon Ultra Centrifugal Filter unit, and applied to a Superdex 200 increase 10/300 gel filtration column equilibrated in buffer A + 150 mM NaCl, 1 mM EDTA. Peak fractions containing FACT subunits were pooled, spin concentrated, aliquoted, frozen in liquid N_2 and stored at -80 °C.

The same strategy was used for all FACT constructs, detailed in Table 3.

3.1.3. Tof1 truncations & Csm3 purification

Tof1 and Csm3 were codon optimized for bacterial purification, cloned into a pET GST-His6-TEV vector and transformed in *E. coli* BL21 (DE3) codon plus RIL (Agilent) cells. Cells were grown in ZYP-5052 auto-induction medium at 37 °C up to OD_{600} = 0.8. The temperature was lowered to 18 °C and expression continued overnight. All subsequent purification steps were performed at 4 °C. Cells were harvested by centrifugation (4000 x g, 15 min), resuspended in buffer T (50 mM Tris-HCl, pH 7, 10 % (v/v) glycerol, 1 mM DTT) + 300 mM NaCl, supplemented with 1× protease inhibitor cocktail and lysed by sonication. The cell lysate was cleared by centrifugation (23666 x g, 45 min) and applied to GSTrap HP 5 ml column (GE Healthcare) equilibrated in buffer T + 100 mM NaCl. The column was washed with 20 CV buffer T + 100 mM NaCl, followed by 5 CV wash with buffer T + 1 M NaCl, and buffer T + 100 mM NaCl, 50 mM KCl, 10 mM Mg(OAc)2, 2mM ATP. Protein was eluted in buffer T + 100 mM NaCl, 20 mM reduced glutathione. Peak fractions were pooled and applied on ENrich™ Q 10 x 100 column (Bio-Rad), equilibrated in buffer T (pH 7.5) + 100 mM NaCl. Following the 5 CV wash, protein was eluted with gradient from 100 – 1000 mM NaCl. Peak fractions were spin concentrated, applied on Superdex 200 increase 10/300 gel filtration column (GE Healthcare) equilibrated in buffer T1 (25 mM HEPES, pH 7.5, 200 mM NaCl, 5 % glycerol, 1 mM DTT). Peak fractions containing the protein of interest were pooled, spin concentrated, frozen in aliquots in liquid N_2 and stored at -80 °C.

The same strategy was used for all Tof1 truncations (Tof1_N (1-638 aa), Tof1_M (793-937 aa), Tof1_C (938-1238 aa), Tof1ΔN (639-1238 aa)) and Csm3.

S. cerevisiae Tof1ΔC (1-937 aa) and Csm3 were amplified from genomic template into 12-Ade-B and 12-Trp-U vectors (a kind gift from S. Gradia, UC Berkeley, Addgene plasmids #48298 and #48303, Addgene) following standard genetic procedures. Expression and purification of the complex was done as described above for FACT.

3.1.4. Nhp6 purification

Nhp6 was amplified from yeast genomic DNA into a pET28a (#69864, Novagen), transformed into BL21(DE3) Competent Cells (Novagen), and expressed in ZYP-5052 auto-induction medium at 37 °C up to OD_{600} = 0.8. The temperature was lowered to 18 °C and expression continued overnight. All subsequent purification steps were performed at 4 °C. Cells were harvested by centrifugation (4000 x g, 15 min), resuspended in buffer N6 (20 mM Tris-NaOH, pH 8, 10 % (v/v) glycerol, 1 mM DTT) + 1 M NaCl, 30 mM imidazole, supplemented with 1× protease inhibitor cocktail and lysed by sonication. The cell lysate was cleared by centrifugation (23666 x g, 45 min) and applied to HisTrap HP 5 ml column (GE Healthcare) equilibrated in buffer A + 1 M NaCl. The columns were washed with 15 CV buffer N6 + 1 M NaCl, 30 mM imidazole, and protein was eluted using a 30 – 500 mM imidazole gradient in buffer N6 + 500 mM NaCl. Peak fractions were pooled, buffer exchanged to buffer N6 + 100 mM NaCl, and the His-tag was cleaved by TEV protease overnight at 4 °C. Cleaved protein was purified over HiTrap NiNTA HP 5 ml, the flowthrough was applied to a HP S column. Protein was eluted on a 100 – 1 M NaCl gradient, peak fractions were pooled, spin concentrated with a MWCO 10000 Amicon Ultra Centrifugal Filter unit and applied to Superdex 200 increase 10/300 gel filtration column (GE Healthcare) equilibrated in buffer N6 + 150 mM NaCl. Final peak fractions containing Nhp6 were pooled, spin concentrated, frozen in aliquots in liquid N_2 and stored at -80 °C.

3.1.5. Asf1 purification

E. coli BL21(DE3) codon plus RIL cells were transformed with pSmt3-Asf1 (a kind gift from Remus lab), expressed in ZYP-5052 auto-induction medium at 37 °C up to OD_{600} = 0.8. The temperature was lowered to 18 °C and expression continued overnight. All subsequent purification steps were performed at 4 °C. Cells were harvested by centrifugation (4000 x g, 15 min), resuspended in buffer A + 500 mM NaCl, 30 mM imidazole, supplemented with 1× protease inhibitor cocktail and lysed by sonication. The cell lysate was cleared by centrifugation (23666 x g, 45 min) and applied to two HisTrap HP 5 ml columns equilibrated in buffer A + 500 mM NaCl. Each column was washed with 15 CV buffer A + 500 mM NaCl, 30 mM imidazole, and SUMO-His-Asf1 was eluted using a 30 – 500 mM imidazole gradient. Peak fractions were pooled, and buffer exchanged against buffer A + 100 mM NaCl, followed by Upl1 cleavage. The cleaved tags were separated over a HisTrap HP 5 ml column. The cleaved protein was further purified on ENrich™ Q 10 x 100 Column

(Bio-Rad) column, washed with 15 CV buffer A + 100 mM NaCl, and eluted on an 100 – 500 mM NaCl gradient over 20 CV. Peak fractions were spin concentrated with a MWCO 10000 Amicon Ultra Centrifugal Filter unit, applied on Superdex 200 increase 10/300 gel filtration column (GE Healthcare) equilibrated in buffer A + 100 mM NaCl. Peak fractions containing Asf1 were pooled, spin concentrated, frozen in aliquots in liquid N_2 and stored at -80 °C.

3.1.6. MCM2$_{1-200}$ purification

The N terminal peptide of MCM2$_{1-200}$ was amplified from the yeast genomic sequence, cloned into a pET GST-His6-TEV vector and transformed in *E. coli* BL21(DE3) codon plus RIL cells. Cells were grown in LB medium at 37 °C up to OD_{600} = 0.5, chilled on ice, followed by induction of expression by addition of 1 mM IPTG. Expression proceeded overnight at 15 °C. All subsequent purification steps were performed at 4 °C. Cells were harvested by centrifugation (4000 x g, 15 min), resuspended in buffer M (50 mM Tris-HCl, pH 7.5, 10 % (v/v) glycerol, 1 mM DTT, 1 mM EDTA) + 1 M NaCl, supplemented with 1× protease inhibitor cocktail and lysed by sonication. The cell lysate was cleared by centrifugation (23666 x g, 45 min) and applied to GSTrap HP 5 ml column (GE Healthcare) equilibrated in buffer M + 300 mM NaCl. The column was washed with 15 CV buffer M + 300 mM NaCl, and GST- MCM2$_{1-200}$ was eluted in buffer M + 300 mM NaCl, 10 mM reduced Glutathione. Peak fractions were pooled, and buffer exchanged against buffer M + 100 mM NaCl, followed by TEV cleavage. The cleaved protein was further purified over HisTrap HP 5 ml column. The flowthrough was spin concentrated with a MWCO 10000 Amicon Ultra Centrifugal Filter unit, applied on HiLoad 26/600 Superdex 75 pg (GE Healthcare) column equilibrated in buffer M + 150 mM NaCl. Peak fractions containing MCM2$_{1-200}$ were pooled, spin concentrated, frozen in aliquots in liquid N_2 and stored at -80 °C.

3.1.7. Pol α, GINS, Ctf4, Cdc45, MCM-Cdt1 and Tof1Csm3 purification

Yeast strains and plasmids used for expression of Pol α, Ctf4, GINS, Cdc45, MCM-Ct1 and Tof1-Csm3 were a gift from the Remus lab. The proteins were purified as detailed in Devbhandari and Remus (2020). The plasmid used for expression of GINS was a gift from the Labib lab. GINS complex was purified as described in Yeeles et al. (2015b).

A list of all plasmids and yeast strains used in this study can be found in the Table 10 and Table 11.

3.2. Nucleosome reconstitution

For the nucleosome reconstitution, a template DNA containing the 147 bp 601 Widom sequence was used (pGEM-3z/601 was a gift from Jonathan Widom, Addgene plasmid # 26656) . Fluorescent labels were introduced via PCR with modified primer pairs at positions 35 and 122 with Cy3 and Cy5, or Cy3B and Atto647N, as indicated with asterix (*):
CTGGAGAATCCCGGTGCCGAGGCCGCTCAATTGGT*CGTAGACAGCTCTAG,
and
ACAGGATGTATATATCTGACACGTGCCTGGAGACTA*GGGAGTAATCCCCT.
After PCR, DNA was purified on TSKgel SuperQ-5PW column (Tosoh Bioscience GmbH) equilibrated in 20 mM Tris-HCl, pH 7.5, 1 mM EDTA, and eluted using a 0 – 2 M NaCl gradient. Peak fractions containing DNA were pooled and dialyzed overnight in buffer N (20 mM HEPES, pH 7.6, 10% (v/v) glycerol, 5 mM $MgCl_2$, 1 mM DTT) + 2 M NaCl. The following day, 3 µg of template DNA was mixed with varying amounts of yeast core histones in buffer N + 2 M NaCl, incubated on ice for 2 hours, followed by an overnight dialysis into buffer N + 50 mM NaCl. A dialysis setup with a peristaltic pump was constructed following the instructions in Luger et al. (1999). The reconstituted nucleosomes were visualized on a Novex™ TBE Gels, 6% gel (Invitrogen). Gel electrophoresis was performed with cold 0.5× TBE buffer (4 °C) at 90 V for 90 min. Fluorescence signals were acquired by a Typhoon FLA 9500 (GE Healthcare) using the Cy5 filter.

3.3. Electrophoretic mobility shift assay (EMSA)

Cy3 and Cy5 labeled nucleosomes were incubated with 4 µM Nhp6 and 0.4 µM of FACT or FACT truncations in total volume of 15 µl in the buffer N + 50 mM NaCl, for 30 min on ice. Reactions were loaded on Novex™ TBE Gels, 6% gel (Invitrogen). Gel electrophoresis was performed with cold 0.5× TBE buffer (4 °C) at 90 V for 180 min. Fluorescence signals were acquired by a Typhoon FLA 9500 (GE Healthcare) using the Cy5 filter.

3.4. Single molecule FRET assays by alternating-laser excitation (ALEX)

Labelled nucleosomes were diluted to concentrations of ≈ 50 pM in the imaging buffer (20 mM HEPES-NaOH, pH 7.6, 50 mM NaCl, 10% glycerol, 2 mg/ml BSA, 0.054% PEG-8000, 6% glucose). Prior to measurements, the coverslip was passivated for 5 minutes with a 2 mg/ml BSA solution in the buffer N. All assays were measured in a total sample volume of a 100 µl. In assays where the influence of proteins on nucleosome stability was examined, the proteins were mixed together with the nucleosomes and incubated at RT for 10 min prior to the measurement.

Single molecule FRET assays were carried out on a homebuilt confocal alternating-laser excitation (ALEX) microscope. The microscope set up, and subsequent data analysis are detailed in Gebhardt et al. (2020). In short, the measurements were carried out on an epi-illuminated confocal microscope (Olympus IX71, Hamburg, Germany) with a dual-edge beamsplitter ZT532/640rpc (Chroma/AHF, Germany). Laser light was focused to a diffraction-limited excitation spot by a water immersion objective (UPlanSApo 60x/1.2w, Olympus Hamburg, Germany). Fluorescent probes were excited by a diode laser at 532 nm (OBIS 532-100-LS, Coherent, USA) operated at 60 µW at the sample in alternation mode (50 µs alternating excitation and a 100 µs alternation period) and by a diode laser at 640 nm (OBIS 640-100-LX, Coherent, USA) operated at 25 µW at the sample. The emitted fluorescence was spectrally split into donor and acceptor channel by a single-edge dichroic mirror H643 LPXR (AHF). Fluorescence emission was filtered (donor: BrightLine HC 582/75 (Semrock/AHF), acceptor: Longpass 647 LP Edge Basic (Semroch/AHF) and focused onto avalanche photodiodes (SPCM-AQRH-64, Excelitas). The detector outputs were recorded by a NI-Card (PCI-6602, National Instruments, USA).

3.4.1. Data analysis

Based on the recorded photon arrival times, the bursts were identified with ALEX-Suite, a home written software package for burst search and burst analysis as described in Gouridis et al. (2015). In addition to the burst determination, ALEX-Suite also provides apparent FRET values (E^*), calculated according to the equation (2.8, together with the stoichiometry, calculated according to the equation (2.9. Burst-sorted data was further analyzed and visualized using the Python programming

language (version 3.6.7), in Jupyter Notebook environment (version 5.0), using following Python packages: matplotlib (version 3.1.1), numpy (version 1.12.1), seaborn (version 0.9.0), pandas (version 0.20.1), math (version 0.19) and scipy (version 1.1.0) (PyPI.org).

The main criteria of ALEX data analysis were apparent FRET values. To distinguish between low and high FRET populations, a cut-off threshold of E^* = 0.4 was universally applied. Next, a percentage of the signal in low FRET population, i.e. with FRET values under 0.4, was calculated. This percentage reports on the nucleosome destabilization, reflected in the loss of high FRET signal characteristic of a stable nucleosome. By quantifying the low FRET population, different protein constructs and their effect on nucleosome stability are compared to each other as well as the nucleosome alone. Statistical analysis was done by a one-way ANOVA, followed by post hoc comparisons using the Tukey HSD test. Results of individual FRET assays are visualized by histograms, representing the signal distribution of the FRET population. To compare between different assay conditions and protein constructs, quantified low FRET populations are visualized by bar charts, with errors bars presenting the standard deviation (s.d.). All FRET assays were measured in three biological replicates (n=3).

3.5. Pulldown assays

3.5.1. GST and CBP pulldown assays

In the pulldown assays with the replisome factors, 0.5 µM of GST-Pob3Spt16 was incubated with 1 µM of Pol α, Ctf4, GINS, Cdc45 and Tof1-Csm3, on ice for 30 minutes in a total volume of 50 µl. Proteins were immobilized on 15 µl of Protino™ Glutathione Agarose 4B (Macherey-Nagel) for 90 min at 4 °C. Similarly, CBP-Csm3Tof1, GST fusion proteins (Tof1_N, Tof1_M, Tof1_C) and GST (1.5 µM) were incubated with prey proteins (fl FACT and FACT truncations, 3 µM) and immobilized on 15 µl of Calmodulin Affinity Resin (Agilent) or Protino™ Glutathione Agarose 4B (Macherey-Nagel) for 90 min at 4 °C. Following, beads were washed 3x with buffer G (50 mM HEPES-NaOH, pH 7.6, 300 mM NaCl, 10% (v/v) glycerol, 0.05% NP-40, 1 mM DTT, 1 mM EDTA) for GST pulldowns or buffer C (25 mM HEPES-NaOH, pH 7.6, 300 mM NaCl, 10% (v/v) glycerol, 0.05% NP-40, 1 mM DTT, 2 mM CaCl2) for CBP pulldowns. Proteins were incubated in the buffer C + 5 mM EDTA, 5 mM EGTA, or buffer G + 20 mM reduced glutathione, for 10 min on shaker

at 4 °C, 1000 rpm, eluted by centrifugation (500 x g, 4 °C, 1 min), and analyzed by SDS-PAGE.

3.5.2. Peptide pulldowns

Peptides based on Tof1_C were synthetized with a desthiobiotin linker, and were immobilized on magnetic Dynabeads™ M-280 Streptavidin (Invitrogen), equilibrated with buffer M (25mM HEPES-NaOH, pH 7.6, 50 mM NaCl, 10% (v/v) glycerol, 0.02% NP-40, 1 mM DTT) at RT for 90 min on a spinning wheel. Following 3x wash with buffer M, prey protein (S_N, Top1) was added and further incubated for 1 h. After a wash step, beads were transferred to a fresh tube and incubated for 30 min in the buffer M + 5 mM biotin, at 1000 rmp. Supernatants were recovered and eluted proteins were analyzed by SDS-PAGE.

Full list of peptides queried by pulldowns, and their sequence, is provided in Table 9.

3.6. *In vitro* chromatin replication assay

Replication reactions were carried out as described previously (Kurat et al., 2017). The following concentrations were used, unless stated otherwise: 50 nM FACT, 50 nM SΔN-P, 50 nM SΔC-PΔC, 20 nM Tof1Csm3, 20 nM Tof1ΔC, 10 nM Top1, and 10 nM TopI2. DNA was visualized by incorporation of [α32P] deoxycytidine triphosphate (dCTP) into nascent DNA. Reaction products were separated on a 0.8% alkaline agarose gel and visualized by phosphoimaging. Factors required for Okazaki fragment maturation are omitted from the assay, thus leading and lagging strands are visible.

Gels were analyzed with ImageJ using the Plot Lanes macro (Rasband, 1997). Obtained lane profiles of the replication reactions were fit to a Gaussian distribution, and the center of the distribution was taken as the mean leading strand length. To compare the influence of different replication conditions on chromatin replication enhancement across multiple gels, the lengths of the leading strands were normalized for each gel to the negative (0% enhancement) and positive (100% enhancement) control, i.e. the reactions without and with fl FACT, respectively.

Chapter 4: A single-molecule FRET study of the rearrangements in the nucleosome core by FACT

Structural rearrangements in the nucleosome core are highly dynamic in nature, and traditional approaches fall short in capturing these dynamic events. Therefore, to investigate the rearrangements in the nucleosome core by the histone chaperone FACT in greater detail, I developed a single molecule FRET-based assay. For this, donor and acceptor fluorophores were introduced on the nucleosome template DNA, enabling us to monitor DNA mobility. Taking advantage of the persistence length of double-stranded DNA which is around 50 nm or 150 base pairs (bp) (Hagerman, 1988; Wang et al., 1997), the nucleosome template DNA is considered to behave like a stiff rod. In such case, donor and acceptor fluorophores are far apart and it can be expected that energy transfer from donor to acceptor will not occur. In contrast, upon nucleosome formation, the DNA is significantly bent, bringing the fluorophores in a close proximity. Hence, energy transfer from donor to acceptor will be possible, allowing FRET measurements and monitoring changes in the DNA conformation upon FACT engagement with the nucleosome.

As FACT has a highly modular structure, the contribution of the individual domains to nucleosome rearrangements can be assessed based on the distinct FRET populations different FACT constructs lead to. First, the single-molecule FRET assay confirmed the indispensable role of Nhp6, a helper protein, for FACT engagement with the nucleosome. Interestingly, even though Nhp6 is believed to cause extensive DNA kinging, upon addition of Nhp6 no change in FRET was detected. This is consistent with the hypothesis that Nhp6 captures nucleosome breathing intermediates, thus exposing the histone-DNA interfaces that are, in turn, recognized and captured by FACT. Further, it confirms that the assay set-up in which the fluorophores were placed away from the entrance and exit sites of the nucleosomal DNA is unaffected by dynamic nucleosomal breathing. Next, a crucial contribution of the C-terminal domains of both FACT subunits, Spt16 and Pob3, for the initial engagement with the nucleosome was observed. These domains were previously found to interact with free histone H2A/H2B dimers in solution. Consequently, a double C-terminus truncation, SΔC-PΔC, is not able to reorganize the nucleosome in single-molecule FRET assays. Surprisingly, the N-domain of Spt16 was found not to have a role in FACT interactions with nucleosomes, and its deletion does not impair FACT reorganization activity.

4.1. Single molecule investigations of the nucleosome

Even before the first high resolution crystal structure of a nucleosome was published (Richmond et al., 1984), FRET was used to better understand the arrangement of the histones within the nucleosome core (Eshaghpour et al., 1980). Based on these first experiments in bulk, the authors concluded that H3 and H4 histones both bind very strongly to the DNA and that this could present the first step in nucleosome assembly. Decades of studies that followed confirmed their initial findings. More recently, bulk FRET experiments revealed the trajectory of nucleosomal linker DNA (Tóth et al., 2001), determined the effect of histone acetylation, ionic conditions, and the presence of linker histones on nucleosome compaction (Tóth et al., 2006), and the rates of spontaneous unwrapping and rewrapping of nucleosomal DNA (Li et al., 2004). However, details of the structural changes within the nucleosome core proved to be hard to observe with traditional approaches as ensemble measurements fail in investigating structural heterogeneities due to the intrinsic averaging.

The great technological development over the years amounted to a comprehensive single-molecule toolbox. Numerous force manipulation techniques are now available that provide a direct view of biological pathways by revealing the real-time dynamics of individual molecules and molecular assemblies (Dulin et al., 2013; Neuman and Nagy, 2008). Optical trapping, magnetic tweezing, and flow stretching are the techniques of choice for studying replisome components having well-established DNA manipulation protocols. These methods have been widely applied to study nucleic acid manipulating enzymes and each provides unique advantages depending on the application. Further the unparalleled design flexibility of fluorescence imaging approaches has allowed for their wide application in studies of a diverse range of biological pathways both *in vivo* and *in vitro*. In contrast to mechanical manipulation techniques that only report on functional output, fluorescence imaging techniques also can provide information about the spatial and temporal organization of individual enzymes on substrates and within large complexes.

Single-molecule FRET studies have provided high-resolution information about nucleosome conformations. Confirming the findings of bulk FRET experiments, Gansen et al. (2008) determined the influence of DNA sequence variations on the nucleosome structure and dynamics. Studies of nucleosome disassembly revealed that the interface between the $(H3–H4)_2$ tetramer and H2A/H2B dimers opens up

prior to H2A/H2B dissociation from the DNA, in contrast to a model of a disassembly pathway with one-step histone octamer removal (Böhm et al., 2011). Salt-induced dissociation experiments further demonstrated the influence of the electrostatic environment of the nucleosome in great detail, suggestive of possible pathways for nucleosome opening during DNA-based processes (Hazan et al., 2015). Also, the effect of histone acetylation and phosphorylation on nucleosome dynamics was analyzed (Brehove et al., 2015), together with the dynamics of the nucleosomal histone H3 N-terminal tail (Langowski et al., 2020). In addition to DNA breathing, single-molecule FRET also provided valuable mechanistic insights into nucleosome remodellers, such as ISWI that slides nucleosomes (Deindl et al., 2013), nucleosome translocation by RSC remodeling complexes (Harada et al., 2016), bidirectional sliding by Chd1 (Qiu et al., 2017), and nucleosome repositioning by INO80 (Schwarz et al., 2018).

Taken together, single-molecule FRET have become an ideal tool for studying nucleosome structure and dynamics. Coincidentally, the dimensions of a nucleosome, with a diameter of around 10 nm, conveniently match the distances permissive of the energy resonance. In this thesis, a single-molecule FRET assay based on ALEX (described in detail in Chapter 2) was set up to monitor the dynamics of the nucleosome upon FACT engagement. Previously reported nucleosome immobilization artifacts (Koopmans et al., 2008) were circumvented by confocal microscopy and measuring FRET of freely diffusing nucleosomes. Fluorophores on the DNA positioned close to the nucleosome dyad axis resulted in a stable high-FRET population, upon nucleosome reconstitution. Large scale perturbations of the histone-DNA contact network resulted in a significant increase in the distance between the fluorophores. Therefore, the results presented in the following chapters report on the loss of high-FRET nucleosome populations, reflective of big structural changes in the nucleosome core due to FACT engagement.

4.2. Aims

The histone chaperone FACT was shown to be implicated in multiple processes on chromatin. Prior to the start of the project, multiple interaction sites with different histones dimers on specific FACT domains had been determined. However, whether FACT could bind to both H2A/H2B as well as H3/H4 dimer (or tetramer) simultaneously was not clear. Further, how individual domains interact with histones in the context of a nucleosome was not resolved. Also, a minimal region for nucleosome reorganization was not been identified.

The goal of the first part of this thesis was to clarify how FACT interacts with and reorganizes the nucleosome, the importance of individual domains of FACT for nucleosome reorganization and to gain insight into the underlying FACT mechanism. First, to investigate the contribution of the individual FACT domains to the rearrangements in the nucleosome core, a single-molecule FRET-based assay needed to be developed. Following, a library of FACT truncations were constructed, guided by the modular organization of FACT, and tested for nucleosome reorganization ability in a single-molecule FRET assay. Based on these results, I identified the key domains required for the interactions between FACT and the nucleosome.

4.3. Results

4.3.1. A single-molecule FRET approach to study rearrangements in the nucleosome core

To investigate structural changes within the nucleosome, I established a single-molecule FRET assay which allowed for precise detection of nucleosomal DNA reorganization. Budding yeast nucleosomes were reconstituted as previously described (Luger et al., 1999) using 147-bp DNA substrates containing the Widom 601 sequence. Nucleosome reconstitution was highly efficient with essentially no amounts of free DNA remaining (Figure 4.1).

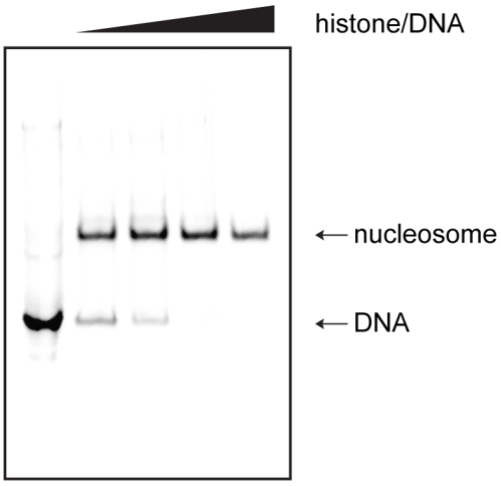

Figure 4.1. Nucleosome reconstitution.
Yeast nucleosomes were reconstituted with an increasing ratio of histones vs. Widom 601 DNA. The efficiency of nucleosome reconstitution is evident as a shift of the complex with decreasing amounts of free DNA, separated on a native gel.

To track DNA mobility, donor and acceptor fluorophores (Cy3 and Cy5) were placed along the dyad axis at positions 35 and 112, at the maximum distance from the entry and exit points of DNA (Figure 4.2). These positions ensured minimal influence of nucleosome breathing on monitored FRET values (Huertas and Cojocaru, 2020). The DNA substrate is considered stiff due to the short length, which is smaller than the persistence length of double-stranded DNA. The construct thus places both dyes at a distance of 77 base pairs, ~26 nm, apart. Considering the Förster radius of the Cy3-Cy5 pair is in the range of ~5 nm (Voith von Voithenberg and Lamb, 2018), it is expected that energy transfer is absent in the construct before nucleosome formation. Based on the budding yeast nucleosome structure (PDB 1ID3), the dyes positioned along the dyad axis are at a distance of ~4.5 nm, thus expected to have a FRET efficiency of ~0.65.

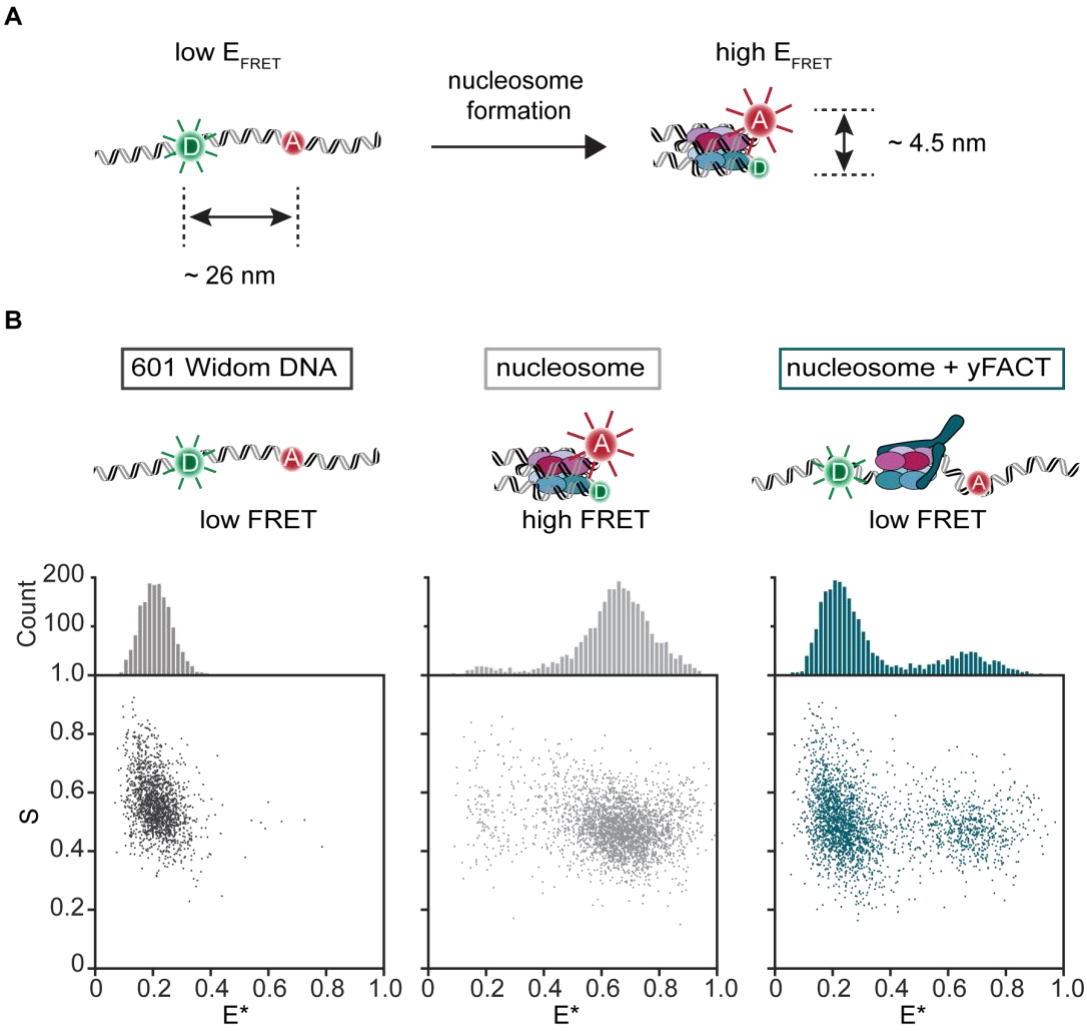

Figure 4.2. Substrates for the single-molecule FRET assays.
(**A**) DNA construct with fluorophores used in the nucleosome reconstitution. Left: Donor and acceptor fluorophores are placed at a distance of 77 bp apart, at positions 35 and 112 bp, corresponding to 26 nm. Right: Upon nucleosome reconstitution, DNA wraps around the core histones, bringing the fluorophores into proximity at a distance of 4.5 nm, based on nucleosome structure (PDB 1ID3). (**B**) Substrates measured in ALEX assays. Top: schematic showing FRET substrates, Bottom: 2D-histograms showing the stoichiometry vs FRET efficiency for individual measurements of the labelled DNA (left), nucleosome (middle) and nucleosome + yFACT (right).

To establish the FRET assay, single, freely-diffusing nucleosomes were imaged in a confocal microscope using alternating laser excitation (ALEX) with rapid switching between green (532 nm) and red (637 nm) lasers at 20 kHz to capture donor and acceptor emission (Hohlbein et al., 2014). Spectral separation of green and red signal provided information on donor (DD) and acceptor (DA) emissions upon donor excitation, as well as acceptor emission (AA) upon direct acceptor excitation. These photon streams allowed us to calculate apparent FRET efficiency (Equation (2.8).

Secondly, stoichiometry S was calculated according to Equation (2.9 and the data were plotted in two dimensional histograms of *E** versus S. A dual-color burst search was used to identify doubly-labelled DNA constructs and nucleosomes (Figure 4.2). The ability of ALEX to image freely-diffusing molecules allows for the collection of thousands of single molecule observations within hours, facilitating rapid screening of buffers and samples.

Analysis of isolated Widom DNA showed a low-FRET (*E** ~ 0.2) population consistent with the large separation of Cy3 and Cy5 on free DNA (Figure 4.3). The non-zero value of *E**, despite the large interdye distance, is mainly caused by donor-leakage of Cy3 into the Cy5-detection channel. Imaging reconstituted nucleosomes revealed a high FRET population with varied stability over time that strongly depended on the buffer conditions (Figure 4.3). The *E** of the high FRET species was 0.7, in a good agreement with the predicted value based on the budding yeast nucleosome structure (PDB 1ID3) for dyes positioned along the dyad axis (Figure 4.2). In intact nucleosomes under optimal buffer conditions, the high FRET species accounted for 90% of the entire FRET signal. The remaining signal was broadly distributed consistent with the expected background of the measurement technique with a minor species at lower FRET corresponding to free DNA (Figure 4.3). Interestingly, upon dilution lower than 50 pM for single-molecule imaging, pronounced nucleosome disassembly was observed within minutes. This observation provides an explanation for the notorious challenges encountered when attempting to purify and reconstitute budding yeast nucleosomes and arises from key differences in the protein-DNA contact network (Leung et al., 2016). Therefore, buffer conditions were extensively screened to find suitable conditions in which nucleosomes remained stable at the low concentration needed for single-molecule assays during the imaging time window of 30–60 minutes. Additives that mimic native crowded conditions (Batra et al., 2009; Shahid et al., 2019) were found to stabilize nucleosomes, consistent with past reports (Torigoe et al., 2013; Vlijm et al., 2017; Vlijm et al., 2012), and allow for continuous imaging. The optimal conditions that emerged from buffer screening were used for all subsequent FRET measurements.

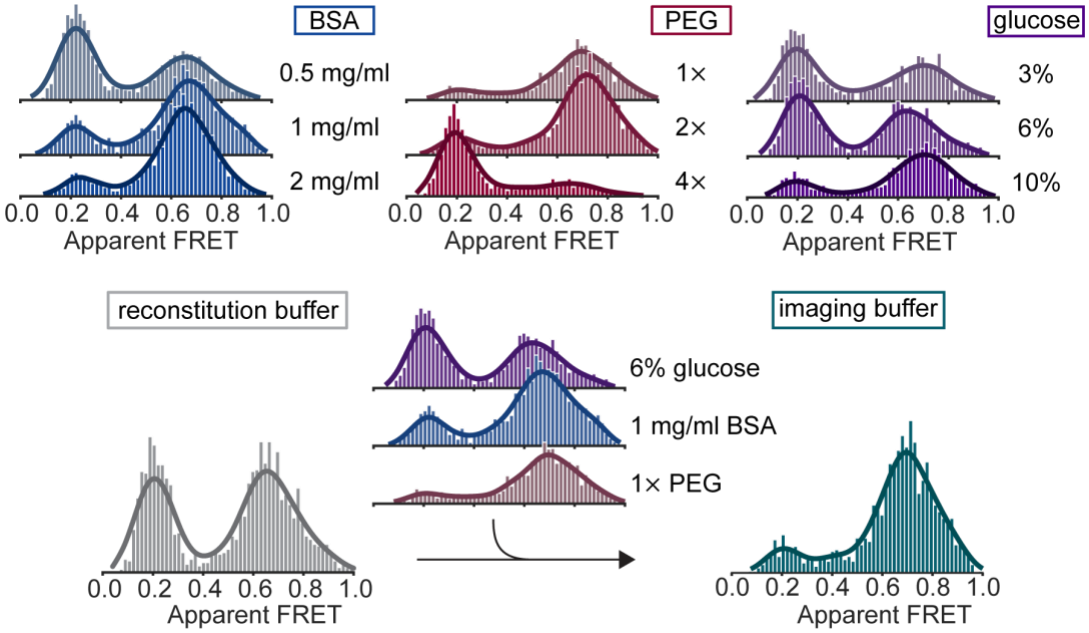

Figure 4.3. Stabilization effect of the imaging buffer.
Top: Screening of different buffer additives to stabilize nucleosomes at low concentrations: BSA (blue), PEG 8000 (red) and glucose (purple), with the concentrations as indicated, 1× PEG=0.054% (v/v). Bottom: Apparent FRET distribution showing stabilization of nucleosomes in the imaging buffer (reconstitution buffer + 1 mg/ml BSA, 0.054% (v/v) PEG and 6% glucose), compared to the reconstitution buffer. All histograms have the same y-axis scale of 200 counts.

4.3.2. yFACT promotes extensive reorganization of yeast nucleosomes

To clarify how FACT interacts with and reorganizes the nucleosome, individual subcomplexes were introduced to labelled nucleosomes. Consistent with EMSA showing formation of higher-order species only with the combination of both factors, and a complete lack of shift with FACT alone, no change in FRET efficiency or the relative abundance of the high- and low-FRET population was observed upon addition of FACT or Nhp6 individually (Figure 4.4). In contrast, simultaneous addition of Nhp6 and FACT, referred to as yFACT, led to extensive destabilization of nucleosomes, defined by almost complete loss of high FRET (Figure 4.4). To quantify the effects of yFACT and its individual components, I calculated the relative percentage of the low FRET population for each condition and compared it to nucleosomes (Table 1). To distinguish between low and high FRET populations, a cut-off threshold of $E^* = 0.4$ was universally applied. Nucleosomes, FACT or Nhp6 all showed a stable ~10% low FRET fraction and only yFACT induced an increase of this value to ~70%. I thus refer to the ratio as loss of FRET throughout the text. Further, statistical analysis showed no significant difference in loss of FRET between nucleosome, Nhp6 and FACT, with a significant difference compared to yFACT, $p<0.001$ (one-way ANOVA with Tukey HSD post hoc test, Table 2). These findings are consistent with EMSA showing formation of higher-order species only with the combination of both factors, and a complete lack of shift with FACT alone (Figure 4.4).

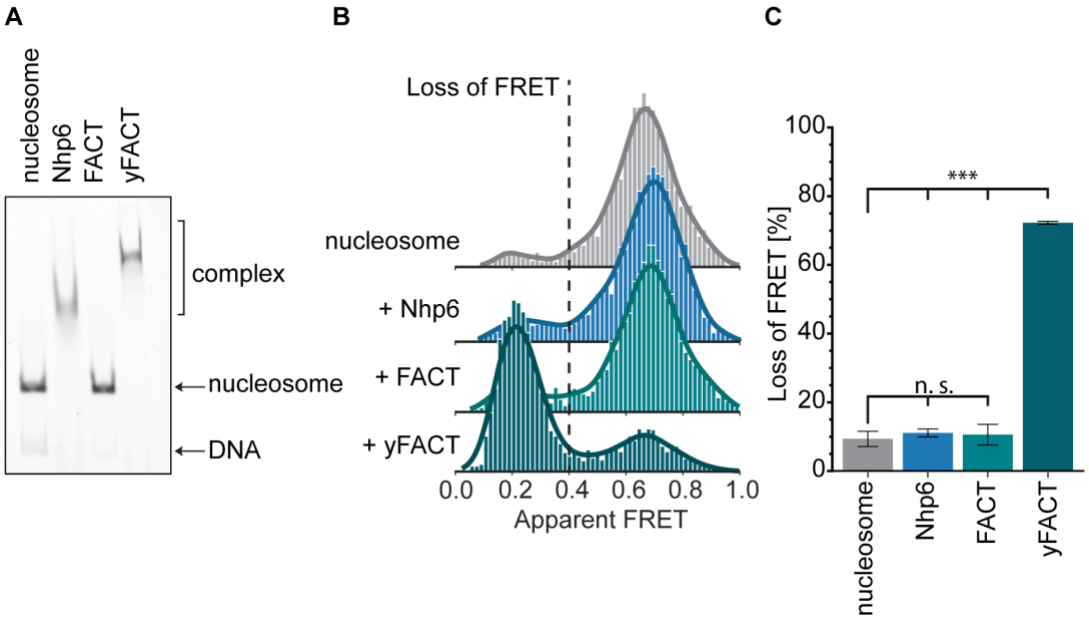

Figure 4.4. Single-molecule FRET assay to study nucleosome dynamics. (**A**) FACT engagement with nucleosomes studied by EMSA. The efficiency of nucleosome reconstitution is evident as a shift of the complex with minor amounts of free DNA (lane 1). Further shift is observed with nucleosome forming a complex upon the addition of Nhp6 (lane 2) and yFACT (Nhp6 together with FACT) (lane 4), but not with FACT alone (lane 3). (**B**) Single-molecule FRET measurements showing the distributions of high FRET population with the efficiency of ~ 0.7 for the complexes as shown in (A): nucleosome (gray), nucleosome + Nhp6 (blue), nucleosome + FACT (green); nucleosome + yFACT (teal) is shifted to a lower FRET population. All histograms have the same y-axis scale of 200 counts. (**C**) yFACT reorganization activity reported as loss of FRET (%), bars and error bars indicate mean ± s.d., respectively, from three independent experiments: nucleosome=9.23 ± 2.20, Nhp6=10.96 ± 1.15, FACT= 10.47 ± 3.01, yFACT=72.12 ± 0.46. Statistical analysis: one-way ANOVA with Tukey HSD post hoc test (n=3), n.s. $p>0.5$, *** $p<0.001$.

Additionally, I confirmed that the higher-order species formed upon yFACT engagement contain all histone dimers. Further, I observed that FACT's ability to form higher order species and disrupt nucleosomes is strongly concentration dependent. To ensure complete reorganization I titrated up to 400 nM, which is much higher than the previously reported *Kd* values ranging between 16 and 64 nM (Chen et al., 2018b; Winkler et al., 2011). In accordance with previously reported EMSA measurements (Ruone et al., 2003), the single-molecule assay demonstrated the prerequisite of a ten-fold higher concentration of Nhp6 for effective recruitment of FACT to nucleosomes (Figure 4.5).

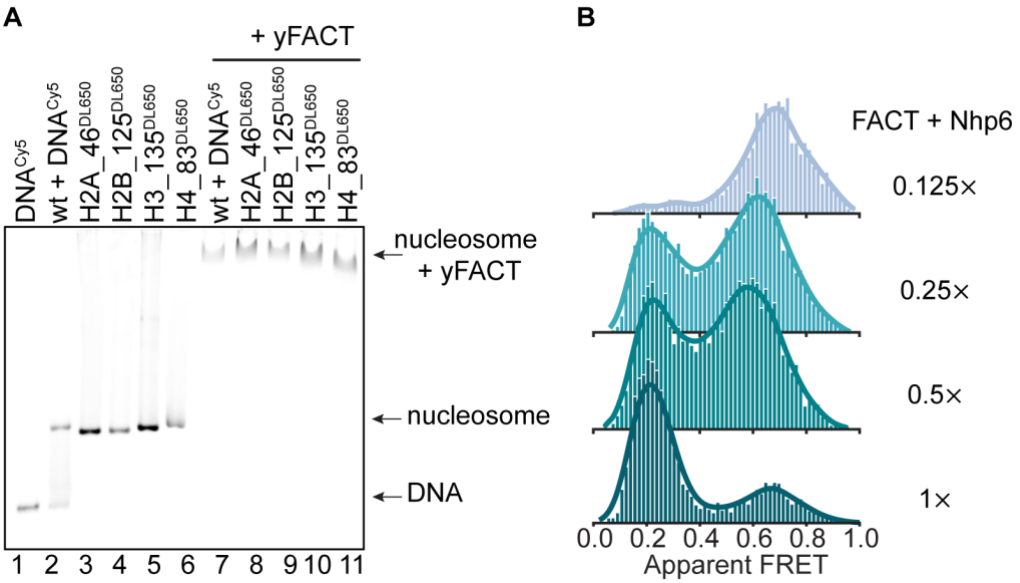

Figure 4.5. Histone conservation and concentration dependent reorganization activity of yFACT.
(**A**) Electrophoretic mobility shift assay (EMSA) showing the higher-order species formed upon yFACT engagement contain all histone dimers. The gel was imaged at the wavelength for the indicated fluorophores. (**B**) Concentration dependent influence of yFACT on nucleosome reorganization based on single-molecule FRET measurements of indicated amounts of Nhp6 and FACT titrated against a fixed nucleosome concentration up to 50 pM. All histograms have the same y-axis scale of 200 counts. The maximum nucleosome reorganization activity of yFACT was found at concentrations 1× = 0.4 µM FACT + 4 µM Nhp6.

To exclude the possibility that FRET changes could occur due to protein-induced fluorescence enhancement (PIFE), control measurements were performed with the donor Cy3B and acceptor ATTO647N, both shown to be insensitive to local environmental changes (Ploetz et al., 2016). In comparison with assays performed with Cy3 and Cy5, these controls revealed no PIFE effects or quenching (Figure 4.6), consistent with all observed FRET changes arising as a consequence of nucleosome reorganization by FACT.

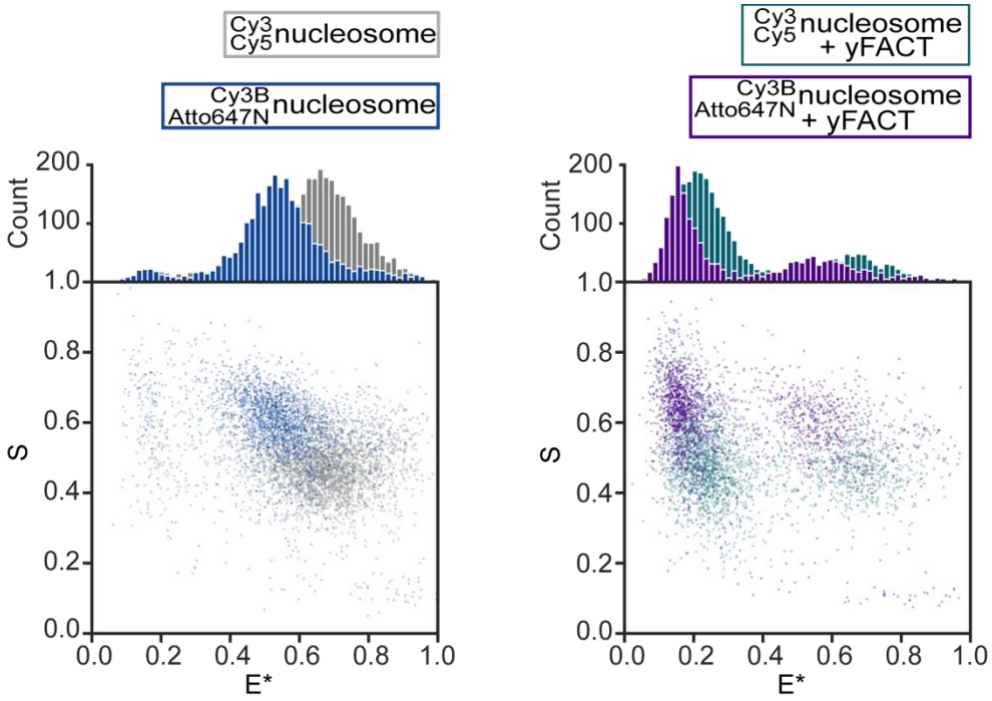

Figure 4.6. Single-molecule ALEX assay with nucleosomes labelled with two different FRET pairs.
Left: 2D-histograms showing individual single-molecule FRET measurements of the Cy3Cy5 labelled nucleosome (gray) vs. Cy3BAtto647N labelled nucleosome (blue). Right: Cy3Cy5 labelled nucleosome + yFACT (teal) vs. Cy3BAtto647N labelled nucleosome + yFACT (purple). No PIFE effect was detected.

4.3.3. Nucleosome reorganization by yFACT is coordinated among several distinct regions

To clarify the importance of individual domains of FACT for nucleosome reorganization, I employed the same assay to study the interaction of nucleosomes with truncated FACT complexes. FACT has a highly modular organization with flexible elements positioned in between histone interacting motifs like beads on a string. Therefore, domains were removed individually and in combination with truncations starting and ending in the naturally flexible regions (Figure 4.7, Figure 4.8).

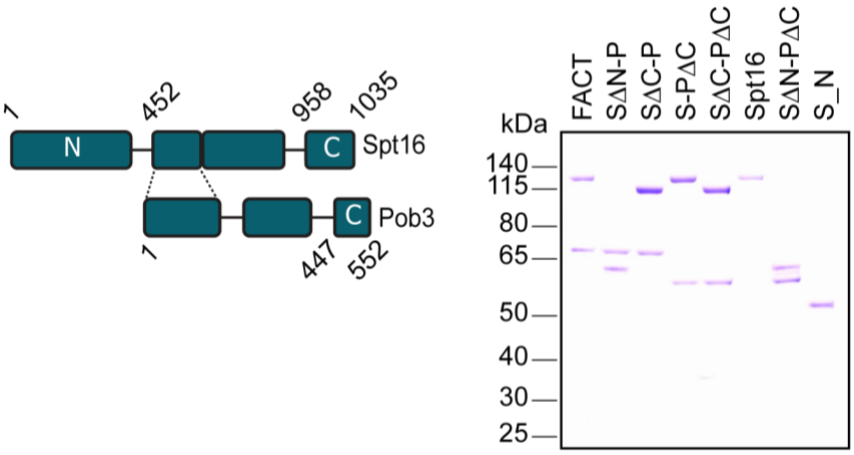

Figure 4.7. Modular organization of yFACT.
Left: schematic showing FACT domains. Right: SDS-PAGE gel of full length FACT and the FACT truncations evaluated in the assays: SΔN-P, S-PΔC, SΔC-P, SΔC-PΔC and Spt16.

Each of the constructs, in combination with Nhp6, caused distinct changes in the FRET populations monitored using labelled nucleosomes (Figure 4.8, Table 4). For further clarity, truncated FACT subunits are noted with S for Spt16, and P for Pob3. Consistent with its suggested role in recruitment and regulation, deletion of the N-terminus of Spt16, SΔN-P, did not significantly impair the reorganization activity of yFACT (p=0.118). Individual C-terminal deletions in either Spt16, SΔC-P, or Pob3, S-PΔC, led to significant loss of FACT reorganization activity. Deletion of the C-terminus of Spt16 was considerably more detrimental as compared to Pob3, with ~22% loss of activity (p<0.001) as compared to ~10% (p=0.029), in agreement with differences in the affinities of each C-terminal domain for H2A/H2B(Kemble et al., 2015). This observation suggests different modes of FACT subunit interaction with the nucleosome. Complete loss of activity was observed when both C-terminal

domains were removed simultaneously, SΔC-PΔC, as reflected by no significant difference compared to nucleosomes alone (p=0.682), demonstrating the indispensable role of the C-terminal domains for FACT reorganization activity. Finally, the observation that the C-terminus of Spt16 alone accounts for the majority of the reorganization activity led us to consider whether Pob3 is required. I therefore performed measurements with Spt16 alone, which showed no significant reorganizing activity compared to nucleosomes alone (p=0.673, one-way ANOVA with Tukey HSD post hoc test, Table 5).

EMSA revealed the formation of large complexes for all truncations that displayed reorganization activity suggesting FACT remains bound to maintain the reorganized state (Figure 4.8). Intermediately sized species, consistent with Nhp6 binding alone, were observed for SΔC-PΔC and Spt16, both of which show no reorganization activity.

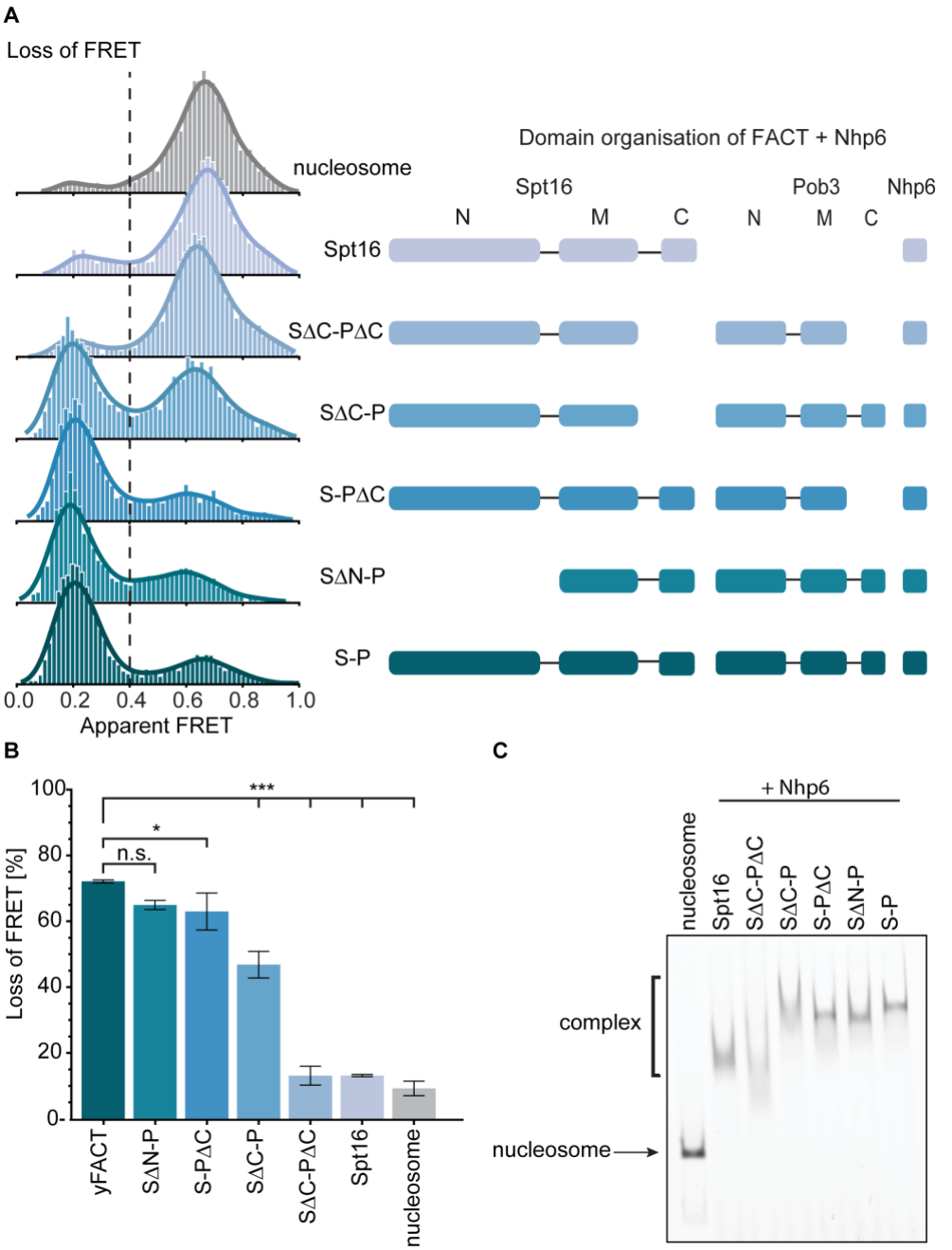

Figure 4.8. Contributions of the individual FACT domains to nucleosome reorganization.
(**A**) Left: single-molecule FRET measurements showing the distributions of FRET populations for individual FACT truncations; Spt16 (S), Pob3 (P). Right: schematic showing the modular domain organization of FACT and the individual truncations. All histograms have the same y-axis scale of 200 counts. (**B**) FACT reorganization activity reported as loss of FRET (%), bars and error bars indicate mean ± s.d., respectively, from three independent experiments: yFACT=72.12 ± 0.46, SΔN-P=64.95 ± 1.37, S-PΔC=62.99 ± 5.62, SΔC-P=46.82 ± 4.04, SΔC-PΔC=13.09 ± 2.87, Spt16=13.13 ± 0.35, nucleosome=9.23 ± 2.20. Statistical analysis: one-way ANOVA with Tukey post hoc test (n=3), n.s. p> 0.5, *p<0.05, *** p<0.001. (**C**) EMSA for the truncations shown in **A**. The nucleosome forms a complex with the addition of Nhp6 and different FACT truncations. The complete shift, compared to the wt FACT, is observed with SΔC-PΔC, S-PΔC and SΔN-P.

Consistent with its suggested role in recruitment and regulation, deletion of the N-terminus of Spt16, SΔN-P, did not significantly impair the reorganization activity of yFACT. Nevertheless, a small reproducible reduction in activity was observed (*p*=0.118). To further assess the reduction in activity I combined the Spt16 N-terminal deletion with the C-terminal deletion of Pob3, creating SΔN-PΔC. As expected, SΔN-PΔC exhibited a loss in activity equivalent to the sum of the individual losses from each truncation. However, I evaluated the N-terminus of Spt16 alone, S_N, and observed no influence on the nucleosome stability (Figure 4.9). Therefore, I attribute the small reduction in activity observed for SΔN-P to global changes in structural stability that influence the engagement pathway since I did not observe any interaction between the N-terminal of Spt16 and the nucleosome, the N-terminal domain does not contain any know histone binding motifs, and no direct interactions have previously been previously reported or been visible in known structures.

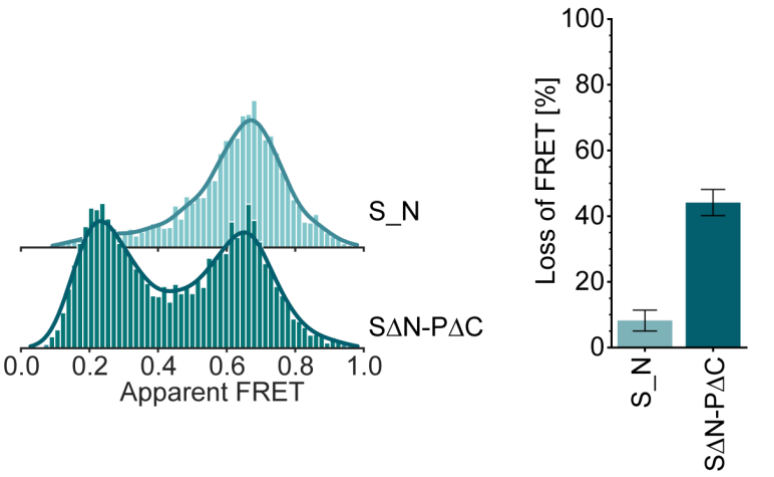

Figure 4.9. Influence of Spt16 N-domain on nucleosome stability.
Left: Single-molecule FRET measurements showing the distributions of FRET populations for the nucleosome in the presence of Spt16 N-domain (top), and SΔN-PΔC (bottom). All histograms have the same y-axis scale of 200 counts. Right: FACT truncation reorganization activity reported as loss of FRET (%), bars and error bars indicate mean ± s.d., respectively, from three independent experiments: S_N=8.20 ± 3.17, SΔN-PΔC=44.11 ± 3.98.

The observation that the C-terminal domains of Spt16 and Pob3 are critical for reorganization activity led us to wonder if these elements alone might be sufficient. To evaluate this hypothesis, I repeated the ALEX assay with peptides containing the C-terminal binding domains from each subunit. However, even at high concentration, no reorganization activity was observed. Next, I attempted to rescue activity by complementing the C-terminal peptides with FACT truncations lacking only the C-terminus of either subunit (Figure 4.10, Table 6). Intriguingly, these attempts

resulted in the same level of activity as without the C-terminal peptides. Taken together, these results highlight the critical importance of multiple points of contact for robust nucleosome reorganization by FACT.

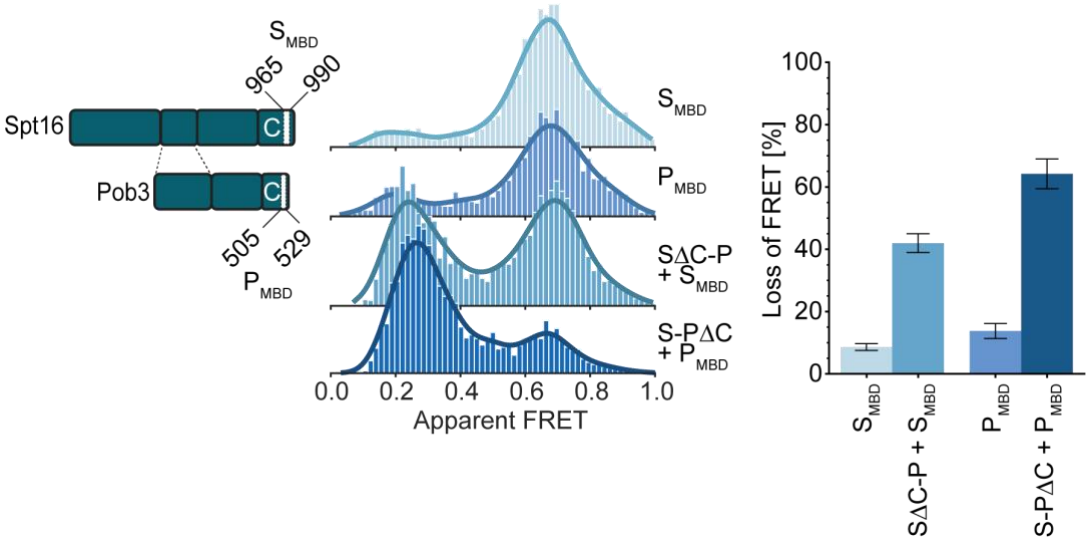

Figure 4.10. Single-molecule FRET measurements showing the distributions of FRET populations with minimal binding regions.
Left: Schematic showing the modular domain organization of FACT and the minimal binding domains (MBD), as reported by Kemble et al. (2015). Middle: Single-molecule FRET measurements showing the distributions of FRET populations for the nucleosome in the presence of S_{MBD}, P_{MBD}, SΔC-P-S_{MBD}, and S-PΔC-P_{MBD}. All histograms have the same y-axis scale of 200 counts. Right: FACT truncation reorganization activity reported as loss of FRET (%), bars and error bars indicate mean ± s.d., respectively, from three independent experiments: S_{MBD}=8.61 ± 1.08, P_{MBD}=13.78 ± 2.42, SΔC-P-S_{MBD}=41.97± 3.03, S-PΔC-P_{MBD}=64.22 ± 4.78.

4.4. Discussion

Nucleosome reorganization by FACT requires multisubunit coordination

The single-molecule FRET observations demonstrate that FACT alone can induce large scale structural changes in the nucleosome core leading to the loss of histone-DNA contacts. Notably, and consistent with past observations (Ruone et al., 2003), this activity required high concentrations of yFACT with a large excess of Nhp6. These conditions shifted the equilibrium toward higher populations of partly opened, FACT-bound nucleosomes, which provided an opportunity to dissect the dynamic roles played by different FACT domains. Systematic removal of the flexibly tethered subdomains of FACT confirmed that at least two points of contact are required for stable formation of open complexes. In particular, truncations lacking the C-terminal domains that bind where H2A/H2B dimers contact DNA were severely compromised, with removal of the C-terminal domain of Spt16 being most detrimental. Intriguingly, the attempts to rescue activity by adding these two critical C-terminal regions as separate polypeptides failed. This demonstrates that the middle domains, known to engage along the dyad axis near the H3 dimerization interface, are needed as an additional anchor to support stable engagement of the C-terminal regions (Figure 4.11). These observations are entirely consistent with the findings of many other recent biochemical and structural studies of FACT (Kemble et al., 2015; Liu et al., 2020; Mayanagi et al., 2019; Tsunaka et al., 2016; Wang et al., 2018; Winkler et al., 2011; Xin et al., 2009). Moreover, they highlight the absolute requirement for coordinated engagement of multiple, connected FACT subdomains for activity and provide a further clue to FACT versatility.

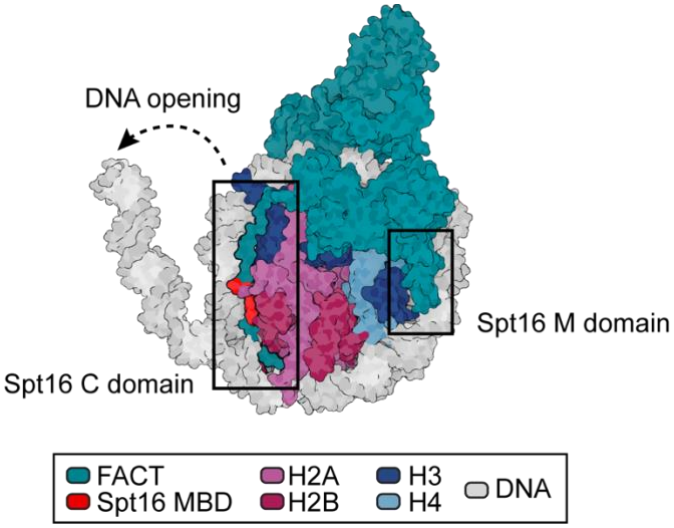

Figure 4.11. Model of FACT engagement with the nucleosome.
FACT (PDB 6UPK) superimposed with the nucleosome core particle (PDB 1ID3) and Spt16 MBD:H2A-H2B (PDB 4WNN). Opening of the DNA allows FACT to engage with the nucleosome via Spt16 MBD located at the C-terminus (shown in red). The entire C terminus of Spt16 engages with H2A/H2B histones along the DNA binding surface, effectively preventing DNA rebinding. Further engagement is carried out by Spt16 M domain contacting H3/H4 and DNA.

The reorganization activity observed with high levels of yFACT would be catastrophic if it occurred uncontrollably throughout chromosomes. However, the cellular conditions differ in several key aspects that ensure the proper regulation of FACT. First, FACT is available at a copy number lower than the number of nucleosomes in the cell. In *S. cerevisiae*, for example, there are 42 thousand copies of FACT as compared with 70 thousand nucleosomes (Formosa and Winston, 2020). Moreover, the pool of available FACT will be continuously depleted by several ongoing processes. Second, I expect that the dense packing in chromatin fibers would lead to greater stability as compared to the mononucleosomes I examined *in vitro*. Further studies beyond the scope of the current work are needed to investigate this possibility and the importance of stacking interactions and extended flanking regions. Nevertheless, heterochromatic regions will surely be far less accessible to FACT (Radman-Livaja and Rando, 2010). Finally, together with these features, I have shown that FACT activity requires several weak interactions between connected subdomains to be coordinated. This appears to be the most potent means of regulation, and the one that most likely underlies the broad versatility that allows the same chaperone to play important roles in vastly differing contexts.

Chapter 5: The fork protection complex recruits FACT to the replication fork

Having resolved the key interaction regions between FACT and the nucleosome, I investigated the possible anchor point(s) of FACT in the replisome. It has been shown in multiple studies that FACT travels with the replisome, but the specific interactions have remained unresolved. The importance of FACT as a histone chaperone was further underlined by the inability of reconstituted replisomes to progress through chromatin *in vitro* in the absence of FACT.

Two studies have reported reconstitutions of chromatin replication *in vitro* using components purified from *S. cerevisiae* which allows for controlled exploration of the minimal sets of required factors. Kurat et al. (2017) demonstrated that FACT was sufficient for chromatin replication, whereas Devbhandari et al. (2017) discovered that the nucleosome-array-forming factors Isw1a and Nap1 allowed for chromatin replication. These divergent findings are reflective of the overlapping functions of many histone chaperones and remodelers. The well-established role of FACT in removing and repopulating nucleosomes during transcription is highly analogous to the demands during replication (Belotserkovskaya et al., 2003; Farnung et al., 2021; Hsieh et al., 2013; Takahata et al., 2009). Together with the observation that FACT travels with the replication fork progression complex (Foltman et al., 2013; Gambus et al., 2006a), these findings suggest it may be the more essential factor in chromatin replication, but how it integrates with the replisome has remained unclear.

Following the data from structural studies, a set of replisome factors was probed for their direct interaction with FACT. Among those, confirming the previous findings, Pol α was shown to interact physically with FACT. Interestingly, I have discovered a new interaction between FACT and the replisome, more specifically, between FACT and the Tof1, a member of the fork protection complex. In line with the recent replisome structures (Baretic et al., 2020), the interaction between FACT and Tof1 would position FACT right at the front of the replisome, placing it in a convenient position to engage with the incoming parental nucleosome and secure parental histones as they are separated from DNA.

5.1. Chromatin replication *in vitro*

Few years after the seminal discovery of DNA structure (Franklin and Gosling, 1953b; Watson and Crick, 1953), in 1955 Arthur Kornberg was first to observe DNA synthesis in *E. coli* cell extract. The following year he discovered and purified DNA assembling enzyme and named it DNA polymerase (Lehman et al., 1958). This discovery earned Kronberg a Nobel Prize for Medicine in 1959, which he shared with Severo Ochoa, his former supervisor, who discovered RNA polymerase. These findings paved way to the first fully *in vitro* studies of DNA replication mechanism. Initial studies were conducted with a bacteriophage T4, which had been investigated in great details by geneticists and it had been known that only several genes are required for DNA synthesis (Cha and Alberts, 1989). In 1975, Bruce Alberts reconstructed bacteriophage T4 DNA replication with purified components (Morris et al., 1975). In 1980, an *in vitro* system of more complex T7 DNA replication was established (Fischer and Hinkle, 1980). Just few years later, DNA replication of the *E. coli* chromosome was reconstituted with purified proteins (Kaguni and Kornberg, 1984).

From the description of the DNA structure, 40 years had passed until the first fully *in vitro* eukaryotic replication assay was established, allowing for a complete replication of DNA from the simian virus 40 (SV40) origin with purified proteins (Waga et al., 1994). Together with T4, T7 and *E. coli in vitro* DNA replication assays, this breakthrough finding provided a powerful technique to study the mechanism of DNA replication in a controlled environment. Further, they allowed for numerous replication proteins to be described. However, the described systems lacked the complexity to elucidate roles of many eukaryotic proteins. A better understanding of the eukaryotic DNA replication was facilitated by development of genomic footprinting (Diffley et al., 1994; Diffley and Cocker, 1992; Santocanale and Diffley, 1996) and chromatin immunoprecipitation (ChIP) (Abi-Ghanem et al., 2015; Aparicio et al., 1997), elucidating details around origin recognition by the origin recognition complex (ORC) and establishment of the pre-replicative complex (pre-RC) (Bell and Stillman, 1992; Cocker et al., 1996; Diffley and Cocker, 1992; Liang and Stillman, 1997; Tanaka et al., 1997). Over the years that followed studies of the yeast cell cycle, extensive biochemical assays, monumental protein purifications and electron microscopy, led to the first reports of eukaryotic DNA replication by a minimal leading-strand replisome (Georgescu et al., 2014) and regulated origin firing with purified proteins (Yeeles et al., 2015a). Though functional, both of these studies reported replication fork speed well below those observed *in vivo*. Then, three fundamental studies were published, reporting *in vitro* reconstituted

eukaryotic DNA replication at *in vivo* fork rates (Yeeles et al., 2017) and the minimum requirements for full chromatin replication *in vitro* (Devbhandari et al., 2017; Kurat et al., 2017). Findings of these studies are briefly described in the following paragraphs as they are the key to understanding the results presented in the following chapters of this thesis.

The efficient eukaryotic DNA replication could be established only upon addition of multiple proteins known to associate with the CMG into the replisome progression complex (RPC) (Yeeles et al., 2017). Next, by the exclusion of the individual RPC factors in the assay, proteins responsible for the increased replication rates were determined - namely Mrc1 (mediator of replication checkpoint), Tof1 (topoisomerase I interacting factor), and Csm3 (chromosome segregation in meiosis), together forming the Fork Protection Complex (FPC). Mrc1 was shown to be primarily responsible for the increased synthesis rate. It is presumed that by directly accelerating the rate of unwinding by CMG, via a so far unknown mechanism, Mrc1 is able to facilitate increased replisome speed. Further, the Csm3-Tof1 complex was crucial for the association of Mrc1 with the replisome. This is supported by earlier ChIP experiments where Csm3 and Tof1 were found to be required for the physical association of Mrc1 with the replication fork (Bando et al., 2009). Additionally, Csm3 and Tof1 were found to be critical in replication fork pausing (Dalgaard and Klar, 2000; Krings and Bastia, 2004), the mechanism of which still remains to be fully resolved. This role is likely separated from promoting replication fork progression, as fork pausing is not dependent on Mrc1 (Calzada, 2005; Mohanty et al., 2006; Tourrière et al., 2005).

The next step in fully understanding eukaryotic replication was to establish *in vitro* replication through chromatin. Building upon the findings by Yeeles et al. (2017), Kurat et al. (2017) was able to establish *in vitro* replication on a chromatinized template. Initially, however, the reconstituted replisome was not functional even though the CMG was readily assembled, and seemed to be inhibited from progression by chromatin. Importantly, the S-phase extract was effective in replicating the same chromatin template, indicating that potential factors are missing in the reconstituted replisome. The relative abundance of proteins in the extract assembled replication complexes revealed the presence of the histone chaperones (Asf1, Nap1, FACT) together with the nucleosome remodelers (INO80, RSC, ISW1A), in addition to proteins already present in the reconstituted replisome. The identified proteins were individually examined for their roles in replication, revealing that FACT is required for chromatin replication and cannot be substituted by any other factor. First, the S-phase extracts depleted of FACT were shown not to be active on chromatin. Upon addition of purified FACT to the

depleted extracts, the replication could be restored. Similarly, addition of FACT to the reconstituted replisome system led to an increase of the replicated leading-strand length and quantity of lagging-strand products. However, the replication fork rates were relatively slow. The search for factors that might stimulate replication on chromatin uncovered a particular importance of Nhp6, confirming the FACT dependence on Nhp6 to engage with nucleosomes, as described in chapter 1.5. Further, ATP-dependent chromatin remodelers INO80 and ISW1A increased the overall productivity of the reconstituted replisome. Finally, the reconstituted replisome supplemented with these additional factors was able to efficiently replicate through the chromatin at *in vivo* rates.

The assay described by Kurat et al. (2017) will be used to assess the contributions of particular FACT domains, identified in Chapter 3 of this thesis, to chromatin replication. The progress of the replisome can be monitored as newly synthetized DNA is labelled by incorporation of [α32P] deoxycytidine triphosphate (dCTP). Upon completion of replication, reaction products are separated on alkaline agarose gel, denaturing dsDNA, and visualized by phosphoimaging. Based on the overall incorporation of [α32P] dCTP, the amount of the nascent DNA can be monitored, while the lengths of the leading strand products reveal the replisome progression through the template (Figure 5.1). Together, these features report on the efficiency of the chromatin replication *in vitro*.

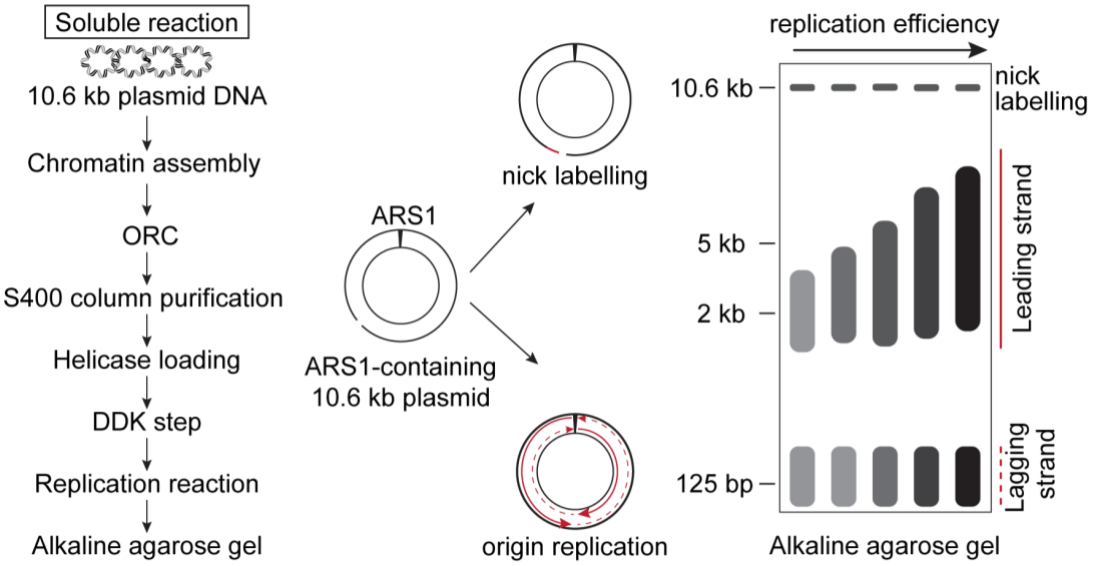

Figure 5.1. Set-up of chromatin replication assay.
Left: Reaction scheme of the *in vitro* chromatin replication assay. Middle: Prominent outcomes of the assay. A potential nick in the plasmid will lead to nick labelling, while proper replication from the origin leads to synthesis of leading strands at around half the length of the plasmid, indicative of an opposing fork collision. Right: Presentation of an alkaline agarose gel depicting results of a replication assay. Increase in the band intensity (from light gray to black) mirrors the increase of [α32P] dCTP incorporation, and longer smears reflect an increase of the leading strand length.

5.2. Aims

A complex network of static and dynamic interactions coordinate histone removal and deposition during replication (Miller and Costa, 2017). Even though it has been shown that FACT travels with the replication machinery, its precise location has not been determined. The goal of this chapter is to determine how FACT interacts with the replisome and which, if any, replication factors cooperate with FACT during chromatin replication. Further, the contribution of individual FACT domains studied in Chapter 3 are assessed for their effect on chromatin replication.

To understand the role of FACT in helping the replication machinery to overcome parental nucleosomes, guided by the recent structural data, replisome factors will be probed for potential interactions with FACT by protein pulldowns. Next, the single-molecule FRET assay described in Chapter 1 is used to study the individual impact of replisome factors on nucleosome stability, and their potential cooperation with FACT during nucleosome reorganization. Based on these experiments, and the findings described in Chapter 3, I have identified the key domains required for the interaction between FACT and replication factors. Finally, to confirm these findings, the identified proteins and truncations are tested in a fully reconstituted *in vitro* chromatin replication assay. The efficiency of DNA replication in the chromatin replication assay shows the contribution of the identified interaction partners to the overall enhancement of replication.

5.3. Results

5.3.1. Direct interactions between FACT and replication factors

Several distinct lines of evidence suggest that FACT may be directly physically coupled to the replisome. FACT has been shown to copurify with core replisome components and travel with the replication fork progression complex (Foltman et al., 2013; Gambus et al., 2006a; Han et al., 2010; Tan et al., 2006). Recent label-free quantitative mass spectrometry measurements have revealed that FACT is present in the replisome at similar levels to other core components (Reusswig et al., 2021). Additionally, low levels of FACT have proven sufficient for chromatin replication *in vitro* (Kurat et al., 2017), consistent with a high local concentration residing at the replication fork. This latter observation may provide an explanation for the large excess of FACT needed for complete reorganization activity in the ALEX experiments. However, the site or sites where FACT might bind and primary location of action within the replisome have remained unclear (Figure 5.2).

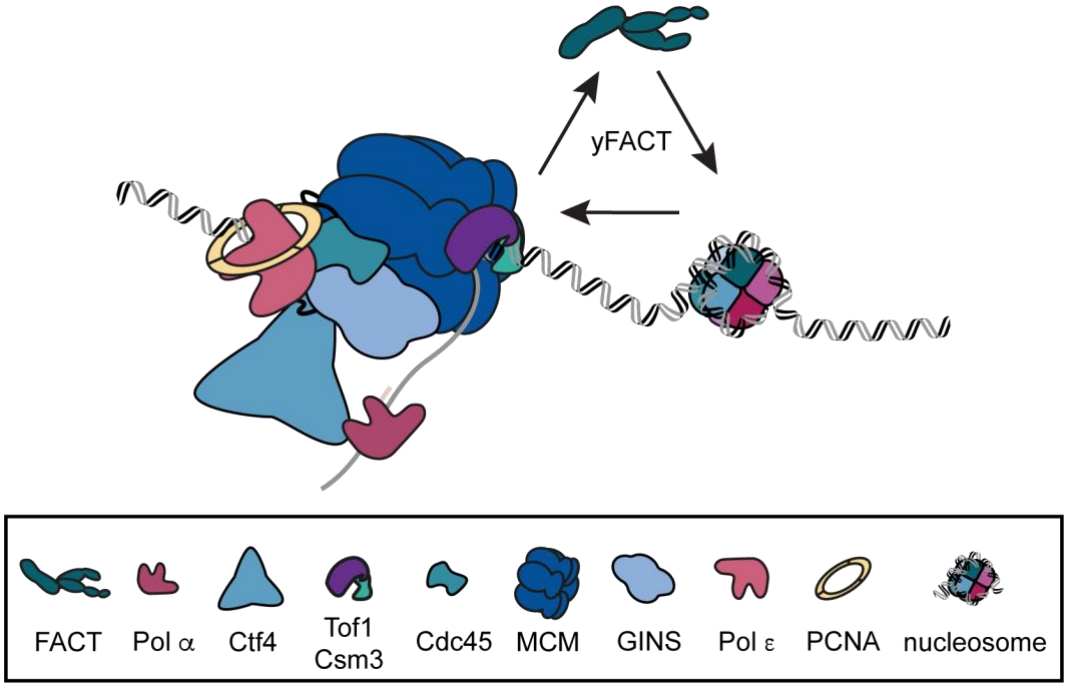

Figure 5.2. Interaction of FACT with the replisome.
Schematic showing the replisome factors, which are potential candidates for anchoring FACT to the replication fork.

To search for physical interactions between FACT and replication factors, I performed pull-down assays with reconstituted replication complexes *in vitro*. To this end, FACT consisting of Spt16 and GST-tagged Pob3 was bound to glutathione beads and used as bait for the replication factors Pol a, Ctf4, Tof1-Csm3, Cdc45, MCM-Cdt1 and

GINS (Figure 5.3), all of which are believed to reside near the site of initial parental nucleosome processing. In agreement with previous reports, I detected a direct interaction between Pol α and FACT (Miles and Formosa, 1992; Wittmeyer and Formosa, 1997). Unexpectedly, I also discovered a novel interaction between Tof1-Csm3 and FACT. None of the other replication factors screened were retained on the beads.

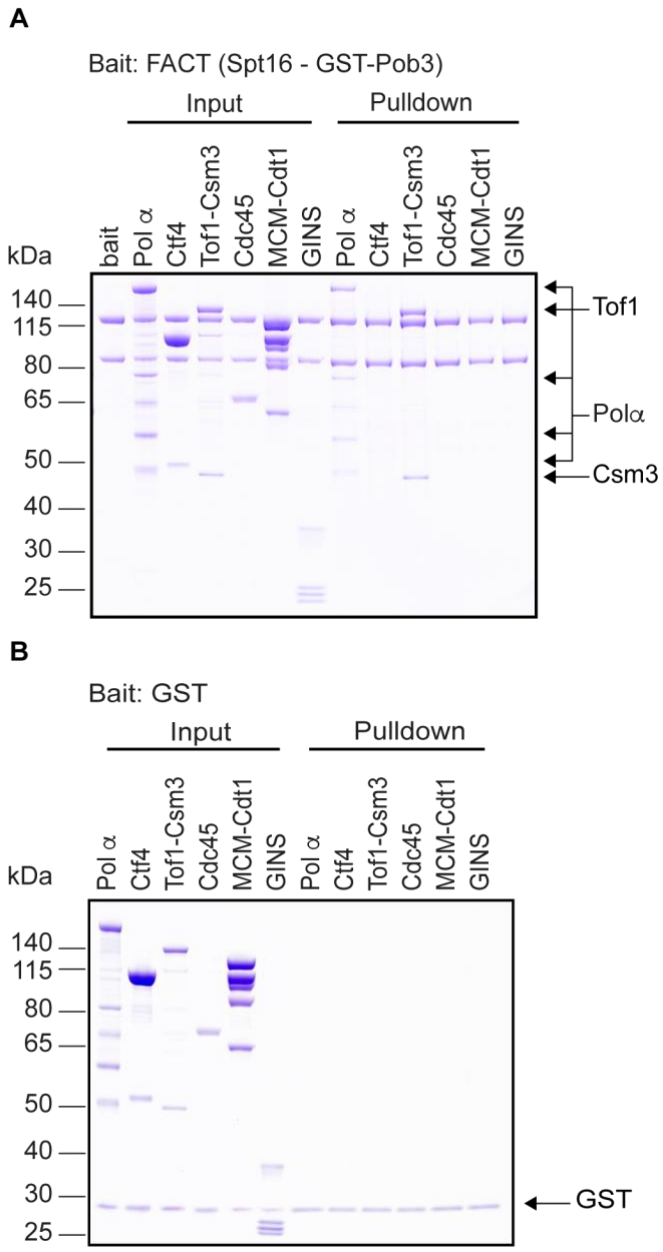

Figure 5.3. Probing for FACT connection with the replisome.
(**A**): Pulldown assay with 0.5 µM GST-tagged Pob3-Spt16 used as a bait to probe for interaction with 1 µM of Pol a, Ctf4, Tof1-Csm3, Cdc45, MCM-Cdt1 and GINS. FACT retained Pol a and Tof1-Csm3. None of the other replisome factors screened were detected. (**B**) Control pulldown assay with GST as a bait. There is no interaction between replisome factors and GST.

Next, I used the FRET assay to investigate whether replisome components might modulate the nucleosome reorganization activity of FACT. I started by evaluating components of the replisome progression complex (Gambus et al., 2006a) individually to exclude any direct nucleosome reorganization activity given that some are known histones binders. In particular, in addition to its interaction with FACT, Pol α has been shown to bind histones H2A/H2B (Evrin et al., 2018) as well as H3/H4 (Li et al., 2020). However, I observed no nucleosome reorganization activity from any of the replication factors tested. The histone chaperone Asf1 and $MCM2_{1\text{-}200}$ (amino acid (aa) 1-200), previously shown to form a complex with H3/H4 dimers, also did not trigger nucleosome reorganization. Next, I introduced replication factors in combination with FACT. None of the factors screened resulted in a significant reduction in FACT activity except Tof1-Csm3, which resulted in a 53% reduction (Figure 5.4, Table 7).

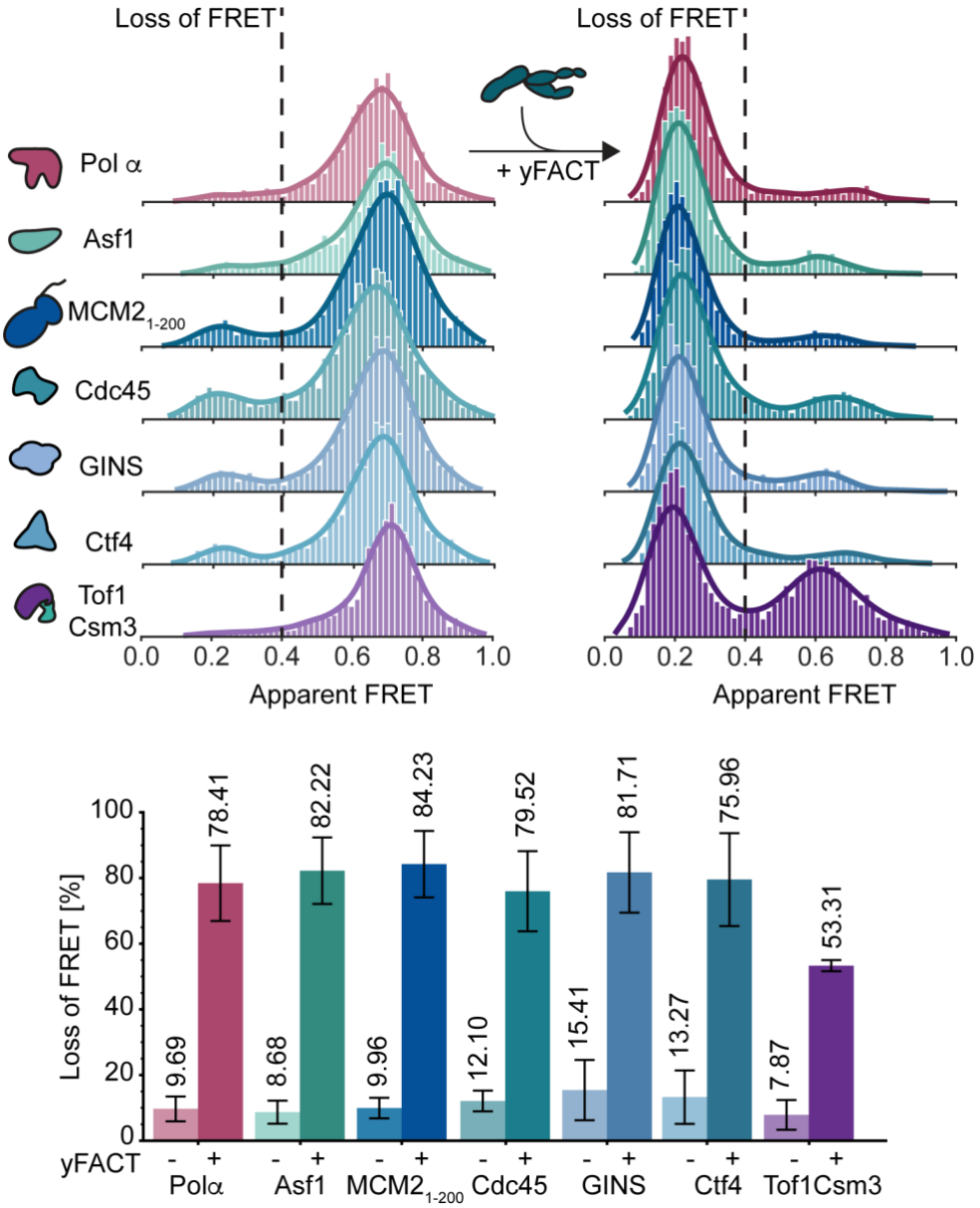

Figure 5.4. Influence of core replisome components on nucleosome stability. Top: Single-molecule FRET measurements showing the distributions of FRET populations for the nucleosome in the presence of respective replisome factor, alone and in the addition of yFACT, as indicated. All histograms have the same y-axis scale of 200 counts. Bottom: Influence of core replisome components on nucleosome stability, alone and with yFACT, reported as loss of FRET (%), bars and error bars indicate mean ± s.d., respectively, from three independent experiments: Pol α=9.69 ± 3.78, Pol α +yFACT= 78,41 ± 11,50, Asf1=8.68 ± 3.51, Asf1+yFACT=82.22 ± 10.13, MCM21-200=9.96 ± 3.12, MCM21-200=84.23 ± 10.11, Ctf4=13.27 ± 8.13, Ctf4+yFACT=79.,52 ± 14.14, Cdc45= 12.10 ± 3.13, Cdc45+yFACT=75.96 ± 12.20, GINS=15.41 ± 9.18, GINS+yFACT=81.71 ± 12.26, Tof1Csm3=7.87 ± 4.53, Tof1Csm3+yFACT= 53.31 ± 1.69.

However, upon further investigation, I discovered that Tof1-Csm3, known to bind DNA (Baretic et al., 2020; Noguchi et al., 2012), engages the nucleosome with a greater affinity than yFACT (Figure 5.5), suggesting the reduction in activity may not be the result of direct modulation of yFACT by Tof1-Csm3, but rather Tof1-Csm3 blocking yFACT engagement. To further investigate this possibility, I removed the N-terminal DNA binding region of Tof1 to generate Tof1ΔN-Csm3 (Tof1DN 639-1238 aa). Using a native shift-assay I confirmed that Tof1ΔN-Csm3 indeed does not bind DNA and it also does not bind nucleosomes (Figure 5.5). Finally, in the FRET assay I probed for an influence of Tof1ΔN-Csm3 on nucleosome stability in the presence of yFACT. Contrary to the results with Tof1-Csm3, Tof1ΔN-Csm3 did not have any effect on nucleosome stability and I detected major loss of high FRET population in the presence of yFACT (Figure 5.5, Table 8). Consequently, the impact of Tof1-Csm3 I observe in the FRET assay can be attributed to Tof1-Csm3 binding to the nucleosomal DNA, thereby hindering access and blocking FACT to engage with the nucleosome. Nevertheless, structural models suggest binding of Tof1-Csm3 to CMG (Baretic et al., 2020) would reduce the direct nucleosomal DNA binding, allowing FACT to play the dominate role in nucleosome engagement at the replication fork.

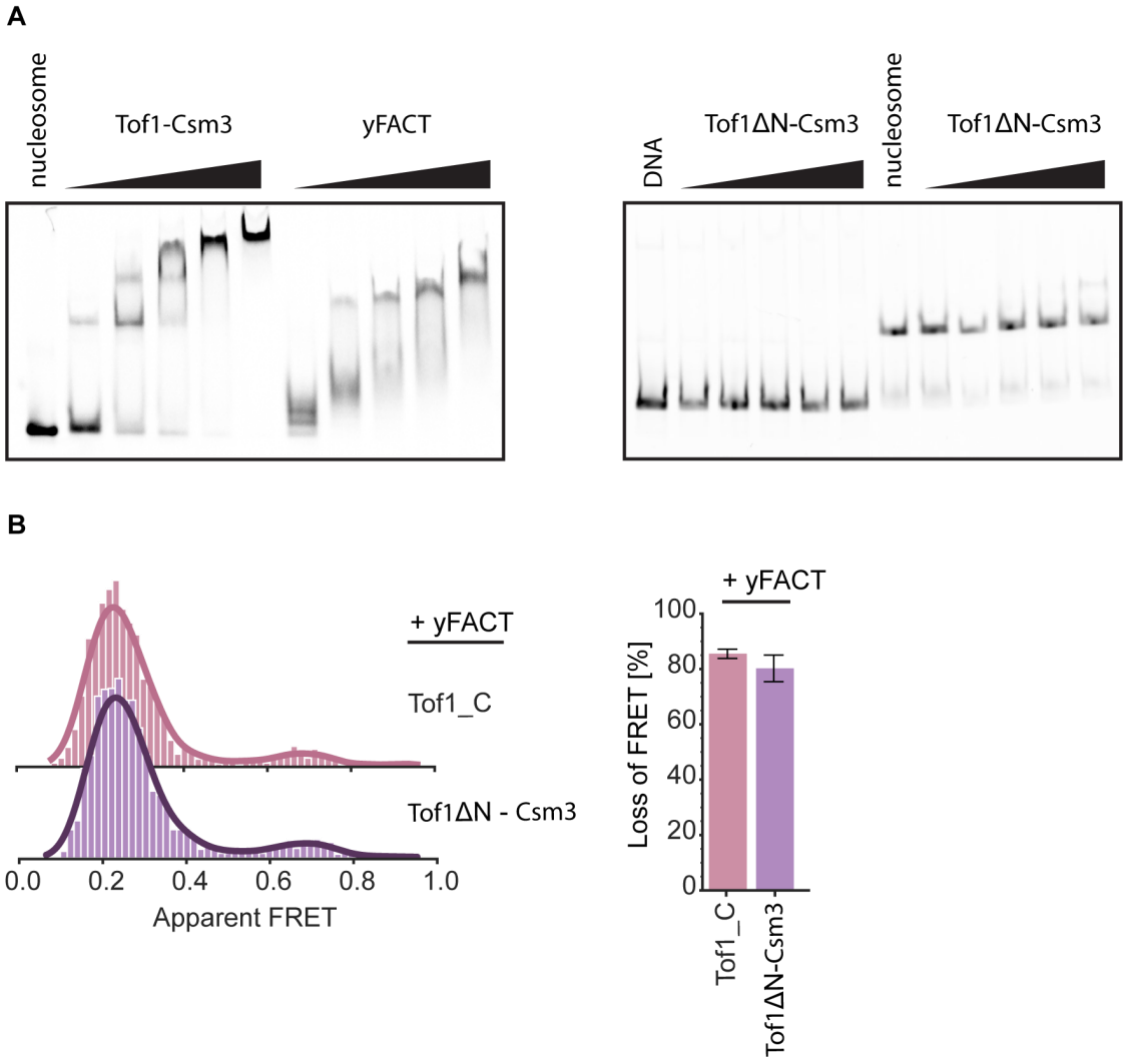

Figure 5.5. DNA binding is responsible for shielding of nucleosome by Tof1. (**A**) Left: EMSA with Tof1Csm3 and yFACT with nucleosome, proteins titrated from 25 to 150 nM. Majority of the nucleosome forms a complex with Tof1Csm3 at a concentration of 50 nM. Right: EMSA with Tof1DN-Csm3 with 146 bp DNA and nucleosome, proteins titrated from 25 to 150 nM. Tof1DN-Csm3 does not bind to free DNA nor the nucleosomes. (**B**) Left: Single-molecule FRET measurements showing the distributions of FRET populations for the nucleosome in the presence of Tof1_C and Tof1DN-Csm3 together with yFACT, as indicated. All histograms have the same y-axis scale of 200 counts. Right: Influence of Tof1_C and Tof1DN-Csm3 on nucleosome stability in the presence of yFACT, reported as loss of FRET (%), bars and error bars indicate mean ± s.d., respectively, from three independent experiments: Tof1_C+yFACT= 85.54 ± 1.69, Tof1DN-Csm3+yFACT= 80.27 ± 4.79.

5.3.2. FACT binds to an interaction hub in the C-terminus of Tof1

Recent structures of the CMG helicase have shown the fork protection complex positioned directly at the front of the replisome, where Tof1-Csm3 can grip dsDNA stabilizing the entire complex (Baretic et al., 2020) (Figure 1.5). Further, in the *in vitro* pull-down assays I found that Tof1-Csm3 was specifically retained by FACT. Moreover, in the FRET assay I noticed that the presence of Tof1-Csm3 appeared to modulate FACT activity (Figure 5.4). Taken together, these observations place FACT in front of the replication fork.

To better understand the interaction between FACT and Tof1-Csm3, I set out to define the interacting region(s) using *in vitro* pull-down assays with purified proteins. First, to confirm the initial finding, I showed that full-length (fl) FACT was also specifically retained by fl CBP-tagged Tof1-Csm3, immobilized on CBP agarose beads. (Figure 5.6). I found that fl FACT was specifically retained by fl CBP-tagged Tof1-Csm3, immobilized on CBP-agarose beads.

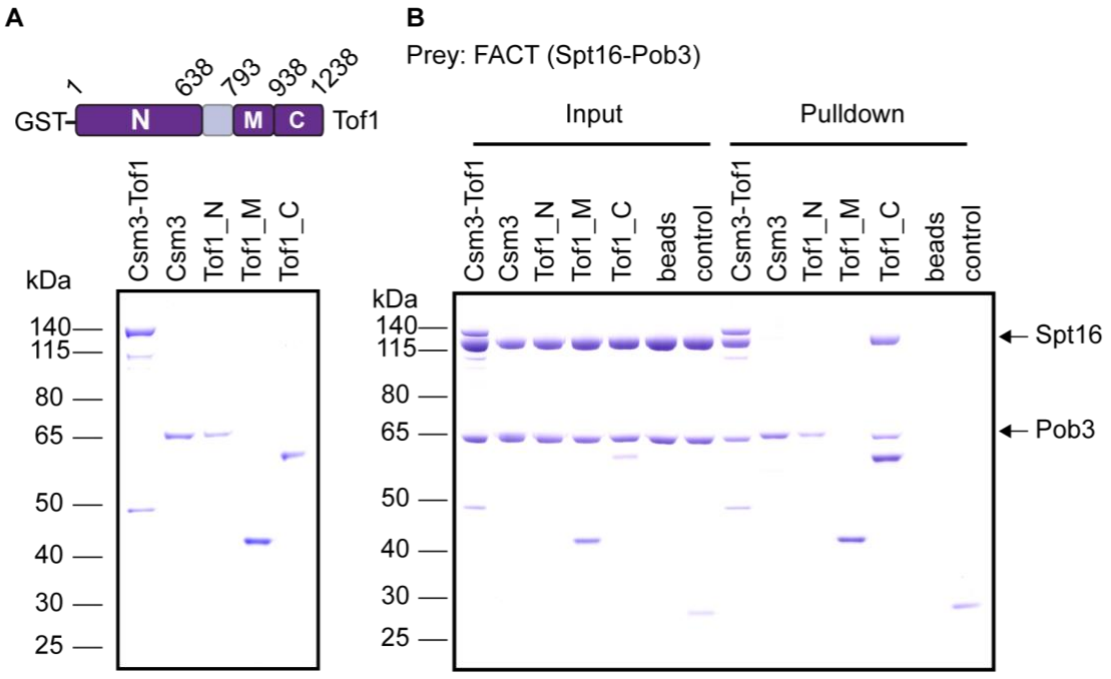

Figure 5.6. Determining the interaction interface of Tof1 and FACT.
(**A**) Top: Schematic showing the domain organization of Tof1 used in the pulldown assays. Bottom: SDS-PAGE of CBP-tagged Csm3-Tof1 and GST-tagged Tof1 truncations used in the pulldown assays. (**B**) Pulldown assay with 1.5 µM CBP-tagged Csm3-Tof1 and GST-tagged Tof1 truncations as shown in A. 3 µM of full length (fl) FACT was used as a prey throughout the assay. Csm3-Tof1 and Tof1_C retained fl FACT. CBP beads and GST control are shown.

To more precisely define the region of Tof1-Csm3 responsible for FACT binding, I constructed a series of GST-tagged Tof1 truncations – Tof1_N (1–638 aa), Tof1_M (793–937 aa) and Tof1_C (938–1238 aa), as well as fl Csm3 (Figure 5.7). In particular, binding of fl FACT to fl Csm3 was not observed. In the same experiment, fl FACT was not retained by Tof1_N or Tof1_M, but a specific interaction with Tof1_C was observed. I examined whether the interaction of FACT with Tof1_C has an influence on nucleosome reorganization by yFACT using the FRET assay. Here, I did not detect any impact of Tof1_C on the ability of yFACT to reorganize nucleosomes (Figure 5.5. B).

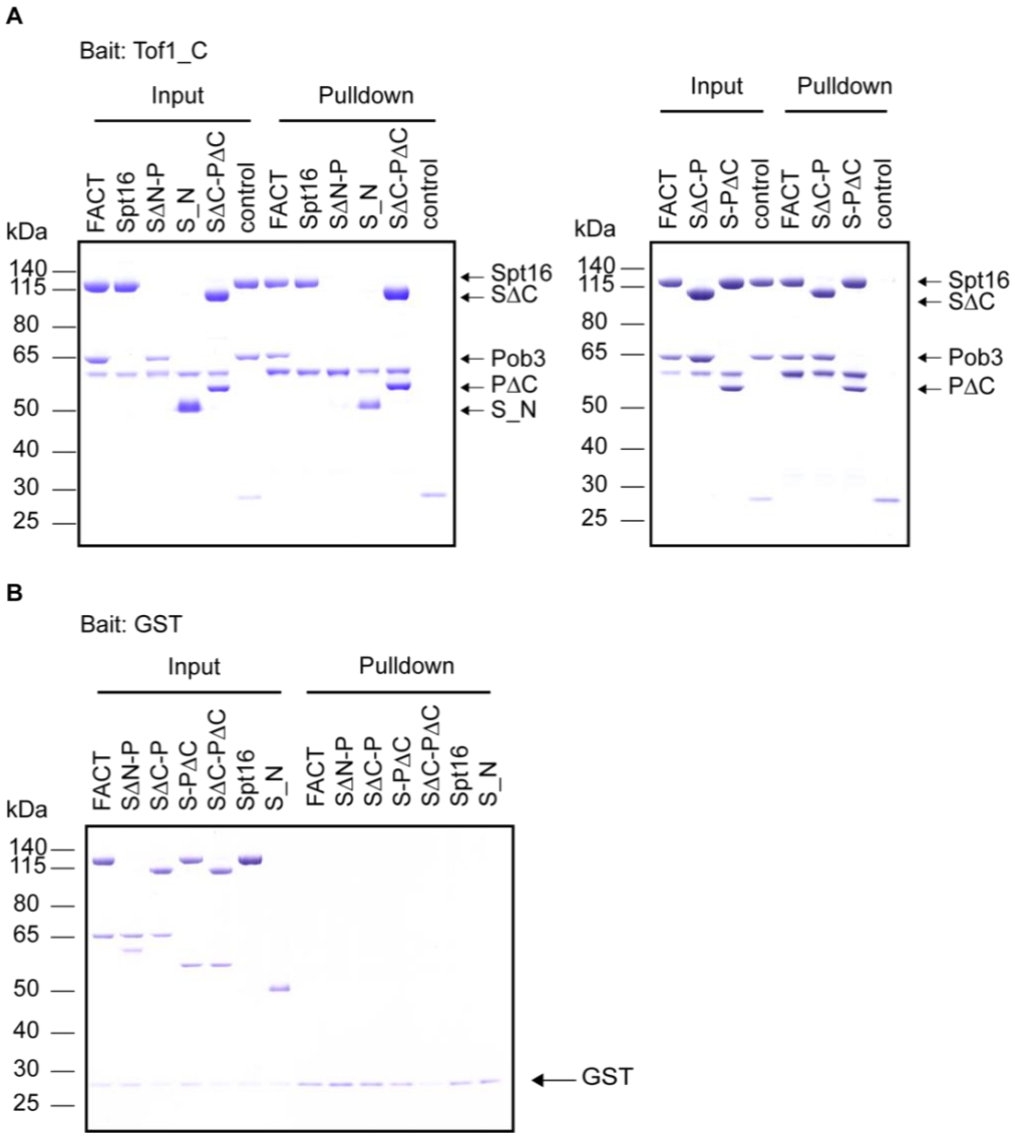

Figure 5.7. Interaction of Tof1_C and FACT truncations.
(**A**) Pulldown assay with 1.5 µM GST-tagged Tof1_C, 3 µM of fl FACT and FACT truncations were used as a prey. Left: Tof1_C retained Spt16, N-domain of Spt16 (S_N) and SΔC-PΔC, in addition to fl FACT. FACT truncations missing Spt16 N-domain, SΔN-P, did not bind to Tof1_C. Right: Tof1_C also retained SΔC-P and S-PΔC. GST control is shown. (**B**) GST-control pulldown assay with all tested FACT truncations, no truncations are retained by GST alone.

Next, I sought to identify the FACT domain responsible for the interaction with Tof1. To this end, I probed a range of FACT truncations, used in FRET assays (Figure 4.7), for their interaction with Tof1_C. In addition to fl FACT, the Spt16 subunit on its own also interacts with Tof1_C. However, the truncation which profoundly destabilized nucleosomes in the FRET assay, SΔN-P, was not retained by Tof1_C. Subsequently, I probed whether the Spt16_N, the domain which seems not to be involved in engaging with the nucleosome, is responsible for the association with Tof1. Indeed, I observed an interaction between Spt16_N and Tof1_C. Finally, the double C-termini truncation, SΔC-PΔC, which is not able to engage with the nucleosome, nevertheless interacts with Tof1_C (Figure 5.7). Taken together, these results indicate that FACT may be recruited to the replication fork by binding to the C-terminus of Tof1 via Spt16 N-domain, leaving the rest of FACT domains free for engagement with the nucleosome.

Interestingly, the C-terminus of Tof1 is also a site housing Top1 (Park and Sternglanz, 1999; Schalbetter et al., 2015; Shyian et al., 2020; Westhorpe et al., 2020), which suggests it could serve as a general interaction hub for recruitment of factors needed ahead of the replication fork. I wondered whether FACT and Top1 can simultaneously bind to Tof1 or their presence is mutually exclusive. Importantly, Top1 and FACT are known interaction partners (Husain et al., 2016). I designed a peptide library with 23 overlapping desthiobiotin-tagged peptides encompassing the Tof1_C in its entirety, which enabled us to screen for specific interaction interfaces between Tof1 and FACT. I found that Spt16_N predominantly interacts with the region of Tof1 between aa 1001 and 1022. Top1 was found to have a more extensive interaction interface spanning multiple peptides, with the most prominent one from aa 1040 to 1074 (Figure 5.8). Based on the peptide pulldowns, Spt16_N and Top1 were found to interact with two distinct, neighboring, sites on Tof1. Given the proximity of the uncovered interaction interfaces, together with the fact that Top1 has been shown to interact with FACT (Husain et al., 2016), one intriguing possibility is the formation of a trimeric Tof1-FACT-Top1 complex.

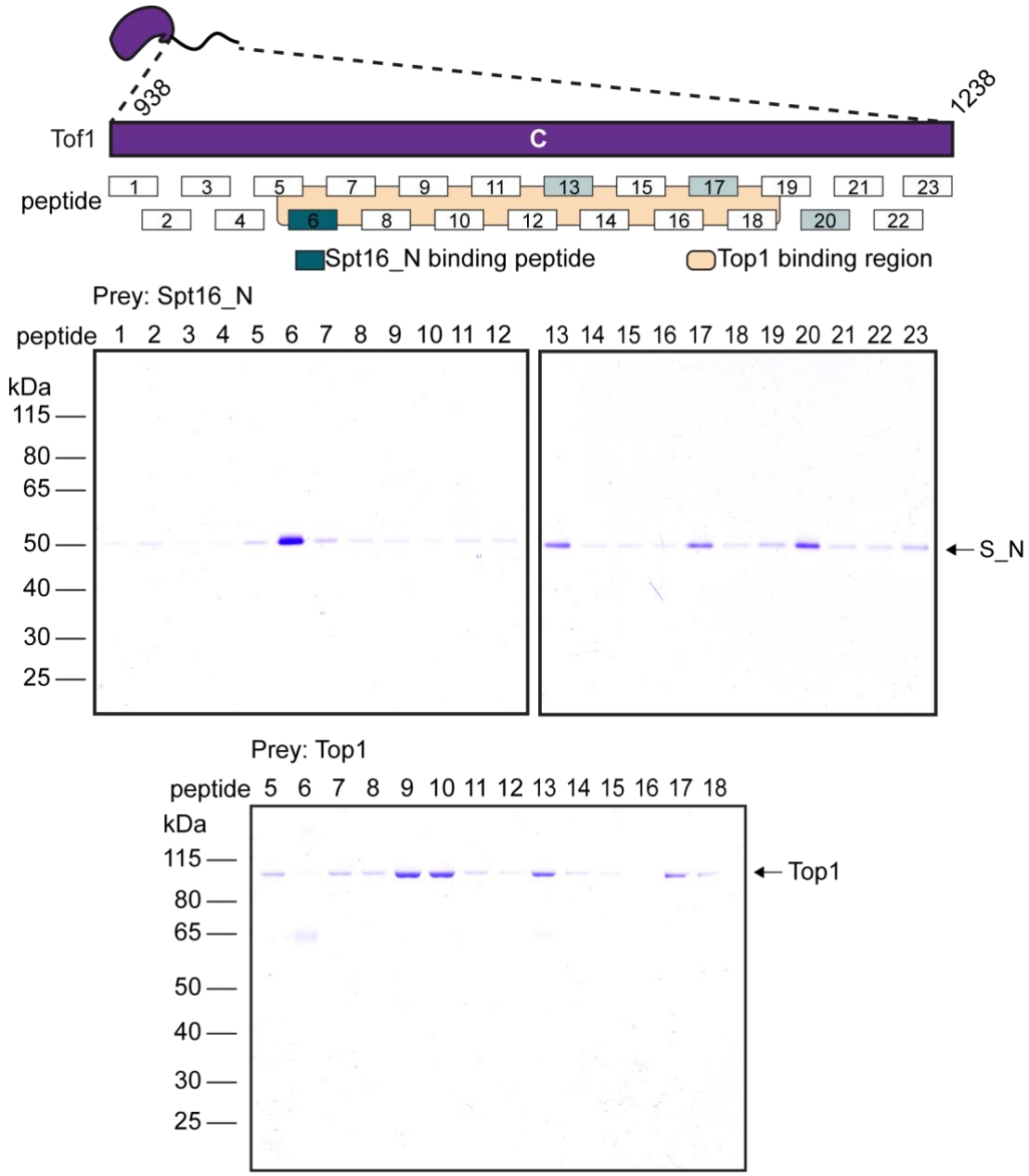

Figure 5.8. Peptide-screen to identify the key residues modulating Tof1 interactions.
Top: Representation of the peptide library coverage of Tof1_C. Top1 interacting region is shown in yellow. Middle: Streptavidin coated magnetic bead pulldown assay with the desthiobiotin-tagged peptides and Spt16 N-domain. The strongest interaction was detected for peptide 6, corresponding to the region of Tof1 between aa 1001 and 1022 (teal). Bottom: Streptavidin coated magnetic bead pulldown assay with the desthiobiotin-tagged peptides and Top1. The strongest interaction was detected for peptides 9 and 10, corresponding to the region of Tof1 between aa 1040 and 1074.

5.3.3. FACT nucleosome reorganization activity and interaction with Tof1 are both required for efficient replication of chromatin

The interaction between FACT and Tof1 I identified could provide an explanation for the requirement of high concentrations of FACT in the single-molecule assays to promote nucleosome reorganization. Clearly, the reorganization activity of FACT must be regulated to avoid random chromatin regions from being remodelled. The interaction with Tof1 would then focus the activity of FACT at the replication fork and contribute to establishing a high local concentration, thus creating a scenario analogous to the artificially high concentration employed in the single-molecule assays. This model is quite appealing and explains many disparate lines of evidence suggesting a direct role of FACT at the replication fork.

To investigate the importance of the activities of FACT I identified for replisome progression through the chromatin, an *in vitro* chromatin replication assay with a minimal set of components was conducted (Figure 5.9). The *in vitro* replication assay allowed us to specifically investigate the contribution of the individual FACT domains to chromatin replication.

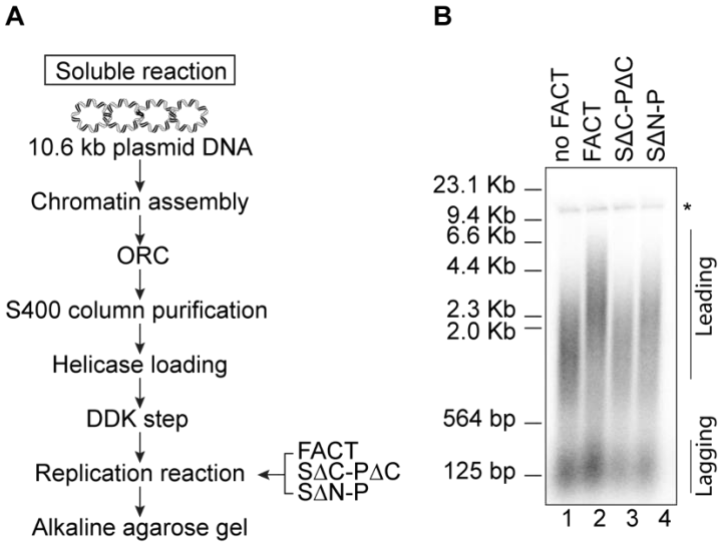

Figure 5.9. Chromatin replication assay.
(**A**) Reaction scheme of the *in vitro* chromatin replication assay. (**B**) Replication reactions on chromatin show loss of enhancement for SΔC-PΔC and SΔN-P as compared to fl FACT. Asterix indicates end labelling of nicked plasmid DNA.

I demonstrated in the FRET assays that FACT reorganizes nucleosomes into a more open complex with many histone-DNA contacts disrupted. These reorganized nucleosomes are more easily removed during unwinding of parental DNA leading to a faster rate of replication fork progression. This FACT enhancement can be monitored by measuring the rate at which the length of the leading-strand product increases because synthesis of the leading strand is directly coupled to unwinding of parental DNA. Notably, the replisome can progress through chromatin even in the absence of dedicated histone chaperones or remodellers. The level of background activity is strongly dependent on the level of chromatinization. This accounts for differences when comparing the results here with those of the previous report Kurat et al. (2017). Nevertheless, substantial FACT enhancement of chromatin replication is observed over background.

First, I asked whether the FACT construct lacking the C-terminal domains, SΔC-PΔC, which is unable to engage with mono-nucleosomes in the FRET assay, is still sufficient to promote replication through chromatin. Consistent with the previous findings (Figure 4.8), replication of chromatinized templates in the presence of SΔC-PΔC is defective to an extent comparable to the complete omission of FACT from the replication reaction (Figure 5.10). As the affinity of SΔC-PΔC for H2A/H2B histones is significantly lower compared to the wild-type FACT (Kemble et al., 2015), we performed *in vitro* chromatin replication across a range of concentrations, up to 400 nM. Even at high concentrations, no increase in the lengths of leading-strand replication products were detected (Figure 5.10).

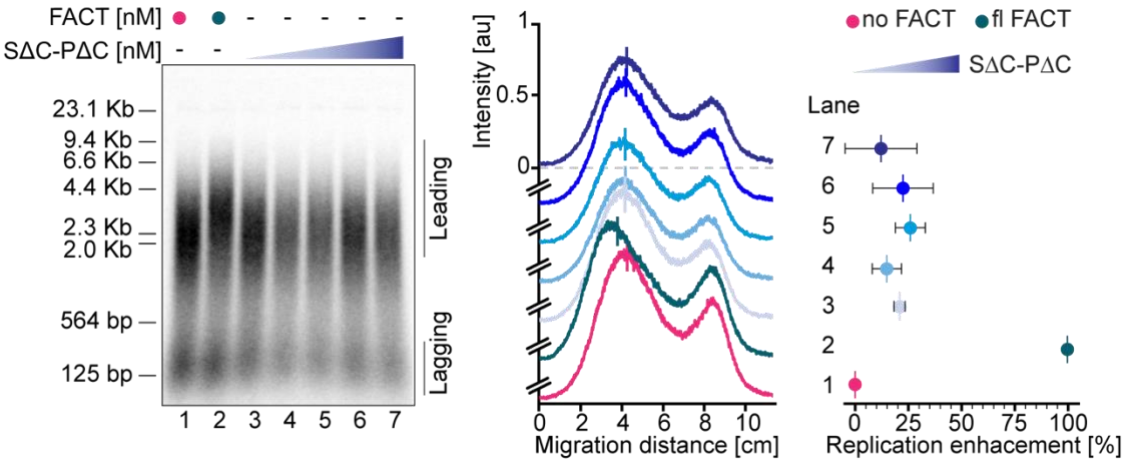

Figure 5.10. Chromatin replication assay with SΔC-PΔC.
Left: Replication reactions on chromatin done as in Figure 5.9, with the titration of SΔC-PΔC up to 400 nM, respectively. Middle: Lane profiles for the replication reactions of left, in the absence of FACT (magenta), with wt FACT (teal), and SΔC-PΔC (blue). Data were fit to a Gaussian distribution. The vertical line shows the mean of the distribution. Right: Enhancement of replication (%) based on the mean migration distance between replication reactions in the absence of FACT and with wt FACT. Recovery of replication enhancement is not observed with higher concentration of SΔC-PΔC.

Next, we investigated the importance of the FACT interaction with Tof1 via the N-terminal domain of Spt16. Unlike SΔC-P ΔC-, the SΔN-P truncation is able to stimulate chromatin replication, albeit not to the same extent as fl FACT (Figure 5.11). As before, we performed replication reactions for a wide range of concentrations to test whether higher concentration of the SΔN-P could restore replication efficiency to that of fl FACT. Interestingly, a positive correlation between the lengths of leading-strand replication products and SΔN-P concentration can be observed (Figure 5.11). Taken together, these assays shows a drastic difference between SΔC-PΔC and SΔN-P in their ability to promote replication on chromatin. The observed concentration dependency of SΔN-P to stimulate replication is consistent with the hypothesis that FACT is recruited by Tof1 to the front of the replication fork, where it can assist in nucleosome reorganization and histone handover, thereby contributing to replication efficiency.

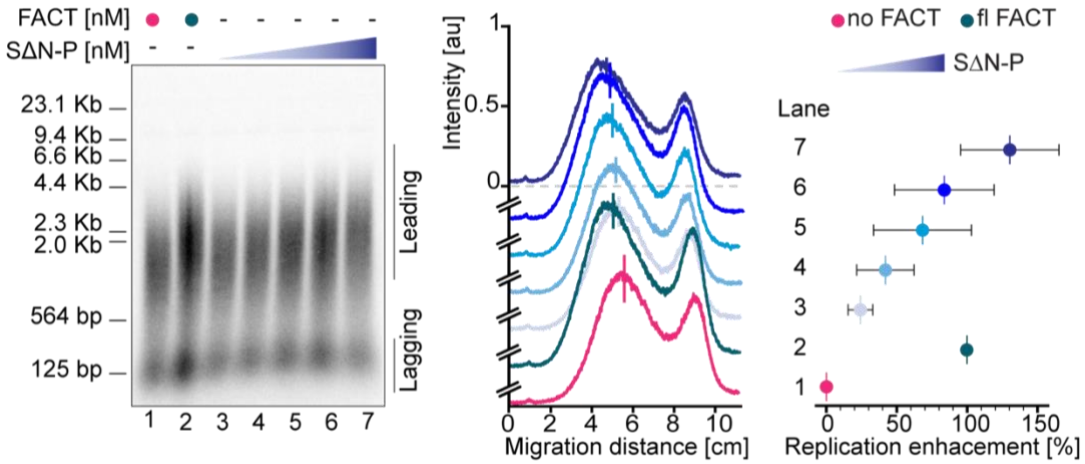

Figure 5.11. Chromatin replication assay with SΔN-P.
Left: Replication reactions on chromatin done as in Figure 5.9, with the titration of SΔN-P up to 400 nM. Middle: Lane profiles for the replication reactions in c and e, respectively, in the absence of FACT (magenta), with wt FACT (teal), and SΔN-P (blue). Data were fit to a Gaussian distribution. Right: Enhancement of replication (%) based on the mean migration distance between replication reactions in the absence of FACT and with wt FACT. Recovery of replication enhancement is observed with higher concentration of SΔN-P.

To further test the hypothesis, we examined the influence of TofΔC-Csm3 on replication. First, we confirmed TofΔC-Csm3 is able to support replication on naked DNA. Next, Tof1ΔC-Csm3 in chromatin replication assays over a range of FACT concentrations was evaluated, which revealed a result similar to assays performed with SΔN-P — in the presence of higher FACT concentration, longer leading-strand replication products could be observed (Figure 5.12). These experiments suggest the C-terminus of Tof1 is the primary location where FACT is recruited to the replication fork.

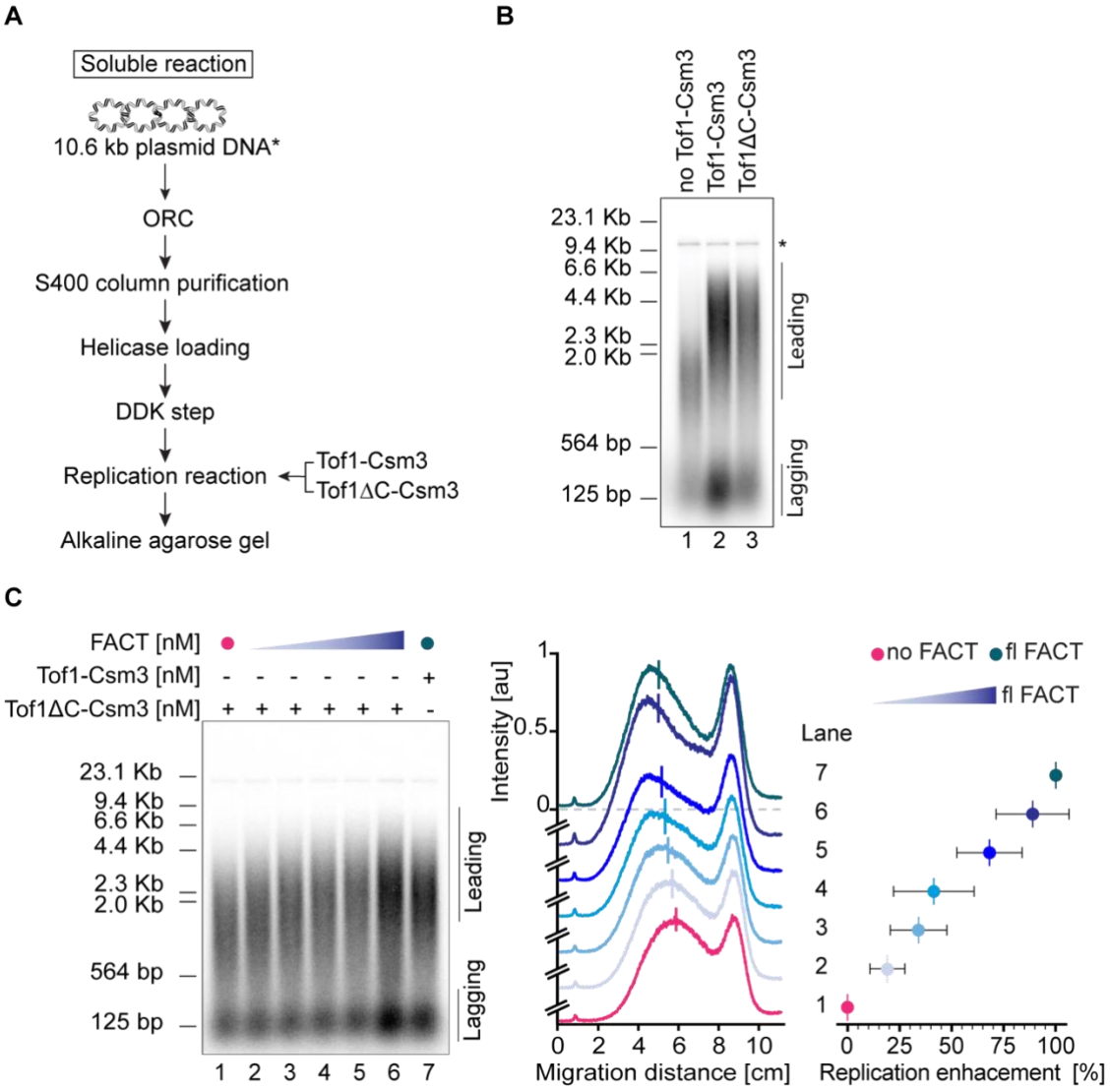

Figure 5.12. Implication of Tof1 in chromatin replication.
(**A**) Reaction scheme of the *in vitro* DNA replication assay probing the function of Tof1. (**B**) Replication reactions on naked DNA show activity of Tof1ΔC-Csm3 comparable to fl Tof1-Csm3. Asterix indicates end labelling of nicked plasmid DNA. (**C**) Left: Replication reactions on chromatin done as in Figure 5.9, with the titration of fl FACT up to 400 nM. Middle: Lane profiles for the replication reactions in c and e, respectively, in the absence of FACT (magenta), with wt FACT (teal), fl FACT and fl Tof1-Csm3 (teal), and Tof1ΔC-Csm3 with fl FACT titration (blue). Data were fit to a Gaussian distribution. The vertical line shows the mean of the distribution. Right: Enhancement of replication (%) based on the mean migration distance between replication reactions in the absence of FACT and with wt FACT. Recovery of replication enhancement is observed with higher concentration of fl FACT even with Tof1ΔC-Csm3

5.4. Discussion

FACT supports chromatin replication by disassembling parental nucleosomes

The recruitment site I have identified between the N-terminus of Spt16 and C-terminus of Tof1 would position FACT adjacent to parental nucleosomes as they approach the replication fork. Structural modelling with nucleosome-bound FACT and Csm3-Tof1-bound CMG demonstrates the feasibility of the resulting spatial organization (Figure 5.13). Moreover, further support for this arrangement comes from numerous studies demonstrating the critical importance of the N-terminal domain of Spt16 as well as biophysical investigations suggesting nucleosome breathing lasts for 50-60 ms. Recruiting FACT to a site directly adjacent to incoming nucleosomes would ensure it could engage during these breaking events to rapidly promote further nucleosome disassembly in a mechanism highly analogous to those proposed for transcription (Li et al., 2005).

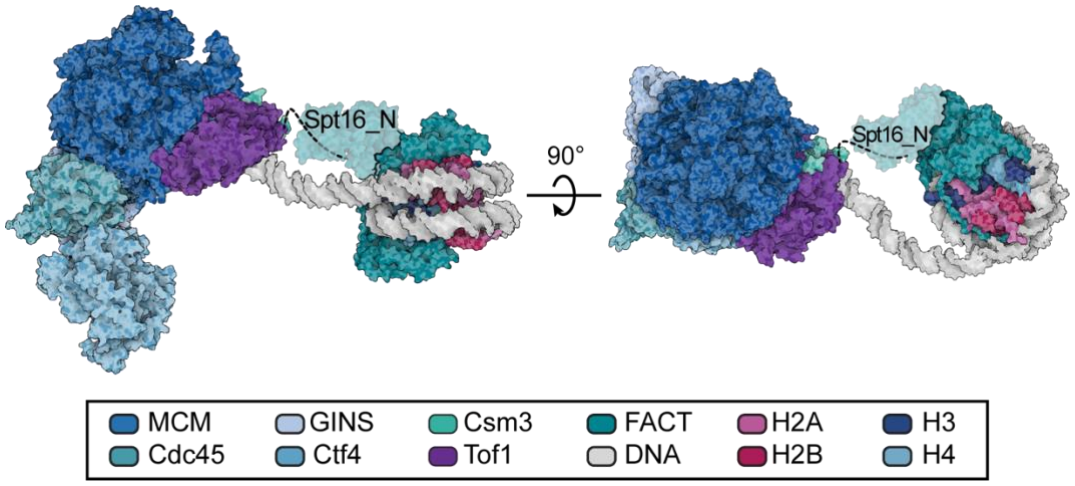

Figure 5.13. Model of CMG approaching the nucleosome with FACT engaged. Model is based on CMG-Ctf4-Tof1Csm3 structure (PDB 6SKL) and coordinates shown in Figure 4.11, with Spt15 N-domain (PDB 5E5B). Tof1 C-terminus (shown as dashed line) acts as an anchor for the N-domain of Spt16 (teal, shaded out).

In addition to the chromatin replication defect observed in this study, upon removal of the N-terminal domain of Spt16, multiple studies, particularly under the conditions of DNA replication stress, have demonstrated the importance of the highly conserved domain. In the absence of the N-domain, yeast cells become very sensitive to hydroxyurea (O'Donnell et al., 2004), while, in combination with mutations of the Pob3 subunit, more severe defects occur (VanDemark et al., 2008). Likewise, FACT was recently shown to be crucial for survival of replication stress in mammalian cells (Prendergast et al., 2020). From a structural perspective, the Spt16 N-domain is a

peptidase domain (Stuwe et al., 2008; VanDemark et al., 2008), which has not been shown to interact with nucleosome and has was not visible in structures showing nucleosome engagement by FACT (Liu et al., 2020). Taken together, FACT positioning at the replication fork by the N-domain of Spt16 through binding to Tof1 would provide an explanation for the indispensability of FACT in cells with high levels of replication stress, across different cell types and organisms.

Chapter 6: Summary and outlook

To understand the role of FACT in helping the replication machinery to overcome parental nucleosomes, I used single-molecule FRET to dissect the key interactions underlying nucleosome destabilization. Robust activity required high levels of FACT suggesting physical coupling to the replication machinery is needed to focus FACT activity. Guided by structures of replisome components, I identified sites of potential integration of FACT into the replication machinery and probed the influence of key factors on nucleosome reorganization activity of FACT. Detailed examination of possible interacting regions using pulldowns revealed that the N-terminus of Spt16, a protein interaction module I found to be dispensable for reorganization activity, binds to the C-terminus of Tof1 adjacent to a predicted Top1 binding site. Taken together, these findings strongly favor a model in which FACT is positioned by Tof1 to destabilize parental nucleosomes ahead of the replication fork. Further support for this model is provided by fully *in vitro* reconstituted chromatin replication assays demonstrating this interaction is required for enhancement of replication by FACT.

The structural model and biochemical insights suggest the following sequence of molecular events take place at the replication fork (Figure 6.1). As the CMG advances, Top1 continuously engages and helps to resolve positive supercoils that may transiently build-up ahead to support robust unwinding. As parental nucleosomes arrive at the replication fork, they become partially destabilized by the advancing helicase. This provides points of entry for FACT, which initially engages with any exposed histone binding site to promote further large-scale reorganization, followed by engagement at secondary and tertiary sites as they become available. As FACT replaces DNA contacts and promotes further opening, other histone binding domains at the replication fork — such as MCM2, Ctf4 and Pol α — would have the opportunity to scavenge for exposed histones. In the absence of binding by additional factors, FACT possesses sites for both the H3/H4 tetramer as well as two H2A/H2B dimers allowing the chaperone to aid in handing off all the protein components of the nucleosome for downstream processing. My observations provide few hints about further downstream events, but I speculate that the individual weaker interactions with each histone dimer could help to facilitate this process by allowing each subdomain of FACT to sequentially disengage as handoff opportunities arise. This process could occur directly during reassembly on the daughter strands or during handoff to intermediate factors, known to bind FACT, such as Pol α.

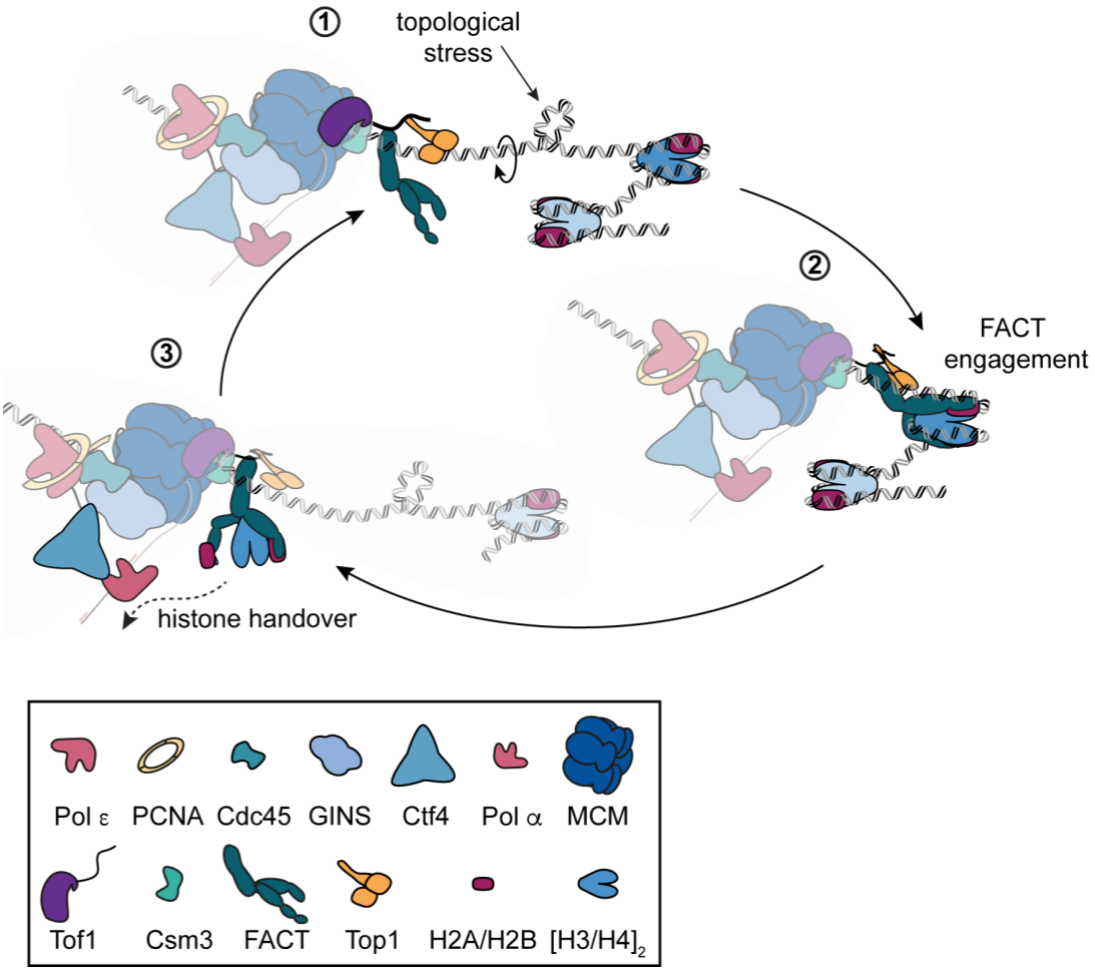

Figure 6.1. Model of FACT recruitment and replication-dependent nucleosome reorganization.
The sequence of molecular events to take place at the replication fork: (1) Topoisomerase 1 (Top1) acts in front of the fork to resolve topological stress that builds up as the replication fork approaches the nucleosome. (2) The advancing replisome pulls on DNA, exposing parts of H2A/H2B where FACT can bind, thus preventing DNA rebinding, and, with further DNA unpeeling from the nucleosome, captures the rest of the histones. (3) Having secured the histones, FACT participates in downstream handover pathways to ensure they are eventually re-incorporated into the newly synthetized DNA strands.

While numerous hints have emerged that suggest histone chaperones and remodelers may be integral members of replication complexes, little is known about the contact network supporting their integration. I speculate that the FACT binding site in Tof1 is only the beginning and that more binding sites are positioned throughout the replication machinery. The observations suggest these sites may not only serve to recruit the histone processing machinery, but also ensure each factor is positioned at the right location and properly regulated. Determining the functional importance of distinct interactions in the context of replication has long been a challenge. Replisomes themselves are highly redundant machines with multiple pathways available to overcome unexpected changes in composition (Scherr et al., 2018). I anticipate, and

recent work suggests, that the nucleosome processing pathway is no different. In fact, the considerable replication through chromatin observed *in vitro*, even in the absence of FACT, represents an intrinsic nucleosome removal activity of the replisome in the absence of dedicated factors. Redundancy often makes it difficult to clearly delineate the roles of distinct factors and interactions. However, single-molecule studies of *in vitro* reconstituted replication factors and complexes provide high spatial and temporal resolution and provide an opportunity to gain a direct view of the network of distinct interactions that underlie the molecular wiring of the megamachines of the cell.

If the incredible methodological developments and major breakthroughs in the field since the beginning on this project are any indication of things to come, in the next few years we might very well understand the orchestration of the remarkable molecular machine responsible for chromatin replication.

Appendix

Table 1. Analysis of single-molecule FRET assays of FACT engagement with nucleosomes.
Data visualized in Figure 4.4, reporting on the loss of FRET (%).

Sample	Loss of FRET (%)	Group mean	s.d.
nucleosome_1	6.70	9.23	2.20
nucleosome_2	10.67		
nucleosome_3	10.33		
Nhp6_1	10.76	10.96	1.15
Nhp6_2	12.20		
Nhp6_3	9.93		
FACT_1	12.90	10.47	3.01
FACT_2	7.10		
FACT_3	11.41		
yFACT_1	72.08	72.12	0.46
yFACT_2	72.60		
yFACT_3	71.69		

Table 2. Statistical analysis of FRET assays in Table 1.
One-way ANOVA with Tukey HSD post hoc test reporting the *p* values.

ANOVA		
F(3,9) = 744.80, p=3.98e-10		
Tukey HSD post hoc test		
Group 1	**Group 2**	***p* value**
nucleosome	Nhp6	0.696
nucleosome	FACT	0.853
FACT	Nhp6	0.900
FACT	yFACT	0.001
Nhp6	yFACT	0.001
nucleosome	yFACT	0.001

Table 3. FACT truncations sizes.

Protein	**aa range**
Spt16 wt	1 - 1035
Spt16ΔN	452 -1035
Spt16ΔC	1 - 958
Spt16 MBD	965 - 990
Pob3 wt	1 - 552
Pob3ΔC	1 - 477
Pob3 MBD	505-529

Table 4. Analysis of single-molecule FRET assays with FACT truncations.
Data visualized in Figure 4.8 reporting on the loss of FRET (%).

Sample	Loss of FRET %	Group mean	s.d.
yFACT_1	72.08	72.12	0.46
yFACT_2	72.60		
yFACT_3	71.69		
SΔNP_1	63.44	64.95	1.39
SΔNP_2	65.24		
SΔNP_3	66.18		
SPΔC_1	62.37	62.99	5.62
SPΔC_2	68.9		
SPΔC_3	57.71		
SΔCP_1	49.9	46.82	4.04
SΔCP_2	48.32		
SΔCP_3	42.25		
ΔCΔC_1	11.34	13.09	2.87
ΔCΔC_2	11.52		
ΔCΔC_3	16.4		
Spt16_1	13.52	13.13	0.35
Spt16_2	12.84		
Spt16_3	13.03		
nucleosome_1	6.70	9.23	2.20
nucleosome_2	10.67		
nucleosome_3	10.33		

Table 5. Statistical analysis of FRET assays in Table 4.
One-way ANOVA with Tukey HSD post hoc test reporting the *p* values.

ANOVA		
F(6,15)=255.72, p=1.75e-13		
Tukey HSD post hoc test		
Group 1	**Group 2**	***p* value**
nucleosome	ΔCΔC	0.682
nucleosome	Spt16	0.673
Spt16	ΔCΔC	0.900
nucleosome	SΔCP	0.001
nucleosome	SPΔC	0.001
nucleosome	SΔNP	0.001
nucleosome	yFACT	0.001
Spt16	SΔNP	0.001
Spt16	yFACT	0.001
ΔCΔC	SΔNP	0.001
ΔCΔC	yFACT	0.001
SΔCP	Spt16	0.001
SΔCP	ΔCΔC	0.001
SΔCP	SΔNP	0.001
SΔCP	yFACT	0.001
SPΔC	SΔCP	0.001
SPΔC	Spt16	0.001
SPΔC	ΔCΔC	0.001
SPΔC	SΔNP	0.900
SPΔC	yFACT	0.029
SΔNP	yFACT	0.118

Table 6. Analysis of single-molecule FRET assays with minimal binding regions.
Data visualized in Figure 4.10, reporting on the loss of FRET (%).

Sample	Loss of FRET %	Group mean	s.d.
S_N_1	10.40	8.20	3.17
S_N_2	9.64		
S_N_3	4.57		
SΔNPΔC_1	44.92	44.11	3.98
SΔNPΔC _2	47.63		
SΔNPΔC _3	39.79		
S_{MBD}_1	9.81	8.61	1.08
S_{MBD}_2	7.70		
S_{MBD}_3	8.33		
P_{MBD}_1	12.98	13.76	2.42
P_{MBD}_2	11.83		
P_{MBD}_3	16.48		
SΔCP + S_{MBD}_1	39.2	41.97	3.03
SΔCP + S_{MBD}_2	45.2		
SΔCP + S_{MBD}_3	41.52		
SPΔC + P_{MBD}_1	65.5	64.22	4.78
SPΔC + P_{MBD}_2	68.22		
SPΔC + P_{MBD}_3	58.93		

Table 7. Analysis of single-molecule FRET assays with replisome factors.
Data visualized in Figure 5.4, reporting on the loss of FRET (%).

Sample	Loss of FRET (%)	Group mean	s.d.	Loss of FRET (%)	Group mean	s.d.
yFACT		-			+	
Polα_1	13.92	9.69	3.78	65.17	78.41	11.50
Polα_2	6.67			85.93		
Polα_3	8.47			84.13		
Asf1_1	12.69	8.68	3.51	70.98	82.22	10.13
Asf1_2	7.15			85.06		
Asf1_3	6.2			90.63		
MCM2_1	13	9.96	3.12	72.66	84.23	10.11
MCM2_2	6.76			88.61		
MCM2_3	10.13			91.41		
Ctf4_1	22.65	13.27	8.13	63.41	79.52	14.14
Ctf4_2	9.06			85.28		
Ctf4_3	8.11			89.87		
Cdc45_1	14.13	12.10	3.13	62.35	75.96	12.20
Cdc45_2	8.49			79.64		
Cdc45_3	13.67			85.9		
GINS_1	25.99	15.41	9.18	68.96	81.71	12.26
GINS_2	10.62			82.76		
GINS_3	9.61			93.41		
Tof1Csm3_1	13.09	7.87	4.53	55.26	53.31	1.69
Tof1 Csm3_2	5.09			52.28		
Tof1 Csm3_3	5.42			52.39		

Table 8. Analysis of single-molecule FRET assays with Tof1_C and Tof1ΔN-Csm3.
Data visualized in Figure 5.5, reporting on the loss of FRET (%).

Sample	Loss of FRET %	Group mean	s.d.
Tof1_C_1	87.42	85.54	1.69
Tof1_C_2	85.07		
Tof1_C_3	84.14		
Tof1ΔN-Csm3_1	77.02	80.27	4.79
Tof1ΔN-Csm3_2	85.77		
Tof1ΔN-Csm3_3	78.02		

Table 9. Peptides synthesized based on Tof1_C (938-1238 aa).

Peptide	Sequence	aa range
1	Desthiobiotin-PSSSYLLRVRSEKDSFSHNEQD-NH2	938-960
2	Desthiobiotin-EKDSFSHNEQDGWEGDDDYDYN-NH2	949-970
3	Desthiobiotin-EGDDDYDYNDPYIVPDDQILSK-NH2	962-983
4	Desthiobiotin-VPDDQILSKSDAAYFKDLDNNA-NH2	975-996
5	Desthiobiotin-YFKDLDNNASDKLKGTKFSKGI-NH2	988-1009
6	Desthiobiotin-KGTKFSKGIARSKKKDKRKRRK-NH2	1001-1022
7	Desthiobiotin-KKDKRKRRKGEAKTNLPMFGDQ-NH2	1016-1035
8	Desthiobiotin-TNLPMFGDQDDERPQTVRERHG-NH2	1027-1048
9	Desthiobiotin-PQTVRERHGVFSKEFISDSEDD-NH2	1040-1061
10	Desthiobiotin-EFISDSEDDEDLMNPIFFENET-NH2	1053-1074
11	Desthiobiotin-NPIFFENETYMRWLLDKNNGQL-NH2	1066-1087
12	Desthiobiotin-LLDKNNGQLTEDRYIQFAKFAA-NH2	1079-1100
13	Desthiobiotin-YIQFAKFAAERMNNGGVVTGDY-NH2	1092-1113
14	Desthiobiotin-NGGVVTGDYTSLFGGSIPSIES-NH2	1105-1126
15	Desthiobiotin-GGSIPSIESIRATESSSFAPDK-NH2	1118-1139
16	Desthiobiotin-ESSSFAPDKSLISLASHVASEM-NH2	1131-1152
17	Desthiobiotin-LASHVASEMSIFDVNNNNNNQL-NH2	1144-1165
18	Desthiobiotin-VNNNNNNQLSDDDVNSESRNSL-NH2	1157-1178
19	Desthiobiotin-VNSESRNSLGSSQPSNSQNMFQ-NH2	1170-1191
20	Desthiobiotin-PSNSQNMFQSEVYSRKESTKRS-NH2	1183-1204
21	Desthiobiotin-SRKESTKRSLEASAADESDEDE-NH2	1196-1215
22	Desthiobiotin-AADESDEDEEAIRLFGKKSRVV-NH2	1209-1230
23	Desthiobiotin-EEAIRLFGKKSRVVLSQGDSDD-NH2	1217-1238

Table 10. Plasmids used in this study.

Plasmid	Plasmid construction	Reference
pRS306G-CSM3-CBP/TOF1	CSM3 amplified from *S. cerevisiae* W303, C-terminal CBP tag, TOF1 amplified from *S. cerevisiae* W303	Devbhandari and Remus, 2020
pET15b-Ctf4	CTF4 amplified from *S. cerevisiae* W303, N-terminal 6xHis-tag	Devbhandari et al., 2017
pRS304G-Cdc45	CDC45 amplified from *S. cerevisiae* W303	Devbhandari et al., 2017
pFJD5-GINS	Psf3 subunit with an N-terminal His-tag	Yeeles et al., 2015
pSmt3-Asf1	ASF1 amplified from *S. cerevisiae* W303, N-terminal SUMO-tag	Remus lab
pBS42	Pob3 amplified from ScCD00751520 (DNASU), in 12ADE-B (#48298, Addgene)	This study
pBS43	Spt16 amplified from ScCD00751519 (DNASU), in 12TRP-U (#48303, Addgene)	This study
pBS49	synthetic ORFs, H2AH2B in pETDuet	Kingston et al., 2011, this study
pBS50	synthetic ORFs, H3H4 in pCDFDuet	Kingston et al., 2011, this study
pBS04	NHP6 amplified from *S. cerevisiae* W303, in pET28a (#69864, Novagen)	This study
pBS38	MCM2 (1-200 aa) amplified from *S. cerevisiae* W303, in MSV027	This study
MSV069	synthetic ORF, Tof1 (1-638 aa) in MSV027	This study
MSV082	synthetic ORF, Tof1 (793-937 aa) in MSV027	This study
MSV084	synthetic ORF, Tof1 (938-1238 aa) in MSV027	This study
MSV097	synthetic ORF, Tof1 (639-1238 aa) in MSV027	This study
MSV016	synthetic ORF, Csm3 in 1G (#29655, Addgene)	This study
pBS61	SPT16 amplified from *S. cerevisiae* W303, 1B (#29653, Addgene)	This study
pBS63	SPT16 (1-451 aa) amplified from pBS61, in 12ADE-B (#48298, Addgene)	This study
pBS47	SPT16 (452-1035 aa) amplified from pBS61, in 12ADE-B (#48298, Addgene)	This study
pBS46	SPT16 (1-958 aa) amplified from pBS61, in 12ADE-B (#48298, Addgene)	This study
pBS48	POB3 (1-477 aa) amplified pBS42, in 12ADE-B (#48298, Addgene)	This study
pBS65	CSM3 amplified from *S. cerevisiae* W303, in 12TRP-U (#48303, Addgene)	This study
pBS66	TOF1 (1-937 aa) amplified from pBS64, in 12ADE-B (#48298, Addgene)	This study
pBS71	GST-POB3 amplified from pBS42, in 12TRP-U (#48303, Addgene)	This study
MSV027	His6-GST ligated into 9B (#48284, Addgene)	This study

Table 11. Yeast strains used in this study.

Strain	Genotype	Reference
YDR137	MATa ade2-1 ura3-1 his3-11,15 trp1-1 leu2-3,112 can1-100 pep4::kanMX bar::hphNAT1 Gal-GAL4 (HIS3) Gal-CSM3-CBP / TOF1 (URA3)	Devbhandari and Remus, 2020
YSD15	MATa ade2-1 ura3-1 his3-11,15 trp1-1 leu2-3,112 can1-100 pep4::kanMX bar::hphNAT1 (hygromycinB) Gal-Gal4 (HIS3) Gal-Cdc45-IF(TRP1)	Devbhandari et al., 2017
YSD16	MATa ade2-1 ura3-1 his3-11,15 trp1-1 leu2-3,112 can1-100 pep4::kanMX bar::hphNAT1 GalGAL4 (HIS3) GAL-POL1/POL12 (URA3) GAL-CBP-PRI1/PRI2 (LEU2)	Devbhandari et al., 2017
yBS2	MATa leu2-3,112 trp1-1 can1-100 ura3-1 ade2-1 his3-11,15 pep4::kanMX	This study

References

Abi-Ghanem, J., Samsonov, S.A., and Pisabarro, M.T. (2015). Insights into the preferential order of strand exchange in the Cre/loxP recombinase system: impact of the DNA spacer flanking sequence and flexibility. J Comput Aided Mol Des *29*, 271-282.

Ahmad, K., and Henikoff, S. (2002). The histone variant H3.3 marks active chromatin by replication-independent nucleosome assembly. Molecular Cell *9*, 1191-1200.

Alberts, B.M., Barry, J., Bedinger, P., Formosa, T., Jongeneel, C.V., and Kreuzer, K.N. (1983). Studies on DNA replication in the bacteriophage T4 *in vitro* system. Cold Spring Harb Symp Quant Biol *47 Pt 2*, 655-668.

Allain, F.H., Yen, Y.M., Masse, J.E., Schultze, P., Dieckmann, T., Johnson, R.C., and Feigon, J. (1999). Solution structure of the HMG protein NHP6A and its interaction with DNA reveals the structural determinants for non-sequence-specific binding. EMBO J *18*, 2563-2579.

Allfrey, V.G., Faulkner, R., and Mirsky, A.E. (1964). Acetylation and Methylation of Histones and Their Possible Role in Regulation of RNA Synthesis. Proceedings of the National Academy of Sciences of the United States of America *51*, 786-+.

Aparicio, O.M., Weinstein, D.M., and Bell, S.P. (1997). Components and dynamics of DNA replication complexes in *S. cerevisiae*: redistribution of MCM proteins and Cdc45p during S phase. Cell *91*, 59-69.

Avery, O.T., MacLeod, C.M., and McCarty, M. (1944). Studies on the Chemical Nature of the Substance Inducing Transformation of Pneumococcal Types Induction of Transformation by a Desoxyribonucleic Acid Fraction Isolated from Pneumococcus Type Iii. J Exp Med *79*, 137-158.

Bando, M., Katou, Y., Komata, M., Tanaka, H., Itoh, T., Sutani, T., and Shirahige, K. (2009). Csm3, Tof1, and Mrc1 Form a Heterotrimeric Mediator Complex That Associates with DNA Replication Forks. Journal of Biological Chemistry *284*, 34355-34365.

Bannister, A.J., and Kouzarides, T. (2011). Regulation of chromatin by histone modifications. Cell Res *21*, 381-395.

Baretic, D., Jenkyn-Bedford, M., Aria, V., Cannone, G., Skehel, M., and Yeeles, J.T.P. (2020). Cryo-EM Structure of the Fork Protection Complex Bound to CMG at a Replication Fork. Molecular Cell *78*, 926-+.

Batra, J., Xu, K., and Zhou, H.X. (2009). Nonadditive effects of mixed crowding on protein stability. Proteins *77*, 133-138.

Beattie, T.R., Kapadia, N., Nicolas, E., Uphoff, S., Wollman, A.J., Leake, M.C., and Reyes-Lamothe, R. (2017). Frequent exchange of the DNA polymerase during bacterial chromosome replication. Elife *6*, e21763.

Bell, S.P., and Stillman, B. (1992). ATP-dependent recognition of eukaryotic origins of DNA replication by a multiprotein complex. Nature *357*, 128-134.

Bellelli, R., Belan, O., Pye, V.E., Clement, C., Maslen, S.L., Skehel, J.M., Cherepanov, P., Almouzni, G., and Boulton, S.J. (2018). POLE3-POLE4 Is a Histone H3-H4 Chaperone that Maintains Chromatin Integrity during DNA Replication. Mol Cell *72*, 112-126 e115.

Belotserkovskaya, R., Oh, S., Bondarenko, V.A., Orphanides, G., Studitsky, V.M., and Reinberg, D. (2003). FACT facilitates transcription-dependent nucleosome alteration. Science *301*, 1090-1093.

Blomberg, N., Baraldi, E., Nilges, M., and Saraste, M. (1999). The PH superfold: a structural scaffold for multiple functions. Trends Biochem Sci *24*, 441-445.

Blow, J.J., and Laskey, R.A. (1988). A role for the nuclear envelope in controlling DNA replication within the cell cycle. Nature *332*, 546-548.

Böhm, V., Hieb, A.R., Andrews, A.J., Gansen, A., Rocker, A., Tóth, K., Luger, K., and Langowski, J. (2011). Nucleosome accessibility governed by the dimer/tetramer interface. Nucleic Acids Research *39*, 3093-3102.

Boyarchuk, E., Filipescu, D., Vassias, I., Cantaloube, S., and Almouzni, G. (2014). The histone variant composition of centromeres is controlled by the pericentric heterochromatin state during the cell cycle. J Cell Sci *127*, 3347-3359.

Brehove, M., Wang, T., North, J., Luo, Y., Dreher, S.J., Shimko, J.C., Ottesen, J.J., Luger, K., and Poirier, M.G. (2015). Histone Core Phosphorylation Regulates DNA Accessibility. Journal of Biological Chemistry *290*, 22612-22621.

Brewster, N.K., Johnston, G.C., and Singer, R.A. (2001). A bipartite yeast SSRP1 analog comprised of Pob3 and Nhp6 proteins modulates transcription. Molecular and Cellular Biology *21*, 3491-3502.

Burgers, P.M.J., and Kunkel, T.A. (2017). Eukaryotic DNA Replication Fork. Annu Rev Biochem *86*, 417-438.

Buschbeck, M., and Hake, S.B. (2017). Variants of core histones and their roles in cell fate decisions, development and cancer. Nat Rev Mol Cell Bio *18*, 299-314.

Calzada, A. (2005). Molecular anatomy and regulation of a stable replisome at a paused eukaryotic DNA replication fork. Genes & Development *19*, 1905-1919.

Carroll, C.W., Milks, K.J., and Straight, A.F. (2010). Dual recognition of CENP-A nucleosomes is required for centromere assembly. J Cell Biol *189*, 1143-1155.

Cha, T.A., and Alberts, B.M. (1989). The Bacteriophage T4 DNA Replication Fork. Journal of Biological Chemistry *264*, 12220-12225.

Chen, C.C., Bowers, S., Lipinszki, Z., Palladino, J., Trusiak, S., Bettini, E., Rosin, L., Przewloka, M.R., Glover, D.M., and O'Neill, R.J. (2015). Establishment of centromeric chromatin by the CENP-A assembly factor CAL1 requires FACT-Mediated transcription. Dev Cell *34*, 73-84.

Chen, P., Dong, L., Hu, M., Wang, Y.Z., Xiao, X., Zhao, Z., Yan, J., Wang, P.Y., Reinberg, D., and Li, M. (2018a). Functions of FACT in breaking the nucleosome and maintaining its integrity at the single-nucleosome level. et al *71*, 284-293.

Chen, P., Dong, L.P., Hu, M.L., Wang, Y.Z., Xiao, X., Zhao, Z.L., Yan, J., Wang, P.Y., Reinberg, D., Li, M.*, et al.* (2018b). Functions of FACT in Breaking the Nucleosome and Maintaining Its Integrity at the Single-Nucleosome Level. Molecular Cell *71*, 284-+.

Cho, W.H., Kang, Y.H., An, Y.Y., Tappin, I., Hurwitz, J., and Lee, J.K. (2013). Human Tim-Tipin complex affects the biochemical properties of the replicative DNA helicase and DNA polymerases. Proc Natl Acad Sci U S A *110*, 2523-2527.

Clegg, R.M. (2009). Forster resonance energy transfer-FRET what is it, why do it, and how it's done. Lab Tech Biochem Mol *33*, 1-57.

Cocker, J.H., Piatti, S., Santocanale, C., Nasmyth, K., and Diffley, J.F. (1996). An essential role for the Cdc6 protein in forming the pre-replicative complexes of budding yeast. Nature *379*, 180-182.

Corn, J.E., Pease, P.J., Hura, G.L., and Berger, J.M. (2005). Crosstalk between primase subunits can act to regulate primer synthesis in trans. Mol Cell *20*, 391-401.

Costa, A., Ilves, I., Tamberg, N., Petojevic, T., Nogales, E., Botchan, M.R., and Berger, J.M. (2011). The structural basis for MCM2–7 helicase activation by GINS and Cdc45. Nature Structural & Molecular Biology *18*, 471-477.

Costa, A., Renault, L., Swuec, P., Petojevic, T., Pesavento, J.J., Ilves, I., MacLellan-Gibson, K., Fleck, R.A., Botchan, M.R., and Berger, J.M. (2014). DNA binding polarity, dimerization, and ATPase ring remodeling in the CMG helicase of the eukaryotic replisome. Elife *3*, e03273.

Costanzi, C., Stein, P., Worrad, D.M., Schultz, R.M., and Pehrson, J.R. (2000). Histone macroH2A1 is concentrated in the inactive X chromosome of female preimplantation mouse embryos. Development *127*, 2283-2289.

Cucinotta, C.E., Hildreth, A.E., McShane, B.M., Shirra, M.K., and Arndt, K.M. (2019). The nucleosome acidic patch directly interacts with subunits of the Paf1 and FACT complexes and controls chromatin architecture *in vivo*. Nucleic Acids Res *47*, 8410-8423.

D'Anna, J.A., Jr., and Isenberg, I. (1974). A histone cross-complexing pattern. Biochemistry *13*, 4992-4997.

Dalgaard, J.Z., and Klar, A.J.S. (2000). swi1 and swi3 Perform Imprinting, Pausing, and Termination of DNA Replication in S. pombe. Cell *102*, 745-751.

Davey, C.A., Sargent, D.F., Luger, K., Maeder, A.W., and Richmond, T.J. (2002). Solvent mediated interactions in the structure of the nucleosome core particle at 1.9 angstrom resolution. Journal of Molecular Biology *319*, 1097-1113.

Deindl, S., Hwang, William L., Hota, Swetansu K., Blosser, Timothy R., Prasad, P., Bartholomew, B., and Zhuang, X. (2013). ISWI Remodelers Slide Nucleosomes with Coordinated Multi-Base-Pair Entry Steps and Single-Base-Pair Exit Steps. Cell *152*, 442-452.

Devbhandari, S., Jiang, J.Q., Kumar, C., Whitehouse, I., and Remus, D. (2017). Chromatin Constrains the Initiation and Elongation of DNA Replication. Molecular Cell *65*, 131-141.

Devbhandari, S., and Remus, D. (2020). Rad53 limits CMG helicase uncoupling from DNA synthesis at replication forks. Nature Structural & Molecular Biology *27*, 461-+.

Deyter, G.M., and Biggins, S. (2014). The FACT complex interacts with the E3 ubiquitin ligase Psh1 to prevent ectopic localization of CENP-A. Genes Dev *28*, 1815-1826.

Diffley, J.F., Cocker, J.H., Dowell, S.J., and Rowley, A. (1994). Two steps in the assembly of complexes at yeast replication origins *in vivo*. Cell *78*, 303-316.

Diffley, J.F.X., and Cocker, J.H. (1992). Protein-DNA interactions at a yeast replication origin. Nature *357*, 169-172.

Dixon, N.E. (2009). DNA replication: prime-time looping. Nature *462*, 854-855.

Donham, D.C., Scorgie, J.K., and Churchill, M.E.A. (2011). The activity of the histone chaperone yeast Asf1 in the assembly and disassembly of histone H3/H4-DNA complexes. Nucleic Acids Research *39*, 5449-5458.

Dorigo, B., Schalch, T., Bystricky, K., and Richmond, T.J. (2003). Chromatin fiber folding: requirement for the histone H4 N-terminal tail. J Mol Biol *327*, 85-96.

Douglas, M.E., Ali, F.A., Costa, A., and Diffley, J.F.X. (2018). The mechanism of eukaryotic CMG helicase activation. Nature *555*, 265-268.

Du, J.M., and Patel, D.J. (2014). Structural biology-based insights into combinatorial readout and crosstalk among epigenetic marks. Biochimica Et Biophysica Acta-Gene Regulatory Mechanisms *1839*, 719-727.

Duderstadt, K.E., Geertsema, H.J., Stratmann, S.A., Punter, C.M., Kulczyk, A.W., Richardson, C.C., and van Oijen, A.M. (2016). Simultaneous Real-Time Imaging of Leading and Lagging Strand Synthesis Reveals the Coordination Dynamics of Single Replisomes. Mol Cell *64*, 1035-1047.

Duina, A.A. (2011). Histone Chaperones Spt6 and FACT: Similarities and Differences in Modes of Action at Transcribed Genes. Genet Res Int *2011*, 625210.

Dulin, D., Lipfert, J., Moolman, M.C., and Dekker, N.H. (2013). Studying genomic processes at the single-molecule level: introducing the tools and applications. Nat Rev Genet *14*, 9-22.

Einstein, A. (1905). Über die von der molekularkinetischen Theorie der Wärme geforderte Bewegung von in ruhenden Flüssigkeiten suspendierten Teilchen. Annalen der Physik *322*, 549-560.

Eshaghpour, H., Dieterich, A.E., Cantor, C.R., and Crothers, D.M. (1980). Singlet-singlet energy transfer studies of the internal organization of nucleosomes. Biochemistry *19*, 1797-1805.

Evrin, C., Clarke, P., Zech, J., Lurz, R., Sun, J., Uhle, S., Li, H., Stillman, B., and Speck, C. (2009). A double-hexameric MCM2-7 complex is loaded onto origin DNA during licensing of eukaryotic DNA replication. Proc Natl Acad Sci U S A *106*, 20240-20245.

Evrin, C., Maman, J.D., Diamante, A., Pellegrini, L., and Labib, K. (2018). Histone H2A-H2B binding by Pol alpha in the eukaryotic replisome contributes to the maintenance of repressive chromatin. Embo Journal *37*.

Farnung, L., Ochmann, M., Engeholm, M., and Cramer, P. (2021). Structural basis of nucleosome transcription mediated by Chd1 and FACT. Nat Struct Mol Biol.

Fischer, H., and Hinkle, D.C. (1980). Bacteriophage T7 DNA replication *in vitro*. Stimulation of DNA synthesis by T7 RNA polymerase. Journal of Biological Chemistry *255*, 7956-7964.

Flemming, W. (1882). Zellsubstanz, Kern und Zelltheilung (Leipzig: Vogel).

Foltman, M., Evrin, C., De Piccoli, G., Jones, R.C., Edmondson, R.D., Katou, Y., Nakato, R., Shirahige, K., and Labib, K. (2013). Eukaryotic Replisome Components Cooperate to Process Histones During Chromosome Replication. Cell Reports *3*, 892-904.

Formosa, T. (2012). The role of FACT in making and breaking nucleosomes. Biochimica Et Biophysica Acta-Gene Regulatory Mechanisms *1819*, 247-255.

Formosa, T., Eriksson, P., Wittmeyer, J., Ginn, J., Yu, Y.X., and Stillman, D.J. (2001). Spt16-Pob3 and the HMG protein Nhp6 combine to form the nucleosome-binding factor SPN. Embo Journal *20*, 3506-3517.

Formosa, T., and Winston, F. (2020). The role of FACT in managing chromatin: disruption, assembly, or repair? Nucleic Acids Research *48*, 11929-11941.

Förster, T. (1948). Zwischenmolekulare Energiewanderung und Fluoreszenz. Annalen der Physik *437*, 55-75.

Franklin, R.E., and Gosling, R.G. (1953a). Molecular configuration in sodium thymonucleate. Nature *171*, 740-741.

Franklin, R.E., and Gosling, R.G. (1953b). Molecular structure of nucleic acids. Molecular configuration in sodium thymonucleate. 1953. Ann N Y Acad Sci *758*, 16-17.

Frick, D.N., and Richardson, C.C. (1999). Interaction of bacteriophage T7 gene 4 primase with its template recognition site. J Biol Chem *274*, 35889-35898.

Friedberg, E.C., Walker, G.C., Siede, W., Wood, R.D., Schultz, R.A., and Ellenberger, T. (2006). DNA Repair and Mutagenesis (American Society of Microbiology).

Gambus, A., Jones, R.C., Sanchez-Diaz, A., Kanemaki, M., van Deursen, F., Edmondson, R.D., and Labib, K. (2006a). GINS maintains association of Cdc45 with MCM in replisome progression complexes at eukaryotic DNA replication forks. Nat Cell Biol *8*, 358-U341.

Gambus, A., Jones, R.C., Sanchez-Diaz, A., Kanemaki, M., van Deursen, F., Edmondson, R.D., and Labib, K. (2006b). GINS maintains association of Cdc45 with MCM in replisome progression complexes at eukaryotic DNA replication forks. Nat Cell Biol *8*, 358-366.

Gambus, A., van Deursen, F., Polychronopoulos, D., Foltman, M., Jones, R.C., Edmondson, R.D., Calzada, A., and Labib, K. (2009). A key role for Ctf4 in coupling the MCM2-7 helicase to DNA polymerase alpha within the eukaryotic replisome. EMBO J *28*, 2992-3004.

Gan, H., Serra-Cardona, A., Hua, X., Zhou, H., Labib, K., Yu, C., and Zhang, Z. (2018a). The Mcm2-Ctf4-Polalpha Axis Facilitates Parental Histone H3-H4 Transfer to Lagging Strands. Mol Cell *72*, 140-151 e143.

Gan, H., Serra-Cardona, A., Hua, X., Zhou, H., Labib, K., Yu, C., and Zhang, Z. (2018b). The Mcm2-Ctf4-Polα Axis Facilitates Parental Histone H3-H4 Transfer to Lagging Strands. Molecular Cell *72*, 140-151.e143.

Gansen, A., Tóth, K., Schwarz, N., and Langowski, J. (2008). Structural Variability of Nucleosomes Detected by Single-Pair Förster Resonance Energy Transfer: Histone Acetylation, Sequence Variation, and Salt Effects. The Journal of Physical Chemistry B *113*, 2604-2613.

Gebhardt, C., Lehmann, M., Reif, M.M., Zacharias, M., and Cordes, T. (2020). Molecular and spectroscopic characterization of green and red cyanine fluorophores from the Alexa Fluor and AF series. bioRxiv, 2020.2011.2013.381152.

Geertsema, H.J., Kulczyk, A.W., Richardson, C.C., and van Oijen, A.M. (2014). Single-molecule studies of polymerase dynamics and stoichiometry at the bacteriophage T7 replication machinery. Proc Natl Acad Sci U S A *111*, 4073-4078.

Georgescu, R., Yuan, Z., Bai, L., de Luna Almeida Santos, R., Sun, J., Zhang, D., Yurieva, O., Li, H., and O'Donnell, M.E. (2017). Structure of eukaryotic CMG helicase at a replication fork and implications to replisome architecture and origin initiation. Proc Natl Acad Sci U S A *114*, E697-E706.

Georgescu, R.E., Langston, L., Yao, N.Y., Yurieva, O., Zhang, D., Finkelstein, J., Agarwal, T., and O'Donnell, M.E. (2014). Mechanism of asymmetric polymerase assembly at the eukaryotic replication fork. Nat Struct Mol Biol *21*, 664-670.

Gonzales, T., and Robert Baudouy, J. (1996). Bacterial aminopeptidases: Properties and functions. Fems Microbiol Rev *18*, 319-344.

Gordon, F., Luger, K., and Hansen, J.C. (2005). The core histone N-terminal tail domains function independently and additively during salt-dependent oligomerization of nucleosomal arrays. J Biol Chem *280*, 33701-33706.

Goswami, P., Abid Ali, F., Douglas, M.E., Locke, J., Purkiss, A., Janska, A., Eickhoff, P., Early, A., Nans, A., Cheung, A.M.C.*, et al.* (2018). Structure of DNA-CMG-Pol epsilon elucidates the roles of the non-catalytic polymerase modules in the eukaryotic replisome. Nature Communications *9*.

Gouridis, G., Schuurman-Wolters, G.K., Ploetz, E., Husada, F., Vietrov, R., de Boer, M., Cordes, T., and Poolman, B. (2015). Conformational dynamics in substrate-binding domains influences transport in the ABC importer GlnPQ. Nature Structural & Molecular Biology *22*, 57-64.

Graham, J.E., Marians, K.J., and Kowalczykowski, S.C. (2017). Independent and Stochastic Action of DNA Polymerases in the Replisome. Cell *169*, 1201-1213 e1217.

Groth, A., Corpet, A., Cook, A.J.L., Roche, D., Bartek, J., Lukas, J., and Almouzni, G. (2007). Regulation of replication fork progression through histone supply and demand. Science *318*, 1928-1931.

Hagerman, P.J. (1988). Flexibility of DNA. Annual Review of Biophysics and Biophysical Chemistry *17*, 265-286.

Hamdan, S.M., Loparo, J.J., Takahashi, M., Richardson, C.C., and van Oijen, A.M. (2009). Dynamics of DNA replication loops reveal temporal control of lagging-strand synthesis. Nature *457*, 336-339.

Han, J., Li, Q., McCullough, L., Kettelkamp, C., Formosa, T., and Zhang, Z. (2010). Ubiquitylation of FACT by the cullin-E3 ligase Rtt101 connects FACT to DNA replication. Genes Dev *24*, 1485-1490.

Harada, B.T., Hwang, W.L., Deindl, S., Chatterjee, N., Bartholomew, B., and Zhuang, X. (2016). Stepwise nucleosome translocation by RSC remodeling complexes. eLife *5*.

Hazan, Noa P., Tomov, Toma E., Tsukanov, R., Liber, M., Berger, Y., Masoud, R., Toth, K., Langowski, J., and Nir, E. (2015). Nucleosome Core Particle Disassembly and Assembly Kinetics Studied Using Single-Molecule Fluorescence. Biophysical Journal *109*, 1676-1685.

Heitz, E. (1929). Heterochromatin, Chromocentren, Chromomeren (Komm. Fischer).

Heitz, E., and Bauer, H. (1933). Beweise für die Chromosomennatur der Kernschleifen in den Knäuelkernen von Bibio hortulanus L. Zeitschrift für Zellforschung und Mikroskopische Anatomie *17*, 67-82.

Ho, Y., Gruhler, A., Heilbut, A., Bader, G.D., Moore, L., Adams, S.L., Millar, A., Taylor, P., Bennett, K., Boutilier, K.*, et al.* (2002). Systematic identification of protein complexes in Saccharomyces cerevisiae by mass spectrometry. Nature *415*, 180-183.

Hohlbein, J., Craggs, T.D., and Cordes, T. (2014). Alternating-laser excitation: single-molecule FRET and beyond (vol 43, pg 1156, 2014). Chem Soc Rev *43*, 6472-6472.

Holla, S., Dhakshnamoorthy, J., Folco, H.D., Balachandran, V., Xiao, H., Sun, L.-l., Wheeler, D., Zofall, M., and Grewal, S.I.S. (2020). Positioning Heterochromatin at the Nuclear Periphery Suppresses Histone Turnover to Promote Epigenetic Inheritance. Cell *180*, 150-164.e115.

Holzer, S., Degliesposti, G., Kilkenny, M.L., Maslen, S.L., Matak-Vinkovíc, D., Skehel, M., and Pellegrini, L. (2017). Crystal structure of the N-terminal domain of human Timeless and its interaction with Tipin. Nucleic Acids Research *45*, 5555-5563.

Hondele, M., and Ladurner, A.G. (2013). Catch me if you can: how the histone chaperone FACT capitalizes on nucleosome breathing. Nucleus *4*, 443-449.

Hooke, R. (1667). Micrographia, or, Some physiological descriptions of minute bodies made by magnifying glasses : with observations and inquiries thereupon (London : Printed for James Allestry ... and are to be sold at his shop ..., MDCLXV11 [1667]).

Hsieh, F.K., Kulaeva, O.I., Patel, S.S., Dyer, P.N., Luger, K., Reinberg, D., and Studitsky, V.M. (2013). Histone chaperone FACT action during transcription through chromatin by RNA polymerase II. Proceedings of the National Academy of Sciences of the United States of America *110*, 7654-7659.

Huang, H.D., Stromme, C.B., Saredi, G., Hodl, M., Strandsby, A., Gonzalez-Aguilera, C., Chen, S., Groth, A., and Patel, D.J. (2015). A unique binding mode enables MCM2 to chaperone histones H3-H4 at replication forks. Nature Structural & Molecular Biology *22*, 618-626.

Huertas, J., and Cojocaru, V. (2020). Breaths, Twists, and Turns of Atomistic Nucleosomes. J Mol Biol, 166744.

Husain, A., Begum, N.A., Taniguchi, T., Taniguchi, H., Kobayashi, M., and Honjo, T. (2016). Chromatin remodeller SMARCA4 recruits topoisomerase 1 and suppresses transcription-associated genomic instability. Nature Communications *7*.

Iashina, E.G., Velichko, E.V., Filatov, M.V., Bouwman, W.G., Duif, C.P., Brulet, A., and Grigoriev, S.V. (2017). Additive scaling law for structural organization of chromatin in chicken erythrocyte nuclei. Physical Review E *96*, 012411.

Ito, T., Bulger, M., Kobayashi, R., and Kadonaga, J.T. (1996). Drosophila NAP-1 is a core histone chaperone that functions in ATP-facilitated assembly of regularly spaced nucleosomal arrays. Molecular and Cellular Biology *16*, 3112-3124.

Itsathitphaisarn, O., Wing, R.A., Eliason, W.K., Wang, J., and Steitz, T.A. (2012). The hexameric helicase DnaB adopts a nonplanar conformation during translocation. Cell *151*, 267-277.

Jamai, A., Puglisi, A., and Strubin, M. (2009). Histone chaperone spt16 promotes redeposition of the original h3-h4 histones evicted by elongating RNA polymerase. Mol Cell *35*, 377-383.

Jeronimo, C., Poitras, C., and Robert, F. (2019). Histone Recycling by FACT and Spt6 during Transcription Prevents the Scrambling of Histone Modifications. Cell Rep *28*, 1206-1218 e1208.

Jones, M.L., Baris, Y., Taylor, M.R.G., and Yeeles, J.T.P. (2021). Structure of a human replisome shows the organisation and interactions of a DNA replication machine. The EMBO Journal.

Kaguni, J.M., and Kornberg, A. (1984). Replication initiated at the origin (oriC) of the E. coli chromosome reconstituted with purified enzymes. Cell *38*, 183-190.

Kalashnikova, A.A., Porter-Goff, M.E., Muthurajan, U.M., Luger, K., and Hansen, J.C. (2013). The role of the nucleosome acidic patch in modulating higher order chromatin structure. J R Soc Interface *10*.

Kang, Y.H., Farina, A., Bermudez, V.P., Tappin, I., Du, F., Galal, W.C., and Hurwitz, J. (2013). Interaction between human Ctf4 and the Cdc45/Mcm2-7/GINS (CMG) replicative helicase. Proc Natl Acad Sci U S A *110*, 19760-19765.

Kapadia, N., El-Hajj, Z.W., Zheng, H., Beattie, T.R., Yu, A., and Reyes-Lamothe, R. (2020). Processive Activity of Replicative DNA Polymerases in the Replisome of Live Eukaryotic Cells. Molecular Cell *80*, 114-126.e118.

Katou, Y., Kanoh, Y., Bando, M., Noguchi, H., Tanaka, H., Ashikari, T., Sugimoto, K., and Shirahige, K. (2003). S-phase checkpoint proteins Tof1 and Mrc1 form a stable replication-pausing complex. Nature *424*, 1078-1083.

Keller, D.M., and Lu, H. (2002). P53 serine 392 phosphorylation increases after UV through induction of the assembly of the CK2 center dot hSPT16 center dot SSRP1 complex. Journal of Biological Chemistry *277*, 50206-50213.

Kemble, D.J., McCullough, L.L., Whitby, F.G., Formosa, T., and Hill, C.P. (2015). FACT Disrupts Nucleosome Structure by Binding H2A-H2B with Conserved Peptide Motifs. Molecular Cell *60*, 294-306.

Kemble, D.J., Whitby, F.G., Robinson, H., McCullough, L.L., Formosa, T., and Hill, C.P. (2013). Structure of the Spt16 Middle Domain Reveals Functional Features of the Histone Chaperone FACT. Journal of Biological Chemistry *288*, 10188-10194.

Koopmans, W.J.A., Schmidt, T., and van Noort, J. (2008). Nucleosome Immobilization Strategies for Single-Pair FRET Microscopy. ChemPhysChem *9*, 2002-2009.

Kornberg, A., and Baker, T.A. (1992). DNA Replication (W.H. Freeman).

Kornberg, R.D. (1974). Chromatin structure: a repeating unit of histones and DNA. Science *184*, 868-871.

Kornberg, R.D. (1977). Structure of chromatin. Annu Rev Biochem *46*, 931-954.

Kornberg, R.D., and Thomas, J.O. (1974). Chromatin structure; oligomers of the histones. Science *184*, 865-868.

Krings, G., and Bastia, D. (2004). swi1- and swi3-dependent and independent replication fork arrest at the ribosomal DNA of Schizosaccharomyces pombe. Proceedings of the National Academy of Sciences *101*, 14085-14090.

Kurat, C.F., Yeeles, J.T.P., Patel, H., Early, A., and Diffley, J.F.X. (2017). Chromatin Controls DNA Replication Origin Selection, Lagging-Strand Synthesis, and Replication Fork Rates. Molecular Cell *65*, 117-130.

Lambert, T.J. (2019). FPbase: a community-editable fluorescent protein database. Nature Methods *16*, 277-278.

Langowski, J., Seidel, C.A.M., Tóth, K., Dimura, M., Kühnemuth, R., Felekyan, S., and Lehmann, K. (2020). Dynamics of the nucleosomal histone H3 N-terminal tail revealed by high precision single-molecule FRET. Nucleic Acids Research *48*, 1551-1571.

Langston, L.D., Zhang, D., Yurieva, O., Georgescu, R.E., Finkelstein, J., Yao, N.Y., Indiani, C., and O'Donnell, M.E. (2014). CMG helicase and DNA polymerase epsilon form a functional 15-subunit holoenzyme for eukaryotic leading-strand DNA replication. Proc Natl Acad Sci U S A *111*, 15390-15395.

Lee, J.B., Hite, R.K., Hamdan, S.M., Xie, X.S., Richardson, C.C., and van Oijen, A.M. (2006). DNA primase acts as a molecular brake in DNA replication. Nature *439*, 621-624.

Lee, S.J., and Richardson, C.C. (2002). Interaction of adjacent primase domains within the hexameric gene 4 helicase-primase of bacteriophage T7. Proc Natl Acad Sci U S A *99*, 12703-12708.

Lehman, I.R., Bessman, M.J., Simms, E.S., and Kornberg, A. (1958). Enzymatic Synthesis of Deoxyribonucleic Acid. Journal of Biological Chemistry *233*, 163-170.

Leung, A., Cheema, M., Gonzalez-Romero, R., Eirin-Lopez, J.M., Ausio, J., and Nelson, C.J. (2016). Unique yeast histone sequences influence octamer and nucleosome stability. FEBS Lett *590*, 2629-2638.

Lewis, J.S., Spenkelink, L.M., Jergic, S., Wood, E.A., Monachino, E., Horan, N.P., Duderstadt, K.E., Cox, M.M., Robinson, A., Dixon, N.E.*, et al.* (2017a). Single-molecule visualization of fast polymerase turnover in the bacterial replisome. Elife *6*, e23932.

Lewis, J.S., Spenkelink, L.M., Schauer, G.D., Hill, F.R., Georgescu, R.E., O'Donnell, M.E., and van Oijen, A.M. (2017b). Single-molecule visualization of Saccharomyces cerevisiae leading-strand synthesis reveals dynamic interaction between MTC and the replisome. Proc Natl Acad Sci U S A *114*, 10630-10635.

Lewis, J.S., Spenkelink, L.M., Schauer, G.D., Yurieva, O., Mueller, S.H., Natarajan, V., Kaur, G., Maher, C., Kay, C., O'Donnell, M.E.*, et al.* (2020). Tunability of DNA Polymerase Stability during Eukaryotic DNA Replication. Molecular Cell *77*, 17-25.e15.

Li, G., Levitus, M., Bustamante, C., and Widom, J. (2004). Rapid spontaneous accessibility of nucleosomal DNA. Nature Structural & Molecular Biology *12*, 46-53.

Li, G., Levitus, M., Bustamante, C., and Widom, J. (2005). Rapid spontaneous accessibility of nucleosomal DNA. Nature Structural & Molecular Biology *12*, 46-53.

Li, G., Sudlow, G., and Belmont, A.S. (1998). Interphase cell cycle dynamics of a late-replicating, heterochromatic homogeneously staining region: precise choreography of condensation/decondensation and nuclear positioning. The Journal of cell biology *140*, 975-989.

Li, N., Zhai, Y., Zhang, Y., Li, W., Yang, M., Lei, J., Tye, B.K., and Gao, N. (2015). Structure of the eukaryotic MCM complex at 3.8 A. Nature *524*, 186-191.

Li, X., and Marians, K.J. (2000). Two distinct triggers for cycling of the lagging strand polymerase at the replication fork. J Biol Chem *275*, 34757-34765.

Li, Z., Hua, X., Serra-Cardona, A., Xu, X., Gan, S., Zhou, H., Yang, W.S., Chen, C.L., Xu, R.M., and Zhang, Z. (2020). DNA polymerase alpha interacts with H3-H4 and facilitates the transfer of parental histones to lagging strands. Sci Adv *6*, eabb5820.

Liang, C., and Stillman, B. (1997). Persistent initiation of DNA replication and chromatin-bound MCM proteins during the cell cycle in cdc6 mutants. Genes Dev *11*, 3375-3386.

Liu, Y., Zhou, K.D., Zhang, N.F., Wei, H., Tan, Y.Z., Zhang, Z.N., Carragher, B., Potter, C.S., D'Arcy, S., and Luger, K. (2020). FACT caught in the act of manipulating the nucleosome. Nature *577*, 426-431.

Lowary, P.T., and Widom, J. (1998). New DNA sequence rules for high affinity binding to histone octamer and sequence-directed nucleosome positioning. Journal of Molecular Biology *276*, 19-42.

Luger, K., Mader, A.W., Richmond, R.K., Sargent, D.F., and Richmond, T.J. (1997). Crystal structure of the nucleosome core particle at 2.8 angstrom resolution. Nature *389*, 251-260.

Luger, K., Rechsteiner, T.J., and Richmond, T.J. (1999). Expression and purification of recombinant histones and nucleosome reconstitution. Methods Mol Biol *119*, 1-16.

Mangiameli, S.M., Merrikh, C.N., Wiggins, P.A., and Merrikh, H. (2017). Transcription leads to pervasive replisome instability in bacteria. Elife *6*, e19848.

Manosas, M., Spiering, M.M., Zhuang, Z., Benkovic, S.J., and Croquette, V. (2009). Coupling DNA unwinding activity with primer synthesis in the bacteriophage T4 primosome. Nat Chem Biol *5*, 904-912.

Mao, P., Kyriss, M.N.M., Hodges, A.J., Duan, M.R., Morris, R.T., Lavine, M.D., Topping, T.B., Gloss, L.M., and Wyrick, J.J. (2016). A basic domain in the histone H2B N-terminal tail is important for nucleosome assembly by FACT. Nucleic Acids Research *44*, 9142-9152.

Marino-Ramirez, L., Hsu, B., Baxevanis, A.D., and Landsman, D. (2006). The histone database: A comprehensive resource for histones and histone fold-containing proteins. Proteins *62*, 838-842.

Martire, S., and Banaszynski, L.A. (2020). The roles of histone variants in fine-tuning chromatin organization and function. Nat Rev Mol Cell Biol *21*, 522-541.

Mason, P.B., and Struhl, K. (2003). The FACT complex travels with elongating RNA polymerase II and is important for the fidelity of transcriptional initiation *in vivo*. Molecular and Cellular Biology *23*, 8323-8333.

Mattiroli, F., Gu, Y.J., Yadav, T., Balsbaugh, J.L., Harris, M.R., Findlay, E.S., Liu, Y., Radebaugh, C.A., Stargell, L.A., Ahn, N.G.*, et al.* (2017). DNA-mediated association of two histone-bound complexes of yeast Chromatin Assembly Factor-1 (CAF-1) drives tetrasome assembly in the wake of DNA replication. Elife *6*.

Mayanagi, K., Saikusa, K., Miyazaki, N., Akashi, S., Iwasaki, K., Nishimura, Y., Morikawa, K., and Tsunaka, Y. (2019). Structural visualization of key steps in nucleosome reorganization by human FACT. Sci Rep *9*, 10183.

McBryant, S.J., Klonoski, J., Sorensen, T.C., Norskog, S.S., Williams, S., Resch, M.G., Toombs, J.A., 3rd, Hobdey, S.E., and Hansen, J.C. (2009). Determinants of histone H4 N-terminal domain function during nucleosomal array oligomerization: roles of amino acid sequence, domain length, and charge density. J Biol Chem *284*, 16716-16722.

McCauley, M.J., Huo, R., Becker, N., Holte, M.N., Muthurajan, U.M., Rouzina, I., Luger, K., Maher, L.J., 3rd, Israeloff, N.E., and Williams, M.C. (2019). Single and double box HMGB proteins differentially destabilize nucleosomes. Nucleic Acids Res *47*, 666-678.

McCullough, L.L., Connell, Z., Xin, H., Studitsky, V.M., Feofanov, A.V., Valieva, M.E., and Formosa, T. (2018). Functional roles of the DNA-binding HMGB domain in the histone chaperone FACT in nucleosome reorganization. J Biol Chem *293*, 6121-6133.

McGeoch, A.T., Trakselis, M.A., Laskey, R.A., and Bell, S.D. (2005). Organization of the archaeal MCM complex on DNA and implications for the helicase mechanism. Nat Struct Mol Biol *12*, 756-762.

McGhee, J.D., and Felsenfeld, G. (1980). Nucleosome structure. Annu Rev Biochem *49*, 1115-1156.

Mendel, G. (1866). Versuche über Pflanzen-Hybriden (Brünn :: Im Verlage des Vereines).

Miles, J., and Formosa, T. (1992). Evidence that POB1, a Saccharomyces cerevisiae protein that binds to DNA polymerase a, acts in DNA metabolism *in vivo*. Molecular and Cellular Biology *12*, 5724-5735.

Miller, T.C.R., and Costa, A. (2017). The architecture and function of the chromatin replication machinery. Curr Opin Struc Biol *47*, 9-16.

Mohanty, B.K., Bairwa, N.K., and Bastia, D. (2006). The Tof1p-Csm3p protein complex counteracts the Rrm3p helicase to control replication termination of Saccharomyces cerevisiae. Proceedings of the National Academy of Sciences *103*, 897-902.

Monardes, N. (1565). Dos libros, el uno que trata de todas las cosas que traen de nuestras Indias Occidentales, que sirven al uso de la medicina, y el otro que trata de la piedra Bezaar y de la yerva escuerconera (Diaz).

Morris, C.F., Sinha, N.K., and Alberts, B.M. (1975). Reconstruction of bacteriophage T4 DNA replication apparatus from purified components: rolling circle replication following *de novo* chain initiation on a single-stranded circular DNA template. Proceedings of the National Academy of Sciences *72*, 4800-4804.

Morrison, O., and Thakur, J. (2021). Molecular Complexes at Euchromatin, Heterochromatin and Centromeric Chromatin. Int J Mol Sci *22*, 6922.

Musselman, C.A., Lalonde, M.E., Cote, J., and Kutateladze, T.G. (2012). Perceiving the epigenetic landscape through histone readers. Nature Structural & Molecular Biology *19*, 1218-1227.

Nelson, D.L., and Cox, M.M. (2005). Lehninger Principles of Biochemistry (W. H. Freeman).

Neuman, K.C., and Nagy, A. (2008). Single-molecule force spectroscopy: optical tweezers, magnetic tweezers and atomic force microscopy. Nat Methods *5*, 491-505.

Noguchi, C., Rapp, J.B., Skorobogatko, Y.V., Bailey, L.D., and Noguchi, E. (2012). Swi1 Associates with Chromatin through the DDT Domain and Recruits Swi3 to Preserve Genomic Integrity. Plos One *7*.

O'Donnell, A.F., Brewster, N.K., Kurniawan, J., Minard, L.V., Johnston, G.C., and Singer, R.A. (2004). Domain organization of the yeast histone chaperone FACT: the conserved N-terminal domain of FACT subunit Spt16 mediates recovery from replication stress. Nucleic Acids Research *32*, 5894-5906.

Okada, M., Okawa, K., Isobe, T., and Fukagawa, T. (2009). CENP-H-containing complex facilitates centromere deposition of CENP-A in cooperation with FACT and CHD1. Mol Biol Cell *20*, 3986-3995.

Olins, A.L., and Olins, D.E. (1974). Spheroid Chromatin Units (v Bodies). Science *183*, 330-332.

Orphanides, G., Wu, W.H., Lane, W.S., Hampsey, M., and Reinberg, D. (1999). The chromatin-specific transcription elongation factor FACT comprises human SPT16 and SSRP1 proteins. Nature *400*, 284-288.

Oudet, P., Gross-Bellard, M., and Chambon, P. (1975). Electron microscopic and biochemical evidence that chromatin structure is a repeating unit. Cell *4*, 281-300.

Pandey, M., Syed, S., Donmez, I., Patel, G., Ha, T., and Patel, S.S. (2009). Coordinating DNA replication by means of priming loop and differential synthesis rate. Nature *462*, 940-943.

Park, H., and Sternglanz, R. (1999). Identification and characterization of the genes for two topoisomerase I-interacting proteins from Saccharomyces cerevisiae. Yeast *15*, 35-41.

Pauling, L., Corey, R.B., and Branson, H.R. (1951). The structure of proteins; two hydrogen-bonded helical configurations of the polypeptide chain. Proc Natl Acad Sci U S A *37*, 205-211.

Perez-Arnaiz, P., Bruck, I., Colbert, M.K., and Kaplan, D.L. (2017). An intact Mcm10 coiled-coil interaction surface is important for origin melting, helicase assembly and the recruitment of Pol-alpha to Mcm2-7. Nucleic Acids Res *45*, 7261-7275.

Ploetz, E., Lerner, E., Husada, F., Roelfs, M., Chung, S., Hohlbein, J., Weiss, S., and Cordes, T. (2016). Forster resonance energy transfer and protein-induced fluorescence enhancement as synergetic multiscale molecular rulers. Sci Rep-Uk *6*.

Prendergast, L., Hong, E., Safina, A., Poe, D., and Gurova, K. (2020). Histone chaperone FACT is essential to overcome replication stress in mammalian cells. Oncogene *39*, 5124-5137.

Prendergast, L., Muller, S., Liu, Y., Huang, H., Dingli, F., Loew, D., Vassias, I., Patel, D.J., Sullivan, K.F., and Almouzni, G. (2016). The CENP-T/-W complex is a binding partner of the histone chaperone FACT. Genes Dev *30*, 1313-1326.

PyPI.org. Python Package Index - PyPI (Python Software Foundation).

Qiu, Y., Levendosky, R.F., Chakravarthy, S., Patel, A., Bowman, G.D., and Myong, S. (2017). The Chd1 Chromatin Remodeler Shifts Nucleosomal DNA Bidirectionally as a Monomer. Molecular Cell *68*, 76-88.e76.

Radman-Livaja, M., and Rando, O.J. (2010). Nucleosome positioning: how is it established, and why does it matter? Dev Biol *339*, 258-266.

Ransom, M., Dennehey, B.K., and Tyler, J.K. (2010). Chaperoning Histones during DNA Replication and Repair. Cell *140*, 183-195.

Rasband, W.S. (1997). ImageJ.

Remus, D., Beuron, F., Tolun, G., Griffith, J.D., Morris, E.P., and Diffley, J.F. (2009). Concerted loading of Mcm2-7 double hexamers around DNA during DNA replication origin licensing. Cell *139*, 719-730.

Reusswig, K.-U., Bittmann, J., Peritore, M., Wierer, M., Mann, M., and Pfander, B. (2021).

Rhoades, A.R., Ruone, S., and Formosa, T. (2004). Structural features of nucleosomes reorganized by yeast FACT and its HMG box component, Nhp6. Molecular and Cellular Biology *24*, 3907-3917.

Richet, N., Liu, D., Legrand, P., Velours, C., Corpet, A., Gaubert, A., Bakail, M., Moal-Raisin, G., Guerois, R., Compper, C.*, et al.* (2015). Structural insight into how the human helicase subunit MCM2 may act as a histone chaperone together with ASF1 at the replication fork. Nucleic Acids Res *43*, 1905-1917.

Richmond, T.J., Finch, J.T., Rushton, B., Rhodes, D., and Klug, A. (1984). Structure of the Nucleosome Core Particle at 7a Resolution. Nature *311*, 532-537.

Roark, D.E., Geoghegan, T.E., and Keller, G.H. (1974). A two-subunit histone complex from calf thymus. Biochem Biophys Res Commun *59*, 542-547.

Rohs, R., West, S.M., Sosinsky, A., Liu, P., Mann, R.S., and Honig, B. (2009). The role of DNA shape in protein–DNA recognition. Nature *461*, 1248-1253.

Rothenberg, E., Trakselis, M.A., Bell, S.D., and Ha, T. (2007). MCM forked substrate specificity involves dynamic interaction with the 5'-tail. J Biol Chem *282*, 34229-34234.

Ruone, S., Rhoades, A.R., and Formosa, T. (2003). Multiple Nhp6 molecules are required to recruit Spt16-Pob3 to form yFACT complexes and to reorganize nucleosomes. Journal of Biological Chemistry *278*, 45288-45295.

Santocanale, C., and Diffley, J.F. (1996). ORC- and Cdc6-dependent complexes at active and inactive chromosomal replication origins in Saccharomyces cerevisiae. The EMBO Journal *15*, 6671-6679.

Sarangi, M.K., Zvoda, V., Holte, M.N., Becker, N.A., Peters, J.P., Maher, L.J., and Ansari, A. (2019). Evidence for a bind-then-bend mechanism for architectural DNA binding protein yNhp6A. Nucleic Acids Res *47*, 2871-2883.

Schalbetter, S.A., Mansoubi, S., Chambers, A.L., Downs, J.A., and Baxter, J. (2015). Fork rotation and DNA precatenation are restricted during DNA replication to prevent chromosomal instability. Proceedings of the National Academy of Sciences of the United States of America *112*, E4565-E4570.

Scherr, M.J., Safaric, B., and Duderstadt, K.E. (2018). Noise in the Machine: Alternative Pathway Sampling is the Rule During DNA Replication. Bioessays *40*.

Schwabish, M.A., and Struhl, K. (2004). Evidence for eviction and rapid deposition of histones upon transcriptional elongation by RNA polymerase II. Molecular and cellular biology *24*, 10111-10117.

Schwarz, M., Schall, K., Kallis, E., Eustermann, S., Guariento, M., Moldt, M., Hopfner, K.-P., and Michaelis, J. (2018). Single-molecule nucleosome remodeling by INO80 and effects of histone tails. FEBS Letters *592*, 318-331.

Sengupta, S., van Deursen, F., de Piccoli, G., and Labib, K. (2013). Dpb2 integrates the leading-strand DNA polymerase into the eukaryotic replisome. Curr Biol *23*, 543-552.

Shahid, S., Ahmad, F., Hassan, M.I., and Islam, A. (2019). Mixture of Macromolecular Crowding Agents Has a Non-additive Effect on the Stability of Proteins. Appl Biochem Biotech *188*, 927-941.

Shakya, A., Callister, C., Goren, A., Yosef, N., Garg, N., Khoddami, V., Nix, D., Regev, A., and Tantin, D. (2015). Pluripotency transcription factor Oct4 mediates stepwise nucleosome demethylation and depletion. Mol Cell Biol *35*, 1014-1025.

Shyian, M., Albert, B., Zupan, A.M., Ivanitsa, V., Charbonnet, G., Dilg, D., and Shore, D. (2020). Fork pausing complex engages topoisomerases at the replisome. Genes & Development *34*, 87-98.

Simon, A.C., Zhou, J.C., Perera, R.L., van Deursen, F., Evrin, C., Ivanova, M.E., Kilkenny, M.L., Renault, L., Kjaer, S., Matak-Vinkovic, D.*, et al.* (2014). A Ctf4

trimer couples the CMG helicase to DNA polymerase alpha in the eukaryotic replisome. Nature *510*, 293-297.

Stinchcomb, D.T., Struhl, K., and Davis, R.W. (1979). Isolation and characterisation of a yeast chromosomal replicator. Nature *282*, 39-43.

Stokes, G.G. (1852). On the change of refrangibility of light. Philosophical transactions of the Royal Society of London, 463-562.

Strahl, B.D., and Allis, C.D. (2000). The language of covalent histone modifications. Nature *403*, 41-45.

Stuwe, T., Hothorn, M., Lejeune, E., Rybin, V., Bortfeld, M., Scheffzek, K., and Ladurner, A.G. (2008). The FACT Spt16 "peptidase" domain is a histone H3-H4 binding module. Proceedings of the National Academy of Sciences of the United States of America *105*, 8884-8889.

Sun, J., Evrin, C., Samel, S.A., Fernández-Cid, A., Riera, A., Kawakami, H., Stillman, B., Speck, C., and Li, H. (2013). Cryo-EM structure of a helicase loading intermediate containing ORC–Cdc6–Cdt1–MCM2-7 bound to DNA. Nature Structural & Molecular Biology *20*, 944-951.

Sun, J., Fernandez-Cid, A., Riera, A., Tognetti, S., Yuan, Z., Stillman, B., Speck, C., and Li, H. (2014). Structural and mechanistic insights into Mcm2–7 double-hexamer assembly and function. Genes & Development *28*, 2291-2303.

Sun, J., Shi, Y., Georgescu, R.E., Yuan, Z., Chait, B.T., Li, H., and O'Donnell, M.E. (2015). The architecture of a eukaryotic replisome. Nat Struct Mol Biol *22*, 976-982.

Tachiwana, H., Dacher, M., Maehara, K., Harada, A., Seto, Y., Katayama, R., Ohkawa, Y., Kimura, H., Kurumizaka, H., and Saitoh, N. (2021). Chromatin structure-dependent histone incorporation revealed by a genome-wide deposition assay. Elife *10*.

Tachiwana, H., Kagawa, W., Shiga, T., Osakabe, A., Miya, Y., Saito, K., Hayashi-Takanaka, Y., Oda, T., Sato, M., Park, S.Y.*, et al.* (2011). Crystal structure of the human centromeric nucleosome containing CENP-A. Nature *476*, 232-U135.

Tagami, H., Ray-Gallet, D., Almouzni, G., and Nakatani, Y. (2004). Histone H3.1 and H3.3 complexes mediate nucleosome assembly pathways dependent or independent of DNA synthesis. Cell *116*, 51-61.

Takahata, S., Yu, Y.X., and Stillman, D.J. (2009). FACT and Asf1 Regulate Nucleosome Dynamics and Coactivator Binding at the HO Promoter. Molecular Cell *34*, 405-415.

Tan, B.C.M., Chien, C.T., Hirose, S., and Lee, S.C. (2006). Functional cooperation between FACT and MCM helicase facilitates initiation of chromatin DNA replication. Embo Journal *25*, 3975-3985.

Tanaka, T., Knapp, D., and Nasmyth, K. (1997). Loading of an Mcm Protein onto DNA Replication Origins Is Regulated by Cdc6p and CDKs. Cell *90*, 649-660.

Tanner, N.A., Hamdan, S.M., Jergic, S., Loscha, K.V., Schaeffer, P.M., Dixon, N.E., and van Oijen, A.M. (2008). Single-molecule studies of fork dynamics in Escherichia coli DNA replication. Nat Struct Mol Biol *15*, 998.

Torigoe, S.E., Patel, A., Khuong, M.T., Bowman, G.D., and Kadonaga, J.T. (2013). ATP-dependent chromatin assembly is functionally distinct from chromatin remodeling. Elife *2*.

Tóth, K., Brun, N., and Langowski, J. (2001). Trajectory of Nucleosomal Linker DNA Studied by Fluorescence Resonance Energy Transfer. Biochemistry *40*, 6921-6928.

Tóth, K., Brun, N., and Langowski, J. (2006). Chromatin Compaction at the Mononucleosome Level. Biochemistry *45*, 1591-1598.

Tourrière, H., Versini, G., Cordón-Preciado, V., Alabert, C., and Pasero, P. (2005). Mrc1 and Tof1 Promote Replication Fork Progression and Recovery Independently of Rad53. Molecular Cell *19*, 699-706.

Tsunaka, Y., Fujiwara, Y., Oyama, T., Hirose, S., and Morikawa, K. (2016). Integrated molecular mechanism directing nucleosome reorganization by human FACT. Genes & Development *30*, 673-686.

Turner, B.M. (1993). Decoding the Nucleosome. Cell *75*, 5-8.

Valieva, M.E., Armeev, G.A., Kudryashova, K.S., Gerasimova, N.S., Shaytan, A.K., Kulaeva, O.I., McCullough, L.L., Formosa, T., Georgiev, P.G., Kirpichnikov, M.P.*, et al.* (2016). Large-scale ATP-independent nucleosome unfolding by a histone chaperone. Nature Structural & Molecular Biology *23*, 1111-1116.

van der Meer, B.W. (2002). Kappa-squared: from nuisance to new sense. J Biotechnol *82*, 181-196.

VanDemark, A.P., Xin, H., McCullough, L., Rawlins, R., Bentley, S., Heroux, A., Stillman, D.J., Hill, C.P., and Formosa, T. (2008). Structural and functional analysis of the Spt16p N-terminal domain reveals overlapping roles of yFACT subunits. Journal of Biological Chemistry *283*, 5058-5068.

Vlijm, R., Kim, S.H., De Zwart, P.L., Dalal, Y., and Dekker, C. (2017). The supercoiling state of DNA determines the handedness of both H3 and CENP-A nucleosomes. Nanoscale *9*, 1862-1870.

Vlijm, R., Smitshuijzen, J.S., Lusser, A., and Dekker, C. (2012). NAP1-assisted nucleosome assembly on DNA measured in real time by single-molecule magnetic tweezers. PLoS One *7*, e46306.

Voith von Voithenberg, L., and Lamb, D.C. (2018). Single Pair Forster Resonance Energy Transfer: A Versatile Tool To Investigate Protein Conformational Dynamics. Bioessays *40*.

Waga, S., Bauer, G., and Stillman, B. (1994). Reconstitution of complete SV40 DNA replication with purified replication factors. J Biol Chem *269*, 10923-10934.

Waldeyer, W. (1888). Ueber Karyokinese und ihre Beziehungen zu den Befruchtungsvorgängen. Archiv für mikroskopische Anatomie *32*, 1.

Wang, M.D., Yin, H., Landick, R., Gelles, J., and Block, S.M. (1997). Stretching DNA with optical tweezers. Biophysical Journal *72*, 1335-1346.

Wang, T., Liu, Y., Edwards, G., Krzizike, D., Scherman, H., and Luger, K. (2018). The histone chaperone FACT modulates nucleosome structure by tethering its components. Life Science Alliance *1*, 13.

Watson, J.D., and Crick, F.H. (1953). Molecular structure of nucleic acids; a structure for deoxyribose nucleic acid. Nature *171*, 737-738.

Westhorpe, R., Keszthelyi, A., Minchell, N.E., Jones, D., and Baxter, J. (2020). Separable functions of Tof1/Timeless in intra-S-checkpoint signalling, replisome stability and DNA topological stress. Nucleic Acids Research *48*, 12169-12187.

Widom, J. (1989). Toward a unified model of chromatin folding. Annu Rev Biophys Biophys Chem *18*, 365-395.

Winkler, D.D., Muthurajan, U.M., Hieb, A.R., and Luger, K. (2011). Histone Chaperone FACT Coordinates Nucleosome Interaction through Multiple Synergistic Binding Events. Journal of Biological Chemistry *286*, 41883-41892.

Wittmeyer, J., and Formosa, T. (1997). The Saccharomyces cerevisiae DNA polymerase alpha catalytic subunit interacts with Cdc68/Spt16 and with Pob3, a protein similar to an HMG1-like protein. Molecular and Cellular Biology *17*, 4178-4190.

Woodcock, C.L. (1973). Ultrastructure of Inactive Chromatin. J Cell Biol *59*, A368-A368.

Woodcock, C.L., and Dimitrov, S. (2001). Higher-order structure of chromatin and chromosomes. Current Opinion in Genetics & Development *11*, 130-135.

Wu, R.S., Panusz, H.T., Hatch, C.L., and Bonner, W.M. (1986). Histones and Their Modifications. Crit Rev Biochem Mol *20*, 201-263.

Xin, H., Takahata, S., Blanksma, M., McCullough, L., Stillman, D.J., and Formosa, T. (2009). yFACT Induces Global Accessibility of Nucleosomal DNA without H2A-H2B Displacement. Molecular Cell *35*, 365-376.

Xu, M., Long, C.Z., Chen, X.Z., Huang, C., Chen, S., and Zhu, B. (2010). Partitioning of Histone H3-H4 Tetramers During DNA Replication-Dependent Chromatin Assembly. Science *328*, 94-98.

Yeeles, J.T., Deegan, T.D., Janska, A., Early, A., and Diffley, J.F. (2015a). Regulated eukaryotic DNA replication origin firing with purified proteins. Nature *519*, 431-435.

Yeeles, J.T.P., Deegan, T.D., Janska, A., Early, A., and Diffley, J.F.X. (2015b). Regulated eukaryotic DNA replication origin firing with purified proteins. Nature *519*, 431-+.

Yeeles, J.T.P., Janska, A., Early, A., and Diffley, J.F.X. (2017). How the Eukaryotic Replisome Achieves Rapid and Efficient DNA Replication. Molecular Cell *65*, 105-116.

Yu, C., Gan, H., Serra-Cardona, A., Zhang, L., Gan, S., Sharma, S., Johansson, E., Chabes, A., Xu, R.M., and Zhang, Z. (2018). A mechanism for preventing asymmetric histone segregation onto replicating DNA strands. Science *361*, 1386-1389.

Yuan, Z., Georgescu, R., Santos, R.d.L.A., Zhang, D., Bai, L., Yao, N.Y., Zhao, G., O'Donnell, M.E., and Li, H. (2019). Ctf4 organizes sister replisomes and Pol α into a replication factory. eLife *8*.

Yuzhakov, A., Kelman, Z., and O'Donnell, M. (1999). Trading places on DNA--a three-point switch underlies primer handoff from primase to the replicative DNA polymerase. Cell *96*, 153-163.

Zhang, T., Cooper, S., and Brockdorff, N. (2015). The interplay of histone modifications – writers that read. EMBO reports *16*, 1467-1481.

Zhou, J.C., Janska, A., Goswami, P., Renault, L., Abid Ali, F., Kotecha, A., Diffley, J.F.X., and Costa, A. (2017). CMG-Pol epsilon dynamics suggests a mechanism for the establishment of leading-strand synthesis in the eukaryotic replisome. Proc Natl Acad Sci U S A *114*, 4141-4146.

Danksagung

I am grateful to so many people for sharing this journey with me and shaping my PhD experience.

I'll be forever grateful to Karl who gave me the opportunity to embark on my PhD journey as his first ever PhD researcher. I had the unlimited freedom to explore different avenues of the project, with my ideas and suggestions never being turned down, and I was able to freely steer the project into the direction the experiments and intuition pointed towards. I truly appreciate your support for all my numerous endeavors outside the lab. A big thank you for all the positive feedback through the years, and for always believing in me. All of this encouraged me to keep going, even when experiments were not, and I felt out of my depth.

Thank you to my Thesis Advisory Committee members, Dr. Naoko Mizuno and Prof. Ladurner, for their valuable input and feedback. A big thanks to our collaborators on the project — Cordes lab and Kurat lab. Thanks to Thorben for making it possible to do the ALEX experiments in his lab, for all the expertise and feedback. A big thanks to Christian for teaching me the ways of Monique, and many discussions and brainstorming. Thank you to Christoph for joining us on the project to look into chromatin replication. Another big thank you to Erika for expertly doing all the replication assays.

A massive thanks to Matthias, without whom I could not see this project through. Thank you for all your help and support, countless discussions and troubleshooting, all coffee breaks, and keeping me sane at times. Most of the time. I honestly cannot imagine doing this without you.

A big thanks to Geri for your friendship, all the chats and being my sounding board. Thank you to Lionel who helped this project take off from the ground zero, and was there for me when I needed it the most. Thanks to Lorenzo and Kalle for all the late night talks and always helping me out, whenever I needed it. Thanks to Thomas for always being the laid-back, optimistic one. Big thank you to Daniel for all the encouragement, and the guidance with cryo-EM.

A special thank you to Kalina for always having my back, and never stopping encouraging me to keep going. You are my rock. Thank you to my dearest Mili for always being there, your friendship was one of the few steady lines in the last years. We stuck together through thick and thin, and I came out on the other side with a true friend for life. A big thanks to the Balkan cluster for all your support, encouragements, and giving me a part of home I didn't know I was missing. And moruzgvice.

A heartfelt thank you to the PhDnet – what would I do without you? To my dear MPQueer, thank you for giving me the opportunity to stand up for something I believe in, and to be there from the beginning. Thank you to Frauke for all your support. Big thanks to my dear Equal Opportunity team, you are an inspiration and I have learned so much from you all. Thank you to my Offspring family for lots of laughs, random chats, fun times, great articles and puppy pics. My biggest thanks to my Mental Health Collective, together we have started something beautiful.

Velika hvala roditeljima, koji su uvijek vjerovali u mene i omogućili mi da slijedim svoj put u nepoznato.